Every parasite counts?! Improving *in vitro* assay design for Chagas' disease drug discovery

Inauguraldissertation

zur

Erlangung der Würde eines Doktors der Philosophie

vorgelegt der

Philosophisch-Naturwissenschaftlichen Fakultät

der Universität Basel

von

Anna Frieda Fesser

aus Nürtingen, Deutschland

2021

Dieses Werk ist lizenziert unter einer Creative Commons Namensnennung 4.0 International Lizenz.

Originaldokument gespeichert auf dem Dokumentenserver der Universität Basel edoc.unibas.ch.

Genehmigt von der Philosophisch-Naturwissenschaftlichen Fakultät

auf Antrag von

Prof. Dr. Pascal Mäser, Prof. Dr. Nicolas Fasel

Basel, den 19.11.2019

(Datum der Genehmigung durch die Fakultät)

Prof. Dr. Martin Spiess

Summary

Chagas' disease is caused by the protozoan parasite *Trypanosoma cruzi*. Symptoms of the chronic disease occur decades after infection in about 30% of the infected people. The major symptoms of chronic disease are cardiomyopathies and mega-syndromes of the digestive tract. Antiparasitic treatment is important to prevent and reduce chronic symptoms. However, the only two licensed antichagasic drugs, benznidazole and nifurtimox, are compromised by limited efficacy and side effects. Therefore, new drugs are urgently needed. Surprisingly high numbers of relapses in the clinical trials of ergosterol inhibitors questioned the preclinical drug discovery pipeline for Chagas' disease. In recent years, progress has been made in *in vitro* drug discovery towards higher throughput in screening, testing against strain panels, and testing against reversibility of drug action. However, inhibition of *T. cruzi* amastigote replication is still a dominant feature in the *in vitro* assays in contrast to cidality.

The aim of this PhD project was to develop an *in vitro* assay that contributes new read-outs to the preclinical drug discovery pipeline for Chagas' disease.

As a first step, methods for *T. cruzi* molecular genetics were established in our laboratory: genotyping, a transfection protocol including the prioritization of selection antibiotics, and the sequence of the genome of our *T. cruzi* strain STIB980. Next, we established an eGFP-expressing parasite line and characterized it phenotypically. This eGFP-expressing parasite line was employed in a novel assay design that allows to monitor parasite replication and drug action in four-hour intervals over 6 days with a high-content microscope occupancy of 24 h only. The results of this assay revealed high levels of variability. Statistical modelling of the development of parasite numbers over 24 h led to the fold-change in parasite numbers as a robust read-out. For drug exposed samples, the fold-change in parasite numbers is dependent on the drug concentration and the time of drug exposure. Using the fold-change, we can determine the timepoint when parasite numbers start to drop with statistical confidence. This time-to-kill is a novel pharmacodynamic parameter that enhances the characterization of drug candidates.

The established methods and the novel assay design will hopefully contribute to Chagas' disease drug discovery in our laboratory and promote the discovery of the much needed effective drugs.

Table of Content

Abbreviations

CO_2	carbon dioxide
Ct-value	qPCR cycle, when the detection threshold is passed
DAPI	4’,6-diamidino-2-phenylindole
DMEM	Dulbecco's modified Eagle's (minimal essential) medium
DMSO	dimethyl sulfoxide
DNA	desoxyribonucleic acid
DNDi	Drugs for Neglected Diseases initiative
DTU	discrete typing units
EC50	concentration of half-maximal effect
EdU	5-ethynyl-2’-deoxyuridine
eGFP	enhanced green fluorescent protein
EMA	European Medicines Agency
ePMM	expanded peritoneal mouse macrophages
G12	GFP-expressing T. cruzi STIB980 clone 12
G6PI	glucose-6-phosphate isomerase
GAPDH	glyceraldehyde 3-phosphate dehydrogenase
gDNA	genomic DNA
GPI	glycosylposphatidylinositol
hpi	hours post infection
HSP60	heat-shock protein 60
iFCS	heat-inactivated fetal calf serum
i.p.	intra-peritoneal
kDNA	kinetoplastid DNA
LacZ	β-galactosidase
LIT	liver infusion tryptose
LSHTM	London School of Hygiene and Tropical Medicine
LSU	large ribosomal subunit
MEF	mouse embryonic fibroblasts
MOI	multiplicity of infection
mTORC	mammalian target of rapamycin complex
PBS	phosphate-buffered saline
PCR	polymerase chain reaction
PD	pharmacodynamics

PK	pharmacokinetics
PolI	RNA polymerase I
PolII	RNA polymerase II
pTcRG	pTCRenillaeGFP
qPCR	quantitative PCR
qRT-PCR	quantitative reverse-transcription PCR
RNA	ribonucleic acid
RNAi	induced suppression of RNA levels
RPMI	Roswell Park Memorial Institute 1640 medium
rRNA	ribosomal RNA
TbBSF	*Trypanosoma brucei* bloodstram forms
TcBDF1	*Trypanosoma cruzi* bromodomain factor 1
TcHTE	*T. cruzi* heme transporter
TGFα	transforming growth factor α

Trypanosoma cruzi amastigote replication and its relevance for Chagas' disease drug discovery

Trypanosoma cruzi amastigote replication in Chagas' disease drug discovery

Trypanosoma cruzi is a protozoan parasite of triatomine bugs and mammals. In humans, *T. cruzi* causes Chagas' disease. About 8 million people are infected with *T. cruzi* globally (Stanaway & Roth, 2015). In endemic countries, transmission to humans is mostly linked to triatomine bugs (Rassi, Rassi, & Marin-Neto, 2010). Triatomine bugs can carry the infective forms of *T. cruzi* in their digestive tract. As they defecate during their blood meal, the parasites have easy access to the bite wound, to mucosal tissues or the conjunctiva. Triatomine-infested food or food crops can become the source for oral infection. Other forms of transmission are not bound to the endemic areas, i.e. the vector distribution. Among them is congenital transmission during pregnancy or birth, blood and organ donation, and laboratory accidents (Herwaldt, 2001; Rassi et al., 2010).

In the first months of infection parasite numbers increase readily. Together with the immune response, the symptoms of acute Chagas' disease appear: swelling/edema of the site of infection (chagoma and Romaña sign) and febrile illness. Acute symptoms are often summarized as flu-like. While acute Chagas' disease can be fatal in a small number of cases, most often it passes unrecognized and undiagnosed (Rassi et al., 2010). The cellular immune response reduces parasite numbers below the detection limit (Rassi et al., 2010). However, as far as we know, in most cases, small numbers of parasites manage to survive in some organs. For several decades, the parasitemia can remain below the detection limit. Yet, at least in the mouse model, parasites replicate and regularly infect cells of several organs during this so-called indeterminate phase (Lewis et al., 2014). Over time, parasite replication and immune response cause tissue damage and fibrosis. In about 30% of the infected people, the accumulation of damage leads to chagasic cardiomyopathies, characterized by cardiac fibrosis, increase of cardiac volume, conduction system disturbances, and can end in sudden cardiac death (Rassi et al., 2010). In about another 10% of the infected people, the accumulation of tissue damage leads to denervation of the digestive tract resulting in mega-syndromes of esophagus and colon (Rassi et al., 2010).

New antiparasitic drugs are needed to treat Chagas' disease

Prevention of Chagas' disease relies on vector control, as no vaccine is available. Disease treatment can be symptomatic or etiological (Rassi et al., 2010). The only antiparasitic drugs available are the nitroheterocyclics benznidazole and nifurtimox. Both drugs were developed in the 1960s and 70s. Both are prodrugs, i.e. they are activated by the parasite's nitroreductase, increasing oxidative stress in the parasite (Wilkinson, Taylor, Horn, Kelly, & Cheeseman, 2008). Treatment with benznidazole or nifurtimox in the acute phase is generally seen as curative (WHO, 2012). In the chronic phase, treatment success is more difficult to assess. In a recent study, cardiac disease progression could not be stopped by benznidazole treatment in chagasic cardiomyopathy patients (Morillo et al., 2015). Both

drugs have to be used for a long period (60 days) and can have severe side effects, such as nausea, rash and neurological symptoms. Due to unclear treatment outcome and the side effects, the medical community is very hesitant to use benznidazole and nifurtimox for treatment of chronic Chagas' disease, especially in asymptomatic cases. Therefore, patients are often treated to control the symptoms with amiodarone, pacemakers, and ultimately cardiac transplantation (Rassi et al., 2010). However, when the presence of the parasite was demonstrated to be linked to disease progression (Tarleton, 2001), efforts were resumed to search for new, more effective, and better tolerated drugs.

Trypanosoma cruzi amastigote replication is important for Chagas' disease

The life cycle of *T. cruzi* alternates between the insect vector and the mammalian host. The infective forms found in the hindgut of the triatomine bug are called metacyclic trypomastigotes. Once inside the mammalian host, they are able to infect any nucleated cell they encounter. Invasion of (metacyclic) trypomastigotes happens either in a lysosome-dependent or in a lysosome-independent manner (Andrade & Andrews, 2005). In both cases, trypomastigotes end up in an acidified lysosome-like compartment, where they receive stimuli for differentiation (Tomlinson, Vandekerckhove, Frevert, & Nussenzweig, 1995). Egressing from this lysosome-like department, they differentiate into the replicative amastigotes (amastigogenesis). Approximately 30 hours after invasion, amastigotes start to replicate by binary fission in the host cell cytosol (Dvorak & Hyde, 1973; Hyde & Dvorak, 1973). Upon not well understood signals, amastigotes filling the host cell cease replication, and the amastigotes in one cell differentiate into trypomastigotes (trypomastigogenesis, (Dvorak & Hyde, 1973)). Trypomastigote rupture the host cell membrane by their flagellar movement and are liberated into the extracellular matrix (Abuin, Freitas-Junior, Colli, Alves, & Schenkman, 1999; Dvorak & Hyde, 1973). They either infect a neighboring cell or enter the bloodstream to find a new host cell or to be taken up by a feeding triatomine bug. In the triatomine midgut, trypomastigotes differentiate into the epimastigotes (epimastigogenesis), which replicate extracellularly by binary fission. Upon nutrient deprivation, epimastigotes migrate to the triatomine hindgut, where they attach and differentiate into metacyclic trypomastigotes (metacyclogenesis, (Lucena et al., 2019)).

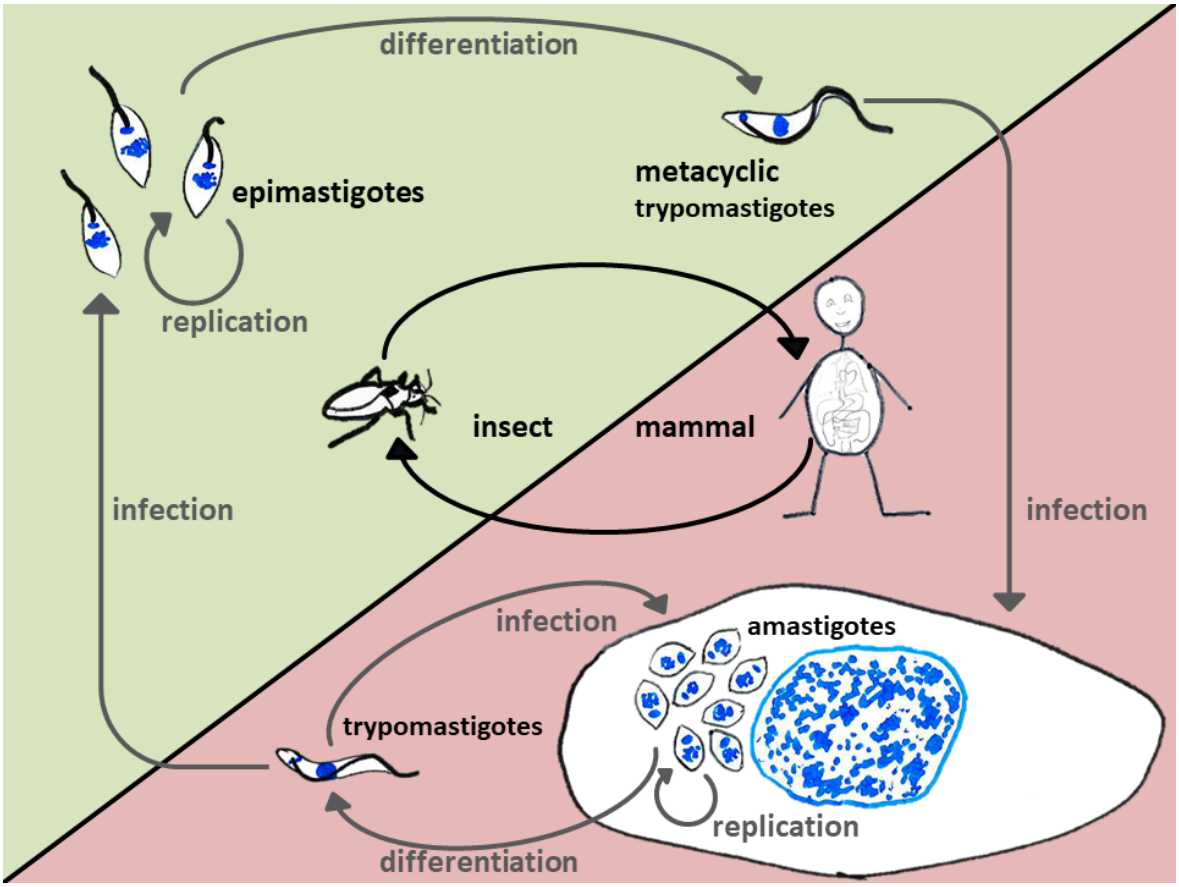

Figure 1 **The life cycle of *Trypanosoma cruzi***

The mammalian stages, amastigotes and trypomastigotes, are the pathogenic stages of human disease. The non-replicating trypomastigotes have a dense glycoprotein coat protecting them from the humoral immune response in the bloodstream (Giorgi & de Lederkremer, 2011). Their protein coat also consists of receptor and effector proteins for invasion. In contrast, amastigotes have an active metabolism and replication machinery (Li et al., 2016). Presumably, intracellular amastigotes are present somewhere in the body throughout the whole period of infection. In recent years, non-replicative (dormant) stages resembling amastigotes but with low metabolic activity were postulated as enduring stages throughout the infection and also under drug treatment (Chatelain, 2015; Sanchez-Valdez, Padilla, Wang, Orr, & Tarleton, 2018). Non-replicating parasite forms have been reported *in vitro* and in mouse models (Sanchez-Valdez et al., 2018). However, it is not yet understood how their induction is regulated, and whether it is regulated at all or stochastic. In general, little is known about the factors influencing amastigote replication, despite its importance for maintenance of infection and therefore for Chagas' disease pathology.

Quantifying *Trypanosoma cruzi* amastigote replication for *in vitro* drug testing

Chagas' disease drug discovery is in a critical phase at the moment (Chatelain, 2015; Franco, Alcantara, Chatelain, Freitas-Junior, & Moraes, 2019). While there are several projects in preclinical phase, the clinical part of the pipeline has been rather empty for the last years (DNDi, 2019), except for three projects: A paediatric formulation of benznidazole, new dosing regimens for benznidazole, and fexinidazole. The latter has recently been approved for treatment of *T. brucei gambiense* (EMA, 2018) and is active against *T. cruzi*. The former most advanced drug candidates were the ergosterol-synthesis inhibitors, posaconazole and E122 - the prodrug of ravuconazole (Torrico et al., 2018; Urbina et al., 1998). Their development as a drug against Chagas' disease was abolished due to the results of the clinical trial of posaconazole in chronic Chagas' disease patients (Molina et al., 2014). Most (94%) benznidazole-treated patients remained PCR-negative over 10 months of follow-up. In contrast, less than 20% of the posaconazole-treated patients remained PCR-negative in the same period of follow-up (Molina et al., 2014). These results did not only empty the Chagas' disease drug discovery pipeline but also reactivated speculations around the existence of drug-tolerant dormant stages (Chatelain, 2015). Primarily, those results questioned the predictability of the preclinical testing, especially of the *in vitro* assays, where the azoles had been highly active (Chatelain, 2015). *In vitro* assays are an artificial situation anyway, as *T. cruzi* parasite replication and reinvasion in a mammalian cell culture seem to be limited only by the availability of host cells. In contrast, we do not really know the parasite behavior *in vivo*, especially in the chronic phase of infection. We do not know which host cells are mainly infected during the chronic phase and at which rate the parasites replicate in the chronic phase. Non-replicating parasites have been reported even in acutely infected mice, demonstrated by the retention of CellTrace Violet and absence of in situ labeling with nucleotide analog 5-ethynyl-2'-deoxyuridine (EdU) (Sanchez-Valdez et al., 2018). In chronically infected mice, a small number of parasites were found to not incorporate EdU over 72 hours. However, it would be rather complicated to prove the existence of long-term dormant parasites in chronically infected mice. Additionally, the question remains, how well those results can be extrapolated to other mammalian species such as humans.

Apart from the questionable comparability of the *in vitro* tests to the *in vivo* situation, there are many further questions around the read-outs of *in vitro* assays. The most prominent *in vitro* assays for Chagas' disease are the LacZ-based assays (Buckner, Verlinde, La Flamme, & Van Voorhis, 1996), assays involving manual counting (Cal, Ioset, Fugi, Maser, & Kaiser, 2016), and high-content assays (Alonso-Padilla et al., 2015; Alonso-Padilla & Rodriguez, 2014; De Rycker et al., 2016; Engel et al., 2010; Moraes et al., 2014; Neitz et al., 2015; Nohara, Lema, Bader, Aguilera, & Almeida, 2010; Yazdanparast et al., 2014). All of these are endpoint assays with the need to fix the cells before read-out. Most of these assays are terminated 72 or 96 hours post infection (hpi). Therefore, the results from those assays can be as promising for compounds inhibiting replication as for cidal compounds. Although

slowly new assay designs are being developed, currently, many *in vitro* assays are biased towards replication inhibition.

Methodology to study *Trypanosoma cruzi* amastigote replication

T. cruzi amastigote replication is an important aspect of Chagas' disease biology. It is furthermore influential for the current *in vitro* assay results. Therefore, understanding amastigote replication is crucial for Chagas' disease control. For these reasons, I reviewed the literature concerning amastigote replication. This review comprises both the methodology applied for quantification of amastigote replication and the factors found to influence amastigote replication.

Pubmed (NCBI) and Web-of-science (Analytics) were searched using the search terms "Trypanosoma AND cruzi AND amastigote AND (replication OR multiplication OR division)". This yielded 111 publications. From those 111 publications, 74 publications were excluded for lack of relevance based on the abstract. Another 2 publications were excluded, as they were not publically available. After reading, 6 publications revealed to lack relevance for amastigote replication and were therefore excluded as well. Another 7 publications were added upon recommendation or accidental encounter. In total, 36 publications were studied for the purpose of this review. Of the studied publications, 7, 27, 3, and 1 publications reported experiments on axenic amastigotes, intracellular amastigotes, amastigotes in mice, and parasites in human organs, respectively.

The different methodology for quantifying amastigote replication was studied and summarized from the Methods and Results sections. Furthermore, the identified factors influencing amastigote replication were identified.

Limited technology to quantify *Trypanosma cruzi* amastigote replication

Counting parasites

Quantifying effects on replication implies counting parasites. In the majority of studies, the number of intracellular parasites were counted using either light microscopy or fluorescence microscopy (Table 1). In three cases, the change in the number of parasites relative to host cells was quantified as the ratio of β-galactosidase-induced luminescence from *LacZ*-expressing parasites to protease-induced fluorescence as a marker of cell viability (Caradonna, Engel, Jacobi, Lee, & Burleigh, 2013; Dumoulin & Burleigh, 2018; Shah-Simpson, Lentini, Dumoulin, & Burleigh, 2017). One of those studies was a screen on host cell genes influencing amastigote replication and therefore needed a quick and easy read-out (Caradonna et al., 2013). The other two took this quick read-out as the basis for further studies (Dumoulin & Burleigh, 2018; Shah-Simpson et al., 2017).

In most of the studies, the cells were fixed and stained. When light microscopy was used, the samples were stained with Giemsa. For fluorescence microscopy, the samples were often stained with nucleic acids stain (DAPI or propidium iodide), sometimes combined with anti-*T. cruzi* antibodies. In one study, eGFP-expressing parasites in phalloidine-stained host cells were used. Three categories of studies have used live sampling techniques: studies on axenically grown amastigotes (Alexander, Villalta, & Lima, 2003; Engel & Dvorak, 1988; Herrera et al., 2016; Lima & Villalta, 1990; Takagi, Akutsu, Doi, & Furukawa, 2019; Villalta & Kierszenbaum, 1982, 1984), mouse studies (Melo & Machado, 2001; Sanchez-Valdez et al., 2018; Silva-Dos-Santos et al., 2017), and one study group (Dvorak & Hyde, 1973; Dvorak & Poore, 1974), which filmed parasite invasion, replication and differentiation using phase-contrast light microscopy.

parasite form	**quantified as**	**technology**	**publications**
amastigotes	densities	LM	(Alexander et al., 2003; Engel & Dvorak, 1988; Herrera et al., 2016; Lima & Villalta, 1990; Takagi et al., 2019; Villalta & Kierszenbaum, 1982, 1984)
	per cell	LM	(Claser et al., 2008; Ritagliati et al., 2016)
	per 100 cells	LM	(Loo & Lalonde, 1984; Schettino, Majumder, & Kierszenbaum, 1995; Yakubu, Basso, & Kierszenbaum, 1992)
		FM	(Stempin, Tanos, Coso, & Cerban, 2004)
	per infected cell	LM	(Cruz-Bustos, Potapenko, Storey, & Docampo, 2018; Nakajima-Shimada, Hirota, & Aoki, 1996)
		FM	(Balcazar et al., 2017; Dumoulin & Burleigh, 2018)
not specified	per cell	LM	(Hyde & Dvorak, 1973)
		FM	(Caradonna et al., 2013; Doyle et al., 2011)
		Lum/Fluo	(Caradonna et al., 2013; Dumoulin & Burleigh, 2018; Shah-Simpson et al., 2017)
	100 cells	LM	(Gonzalez et al., 1996; Schettino et al., 1995; Teixeira, Cruz, Mortara, & Da Silva, 2015; Yakubu et al., 1992; Yakubu, Majumder, & Kierszenbaum, 1993)
		FM	(Andreoli, Taniwaki, & Mortara, 2006)/
	200 cells	LM	(Alexander et al., 2003)
	per infected	LM	(Osuna, Jimenez-Ortiz, Mascaro, & Alonso, 1983)/
	100 infected cells	LM	(Teixeira et al., 2015)
	per 100 vacuoles	FM	(Andreoli et al., 2006)
	per body region (in vivo & ex vivo)	BL	(Silva-Dos-Santos et al., 2017)
	per organ	qPCR	(Silva-Dos-Santos et al., 2017)
	per ml blood	LM	(Silva-Dos-Santos et al., 2017)
amastigote nests		LM	(Melo & Machado, 2001)
to be determined		LM	(Behbehani, 1973)

Table 1 **Quantification of parasite numbers in reviewed studies.** LM light microscopy, FM fluorescence microscopy, Lum/Fluo bioluminescence in relation to fluorescence, BL bioluminescence, qPCR quantitative PCR

Attributing parasite counts to replication

Parasite numbers at any one timepoint after infection are influenced by a variety of factors. Among others, those include invasion and retention capacity of the parasites (Andrade & Andrews, 2005), amastigogenesis efficiency (Schettino et al., 1995; Yakubu et al., 1992), parasite-clearing capacity (i.e. mostly xenophagy, (Matteucci, Pereira, Weinlich, & Bortoluci, 2019)), replication rate, a potential dormancy status (Sanchez-Valdez et al., 2018), parasite death, and trypomastigogenesis. A minor number of the reviewed studies took the percentage of infected host cells at 48 or 72 hpi as a proxy for invasion capacity (Balcazar et al., 2017; Ritagliati et al., 2016). This is misleading, as the percentage of infected host cells has been shown to drop in the course of the first 48 h of infection (Behbehani, 1973), most likely by host cell defense mechanisms as xenophagy. In order to demonstrate effects on replication rate, parasite numbers should be quantified at least at two timepoints after infection to exclude effects on invasion capacity and amastigogenesis. This was done in the majority of the reviewed studies. Most often, parasites were quantified at 24, 48, 72, and 96 hpi and combinations of those timepoints. Some studies included timepoints in between, especially during the first 24 hpi. The animal studies usually took samples several days apart.

Theoretically, a reduced increase in parasite numbers between two timepoints can be due to parasite death, induction of a non-replicative stage or mere reduction of the replication rate. However, especially in the absence of further knowledge, most of the difference in parasite numbers between two timepoints can confidently be assumed to be due to parasite replication.

Looking at other effects in parasite counts

Some studies also looked specifically at effects other than replication rate, e.g. invasion (Behbehani, 1973; Claser et al., 2008; Dvorak & Hyde, 1973; Dvorak & Poore, 1974; Hyde & Dvorak, 1973; Kipnis, Calich, & da Silva, 1979; Ritagliati et al., 2016; Yakubu et al., 1993), amastigogenesis (Schettino et al., 1995; Yakubu et al., 1992), morphological parameters (Andreoli et al., 2006; Behbehani, 1973; Doyle et al., 2011; Dvorak & Hyde, 1973; Gonzalez et al., 1996; Loo & Lalonde, 1984; Melo & Machado, 2001; Villalta & Kierszenbaum, 1982), cell cycle progression (Dumoulin & Burleigh, 2018), number of divisions (Dumoulin & Burleigh, 2018; Shah-Simpson et al., 2017), replicating parasites (Mortara et al., 1999; Sanchez-Valdez et al., 2018), and non-replicating parasites (Sanchez-Valdez et al., 2018).

Factors influencing *Trypanosoma cruzi* amastigote replication

Three major perspectives in the context of amastigote replication have been studied: the parasite machinery, nutrient availability, and host cell contributions.

Parasite machinery influences amastigote replication

Some parts of the parasite machinery have been discovered to influence amastigote replication so far, namely topoisomerase II, glycosylposphatidylinositol (GPI) anchoring, the proteasome, the protease cruzain, glycosomal bromodomain factor, nutrient transporters, polyamine synthesis, and signaling molecules.

Topoisomerase II is important in kinetoplastid DNA (kDNA) replication, which is relevant for parasite replication and differentiation. Pharmacological inhibition of topoisomerase II reduced amastigote replication (Gonzales-Perdomo, de Castro, Meirelles, & Goldenberg, 1990).

The broad majority of trypanosome surface proteins are anchored via glycosylphosphatidylinositol (Ferguson, Duszenko, Lamont, Overath, & Cross, 1986; Giorgi & de Lederkremer, 2011). Heterologous expression of *Trypanosoma brucei* GPI-phospholipase in *T. cruzi* led to drastic reduction of GPI anchored surface proteins (Garg, Tarleton, & Mensa-Wilmot, 1997). Among other effects, this impaired amastigote nuclear division and cytokinesis, while not affecting kinetoplast division. The authors concluded that the GPI deficiency negatively impacts the parasite signaling cascades, or that nuclear division could be directly regulated by GPI-anchored proteins.

Pharmacological inhibition of the proteasome was shown to hamper intracellular parasite development (Gonzalez et al., 1996). The results do not allow to unequivocally conclude that amastigote replication was reduced by proteasome inhibition. Reduction of intracellular amastigogenesis will also lead to reduced amastigote numbers and is a very likely scenario, given that axenic amastigogenesis and trypomastigogenesis were also shown to be reduced upon proteasome inhibition (Gonzalez et al., 1996). The contribution of the proteasome to cellular remodeling and differentiation is conserved across eukaryotic species. Therefore, the role of the proteasome in amastigote replication is not clearly proven.

Cruzain (cruzipain, GP57/51) is a major protease excreted by *T. cruzi* (Cazzulo & Frasch, 1992). Metacyclogenesis and invasion are among the described functions of the protease so far. Additionally, cruzain protected amastigote replication by interfering with host cell signaling cascades (Doyle et al., 2011; Stempin et al., 2004). This parasite protease will therefore be discussed further under the host cell factors influencing amastigote replication.

The bromodomain is involved in the recognition of acetylated proteins (X. J. Yang, 2004). Overexpression of a glycosomal bromodomain factor (TcBDF1) enhanced invasion and amastigote replication (Ritagliati et al., 2016). The authors concluded that TcBDF1 might influence acetylated

enzymes in the glycosome and shift the metabolism more towards gluconeogenesis in amastigotes and hence influence replication. This might explain why inhibition of glycosomal protein import was toxic to amastigotes (Dawidowski et al., 2017) even though the amastigotes do not express glucose transporters (Silber et al., 2009).

Several nutrient uptake systems have been described to influence amastigote replication. Among them are the transferrin receptor (Loo & Lalonde, 1984), the riboflavin transporter (Balcazar et al., 2017), and an ammonium transporter (Cruz-Bustos et al., 2018). Their role highlights the importance of parasite metabolism on amastigote replication and will be discussed further with the influence of nutrient availability on amastigote replication. Pharmacological inhibition of arginine decarboxylase (Yakubu et al., 1992) and adenosyl-methionine decarboxylase (Yakubu et al., 1993) of the polyamine synthesis pathway reduced amastigotes replication.

The role of parasite signaling in amastigote replication is scarcely discussed so far. However, there are hints that amastigote replication, as one possible cell fate decision, is regulated by parasite signaling. A sensory role was ascribed to transporters such as the ammonium transporter (Cruz-Bustos et al., 2018). Another hint is the importance of host TGFα, which will be discussed with the host cell factors, for amastigote replication (Alexander et al., 2003).

Nutrient availability influences amastigote replication

A broad variety of nutrients influences amastigote replication, which was demonstrated in different contexts. Among those nutrients are glucose, glutamine, ion carriers, lipids, nucleotide precursors, and precursors of cofactors.

Glucose-depletion of the growth medium reduces the replication rate of intracellular amastigotes (Dumoulin & Burleigh, 2018; Shah-Simpson et al., 2017). Host cells increase their glucose uptake upon *T. cruzi* infection (Shah-Simpson et al., 2017). This exogenously supplied glucose is partially taken up from the host cell by the intracellular amastigotes and used as a fuel for amastigote glycolysis, mitochondrial respiration, and in anabolic pathways (Shah-Simpson et al., 2017). However, this contrasts with the finding that the amastigotes do not express the *T. cruzi* hexose transporter TcHT (Silber et al., 2009). Glutamine depletion of the growth medium also reduces the replication rate of intracellular amastigotes (Dumoulin & Burleigh, 2018).

Several aspects of iron uptake were shown to have an effect on amastigote replication. The addition of iron chelators to the medium reduced the replication of intracellular amastigotes (Loo & Lalonde, 1984). Cell-free amastigote growth was shown to require ferrotransferrin, which is taken up by a transferrin receptor on the amastigote surface (Lima & Villalta, 1990). A heme transporter (TcHTE) was described to be functional in the replicative forms, epimastigotes and amastigotes, but not in trypomastigotes (Merli et al., 2016). *T. cruzi* has several heme-containing enzymes. Yet, it lacks heme-

biosynthesis enzymes. Therefore, heme has to be supplemented for epimastigote cultivation (Hutner & Bacchi, 1979; Lwoff, 1951). However, TcHTE overexpression reduced epimastigote replication capacity in medium with 20 µM hemin, which is the standard concentration (Merli et al., 2016). The effect of overexpression on amastigote replication was not investigated.

Host enzymes involved in fatty acid oxidation were found to be beneficial for amastigote growth in a screen on the effect of knock-down of host cell genes on amastigote replication (Caradonna et al., 2013). Later, the same group showed that intracellular amastigotes scavenge long chain fatty acids from the host cell (Gazos-Lopes, Martin, Dumoulin, & Burleigh, 2017 369 369). Uptake and oxidation of fatty acids is upregulated in amastigotes on the transcriptomic (Li et al., 2016) and on the proteomic (Atwood et al., 2005) level. Pyrimidine synthesis and purine nucleoside availability were also shown to be supportive of amastigote replication in the host gene knock-down screen (Caradonna et al., 2013).

Riboflavin is the precursor of flavin mononucleotide (FMN) and flavin adenine dinucleotide, which are cofactors of many enzymes. During the characterization of the *T. cruzi* riboflavin transporter, it was noted that the riboflavin analogon roseoflavin inhibits amastigote replication (Balcazar et al., 2017).

Concluding, a variety of nutrients, including glucose, glutamine, iron carriers, fatty acids, and at least one precursor of cofactors, is involved in fueling amastigote replication. The importance was shown in different ways, via medium supplementation, via the host cell's capacity to provide, and via the respective transporter. For many of the nutrients, it remains to be seen (e.g. by concentration-dependence) whether they influence amastigote replication by their availability as building blocks or as signaling molecules informing the parasite's cell fate decision in response to environmental cues.

Host cell elements influence amastigote replication

Probably the first demonstration of the importance of the host cell was, when Osuna et al. infected HeLa cells which had been enucleated with cytochalasin B (Osuna et al., 1983). In contrast to the 30% infected control cells, only 6.5% of the enucleated cells were infected. Not only the invasion capacity was reduced, the intracellular parasites did not proliferate in the enucleated cells. These findings hinted at a significant contribution of host cells towards the parasite's replication capacity. However, the contribution of the host cell has been questioned by numerous reports of axenic replication of amastigotes (Alexander et al., 2003; Lima & Villalta, 1990; Takagi et al., 2019; Villalta & Kierszenbaum, 1982). Axenic amastigote proliferation is not reproducible in everybody's hands. It would be very interesting to know, which exact conditions make axenic amastigotes replicate in one lab and not in another. Amastigote replication was shown to happen in enucleated L929 cells by (Coimbra et al., 2007).

Apart from the nucleus, structural elements of the host cell, its metabolism, and signaling cascades were demonstrated to influence amastigote replication. Cytokeratin 18 is the first structural element shown to influence amastigote replication (Claser et al., 2008). RNAi on cytokeratin 18 led to reduced parasite numbers 48 hpi in HeLa cells, even though neither the frequency of infected cells nor the number of intracellular parasites 2 hpi was changed by silencing cytokeratin 18 (Claser et al., 2008). So far most of the structural elements of the host cells had been demonstrated to influence invasion rather than replication (Andrade & Andrews, 2005).

The metabolism of the parasite is intimately connected to the metabolism of the host cell. As was commented above, a variety of nutrients influence amastigote replication. Parasite and host cell can be competing for the same nutrients. It is therefore not surprising, that infection increases glucose uptake of the host cell (Shah-Simpson et al., 2017). The parasite might modulate the host cell metabolism to serve its own needs, or the host cell might respond to the increased energy need as it is unwillingly feeding the parasite. In the unbiased RNAi screen for host cell factors influencing amastigote replication, lipid metabolism played a prominent role (Caradonna et al., 2013). Disturbances of the host cell's nucleotide metabolism influenced amastigote replication rate as well. Surprisingly, although *T. cruzi* has the intrinsic capacity to synthesize pyrimidines, amastigote replication was reduced when the host cell pyrimidine biosynthesis was disturbed and restored by uridine supplementation. This result allows for the speculation that nutrients are more than mere building blocks for the parasite, but carry information about the environmental situation.

In this same RNAi screen, several host signaling pathways were demonstrated to influence the replication rate of amastigotes (Caradonna et al., 2013). Protein kinase B (Akt)-signalling was shown to promote amastigote replication both in a mammalian target of rapamycin complex 1 (mTORC1)-dependent and a mTORC1-independent manner (Caradonna et al., 2013). Additionally, silencing of subunits of the mTORC1-antagonistic AMP kinase (AMPK) enhanced amastigote replication (Caradonna et al., 2013). The parasite-derived protease cruzain was shown to increase amastigote replication by activating host cell arginase (Stempin et al., 2004). This activation of arginase involves a tyrosine kinase, protein kinase A, and p38 mitogen-activated protein kinase (Stempin et al., 2004). Host arginase activation might provide the parasite with ornithine for polyamine synthesis. However, it also might reduce the generation of nitric oxide (NO), which is a part of the antiparasitic immune response. Cruzain was also shown to reduce host cell IL-12 expression by inhibiting NFkB phosphorylation (Doyle et al., 2011). This way, cruzain would prevent the host immune responses that suppress parasite replication. Additionally, amastigotes reacted on host-derived TGFα with increased replication rate (Alexander et al., 2003). This last result highlights a frequently underestimated point: *T. cruzi* and mammals have many conserved signaling pathways, therefore, activators and inhibitors of signaling pathways might influence both host and parasite signaling, which in turn affect each other. To

disentangle these responses will be very difficult, but will nevertheless be necessary to better understand the replication of the disease relevant forms in the mammalian host.

The special case of axenic amastigotes

Axenic amastigote replication is a special case of *T. cruzi* research. While it has been described very early (Villalta & Kierszenbaum, 1982), not all laboratories are able to cultivate amastigotes axenically. In the context of this review, 7 publications studying the factors influencing axenic amastigote replication were examined. In the majority of these studies, amastigotes were isolated from infected host cells and then grown axenically at 37°C in different media: supplemented ML-15HA (Lima & Villalta, 1990; Villalta & Kierszenbaum, 1982, 1984), supplemented DMEM (Villalta & Kierszenbaum, 1982, 1984), supplemented MEM (Alexander et al., 2003), and supplemented LIT (Takagi et al., 2019). CO_2 (Villalta & Kierszenbaum, 1982) and chelated iron (Lima & Villalta, 1990) were found to be essential for axenic amastigote replication. Concanavalin A (Villalta & Kierszenbaum, 1984) and TGFα (Alexander et al., 2003) were found to enhance replication of axenic amastigotes. One group induced axenic amastigotes from metacyclic trypomastigotes and culture-derived trypomastigotes (Engel & Dvorak, 1988). They cultivated the axenic amastigotes at 26°C in supplemented LIT. However, they reported the need to change medium every 2 days to maintain replication of amastigote. Recently, the induction of axenic amastigogenesis according to an older protocol (Tomlinson et al., 1995) was reported in order to transfect amastigotes (Takagi et al., 2019). As axenic, replicative amastigotes are a valuable tool for drug discovery (Herrera et al., 2016; Takagi et al., 2019), for genetic manipulation, and for the study of the disease-relevant forms of *T. cruzi* (Takagi et al., 2019), I hope the protocol for axenic amastigogenesis and axenic amastigote replicataion will be established in many laboratories across the globe.

Contributions of this thesis

The aim of this PhD thesis is to improve *in vitro* drug screening for Chagas' disease. With this aim, the second chapter of this thesis describes the attempts to establish a transgenic strain for *in vitro* drug screening including the establishment of molecular techniques in our laboratory. In the third chapter, the genome of the wildtype strain is described. In the fourth chapter, we report the use of a eGFP-expressing parasite line for monitoring of replication and drug action.

A molecular toolkit and a transgenic strain for drug discovery

Introduction

Amastigotes, the intracellular form of *Trypanosoma cruzi*, are the parasite stage contributing most to the pathogenesis of Chagas' disease. Therefore, drug discovery for Chagas' disease should focus on the cidality in amastigotes of novel agents. However, as amastigotes are intracellular, they are also the parasite form that is most difficult to quantify.

The classical way of quantification - which is still widely used, especially in academic research settings - is staining and manual counting of the parasites, infected host cells, and total number of host cells. This is extremely laborious and limits the throughput. A more convenient alternative is provided by the transgenic β-galactosidase parasite line engineered by (Buckner et al., 1996), but the simplified colorimetric assay formats do not permit to quantify infection rates. The introduction of high-content microscopy with automated quantification dramatically increased throughput. However, the detection of intracellular parasites based on nuclear staining alone can introduce errors that compromise sensitivity and specificity. These issues can be overcome by parasite lines that express a fluorescent reporter gene (Alonso-Padilla & Rodriguez, 2014; Canavaci et al., 2010; Kessler et al., 2013). Here we perform an in-depth characterization of the *T. cruzi* STIB980 strain aiming to establish a fluorescent derivative of STIB980 as a new tool for high-content based screening.

Results and Discussion

The strain we chose as the assay strain STIB980 belongs to DTU TcI

We have received most of the *T. cruzi* strains in our collection through collaborations. The parasite line I was working with had been received as a *T. cruzi* Y strain from the University of Granada, Spain. The Y strain belongs to discrete typing unit (DTU) TcII, which is distributed all over Southern Latin America. The DTUs are thought to correlate with distinct chronic disease phenotypes (Zingales, 2018). DTU TcII is thought to cause a broad chronic disease phenotype, including asymptomatic, cardiac and digestive symptoms (Zingales, 2018).

As several parasite lines circulate as Y strains, we wanted to make sure that we were really working with a Y strain. Therefore, I genotyped our parasite line (Messenger, Yeo, Lewis, Llewellyn, & Miles, 2015). DNA from reference strains was kindly donated by Dr. M. Lewis (London School of Hygiene and Tropical Medicine, LSHTM). Three PCR were performed: on the glucose-6-phosphate isomerase (G6PI), on the large ribosomal subunit (LSU), and on the heat-shock protein 60 (HSP60). In all three reactions and subsequent digestions of G6PI and HSP60, our parasite line more closely resembled the DTU TcI strains (Silvio, Dm28c, Figure 2 B-F) than the Y strain (DTU TcII). Sanger sequencing of the PCR products did not help to further classify our parasite line. Since it was clearly not a Y strain, we named our parasite line using our internal numbering system: STIB980, belonging to

DTU TcI. TcI is the DTU that circulates most broadly among humans and is correlated m8ostly with cardiomyopathic symptoms (Izeta-Alberdi, Ibarra-Cerdena, Moo-Llanes, & Ramsey, 2016; Zingales, 2018). Therefore, a TcI strain is useful as an assay strain.

Before establishing a transgenic parasite line derived from STIB980, we established a clonal parasite population by employing the gilded paperclip method (Figure 2 A, Methods section).

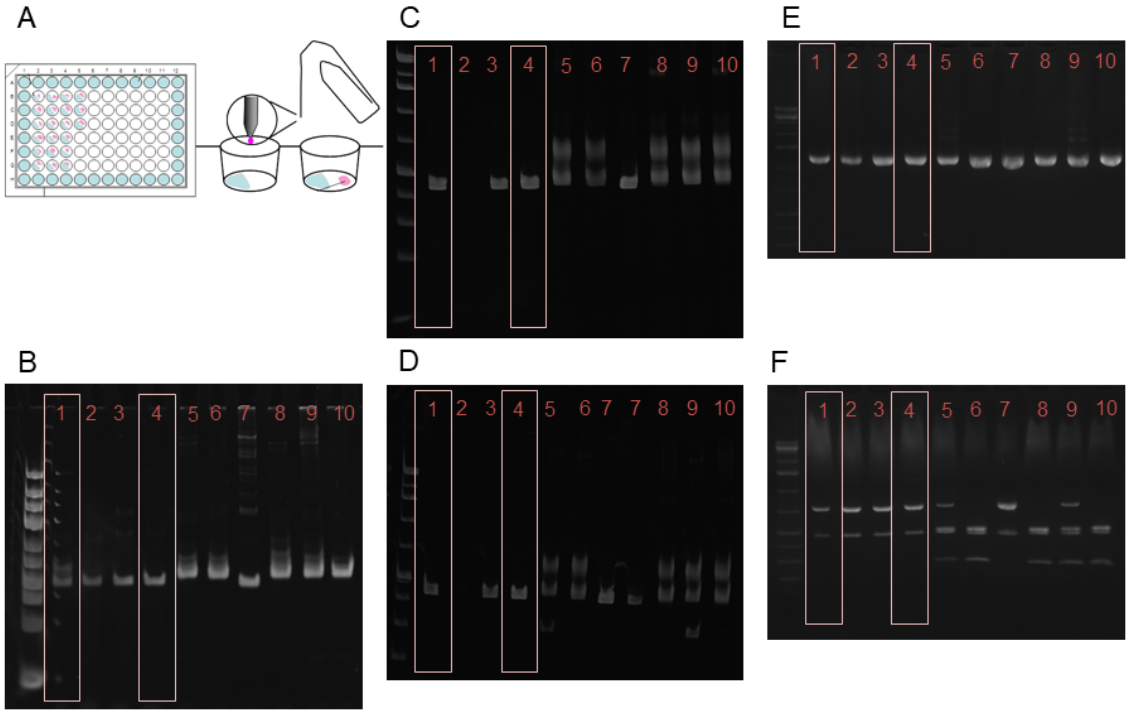

Figure 2 Establishing a clonal parasite line with the gilded paper-clip method (A) and genotyping results (B-F): STIB980 clone 1 (4) is very similar to Dm28c (1, TcI), 2 Sylvio (TcI), 3 STIB980 (?), 5 Tulahuen (TcVI), 6 Esmeraldo (TcII), 7 Sylvio X10/4 (TcI), 8 Y strain (Madrid, TcII), 9 CL Brener (TcVI), 10 Y strain (parental, TcII), PCR products of large ribosomal subunit (B), PCR product of HSP60 before (C) and after (D) digest with *Eco*RV, PCR product of G6PI before (E) and after (F) digest with *Hha*I

Profiling the sensitivity to antibiotics used for selection

In order to determine the best selection marker for use in genetic manipulation, we tested the sensitivity of *T. cruzi* STIB980 epimastigotes against commonly used antibiotics: blasticidin, G418, hygromycin, phleomycin, and puromycin. In addition, we tested the benchmark drugs benznidazole and nifurtimox. As DMSO is generally used as a solvent for test compounds, we also assessed the epimastigotes' sensitivity against it. The sensitivity was tested for 72 and 168 hours of exposure. For the 168 h of exposure, we used two different starting densities (2×10^4 and 10^5 epimastigotes/ml) to differentiate the effects on replication from cidality. The resulting EC50 values were similar across all tested conditions (Table 2). Remarkably, STIB980 epimastigotes had relatively high EC50 values for the commonly used antibiotics G418 and hygromycin, approx. 50 µg/ml and 10 µg/ml, respectively. This is reflected in the high concentrations used for selection with those, e.g. 100 - 500 µg/ml G418, which is in stark contrast to the 1 - 2.5 µg/m and 15 µg/ml used in *Trypanosoma brucei* genetic manipulation

of bloodstream forms (Burkard, Fragoso, & Roditi, 2007) and procyclic forms (Tu & Wang, 2004), respectively.

Besides the sensitivity of untransfected (i.e. wildtype) trypanosomes, other aspects determine the optimal concentration for use in selection. One of these aspects is the intensity of resistance conferred by the resistance gene, which might depend on the mechanism of resistance. To our knowledge, this has not been tested systematically. A critical aspect is the expression level of the resistance gene. In episomal transfections, selection with higher concentrations of antibiotic can lead to increased copy number of the plasmid. For integrated constructs, transfectants with higher expression levels can be selected with higher antibiotic concentrations. This is especially relevant for constructs integrating into the ribosomal locus. In kinetoplastids, RNA polymerase I (PolI) can transcribe protein-coding genes in addition to the *rRNA* genes. PolI transcription starts at the ribosomal promoter. Different ribosomal loci appear to have different expression efficacy (Alsford, Kawahara, Glover, & Horn, 2005). Selection at high concentration of antibiotic therefore favors transfectants that have the construct integrated into highly expressed loci. If endogenous genes are targeted, the expression level of the resistance gene can be substantially lower than for genes under the control of the ribosomal promoter. Apart from the *rRNA* genes, *T. cruzi* genes are expressed as polycistrons by RNA polymerase II (RNAPolII). So far, no promoter has been identified for PolII in kinteoplastids. The expression levels of genes transcribed by RNAPolII are generally lower than those of genes transcribed by RNAPolI.

Overall, we recommend blasticidin or puromycin to select STIB980 transgenes, rather than G418, hygromycin, or phleomycin.

	drug	Benznidazole	Nifurtimox	Blasticidin	Puromycin	Hygromycin	G418	Phleomycin	DMSO (%)
72 h	EC50	1.900	0.870	1.610	1.250	41.1	45.6	89.3	3.84
		(0.670; 3.140)	(0.580; 1.160)	(1.190; 2.020)	(1.080; 1.420)	(29.9; 52.2)	(37.7; 53.5)	(70.0; 109.0)	(3.24; 4.45)
168 h	EC50	1.160	0.411	0.369	1.240	22.0	49.7	70.6	3.16
high dens		(0.902; 1.410)	(0.366; 0.455)	(0.196; 0.542)	(1.060; 1.410)	(13.3; 30.7)	(41.9; 57.4)	(60.4; 80.9)	(-1.09; 7.40)
168 h	EC50	0.664	0.241	0.315	0.558	36.9	31.0	27.4	1.17
low dens		(0.534; 0.794)	(0.201; 0.281)	(0.292; 0.339)	(0.477; 0.640)	(28.1; 45.7)	(24.5; 37.4)	(22.9; 31.9)	(0.93; 1.41)

Table 2. Sensitivity of *T. cruzi* STIB890 epimastigotes (EC50 values in µg/ml) to reference drugs and antibiotics used for selection. 95% CI are given in brackets. Parasite inoculum was for 72 h 5×10^5 epimastigotes/ml, for 168 h 2×10^4 and 10^5 epimastigotes/ml

Testing transfection protocols with the plasmid pTcRG

We use the Lonza nucleofector as the electroporation device for transfections. It provides excellent results, but is a black box: Lonza does not disclose the characteristics of the electric discharge nor the composition of the buffers. The nucleofector offers several programs, which are sequences of electrical stimuli of different quantity, intensity and duration. The differences between the programs are not publically available, but it is very likely that programs with the same starting letter have similar sequences of electroshocks. We investigated which program is best suited for *T. cruzi* STIB890

epimastigotes. Tests on nucleofector programs had already been published for *T. brucei* (Burkard et al., 2007) and *T. cruzi* (Pacheco-Lugo, Diaz-Olmos, Saenz-Garcia, Probst, & DaRocha, 2017).

We first tested the efficiency of the programs to deliver a plasmid into the parasite's nucleus, and afterwards the efficiency of the programs to enable stable integration of a construct into the parasite's genome.

In order to test the efficiency in delivering a plasmid into the nucleus of epimastigote parasites, we transfected epimastigotes with a circular pTcRG plasmid (Figure 6 A). This plasmid contained the *green fluorescent protein* (*GFP*) gene under the control of the 3'UTR of the *glyceraldehyde 3-phosphate dehydrogenase* (*GAPDH)* gene, which confers constitutive expression. We transfected 4×10^7 epimastigotes in the log growth phase with 10 µg plasmid using 10 different nucleofector programs. Shortly after transfection, we counted the surviving parasites. Then, we incubated them for 24 hours in 10 ml LIT at 27°C before we quantified the proportion of eGFP-expressing parasites by flow cytometry using the method of Burkard et al. (Burkard et al., 2007). The overall efficiency was calculated as the product of survival and eGFP positivity.

In general, there were only small differences in the overall efficiency in the same order of magnitude as variability within a given program observed in pretests (Table 3).

	% Survival	% eGFP expression	log10 efficiency
X-001	55.0	6.83	-1.43
X-006	57.5	2.67	-1.81
U-033	42.5	8.15	-1.46
T-020	91.3	1.11	-1.99
X-024	65.0	3.56	-1.64
X-014	58.8	4.16	-1.61
Z-014	60.0	3.18	-1.72
X-013	57.5	4.23	-1.61
Z-001	32.5	7.80	-1.60

Table 3. Efficiency of transient transfection of different Nucleofector programs

The programs X-, Z-, and the U-033 programs had the best overall efficiencies. The most striking difference was in the survival rates, which was low in U-033 and was compensated by a higher eGFP expression rate. In contrast, most X- and Z-programs had a higher survival rate combined with a more moderate eGFP expression rate. Pacheco-Lugo et al. have reported higher proportions of eGFP expression and higher survival rates (Pacheco-Lugo et al., 2017). One reason especially for the higher expression ratios might be that they had used 10 µg of plasmid on only 2×10^7 epimastigotes, a higher DNA to parasite ratio. The higher survival rate can be explained by their different quantification approach. They counted the proportion of parasites that excluded propidium iodide (as a marker of dead cells) 24 hours after transfection. Survival is therefore seen during the 24 hours period after transfection, and not defined as the number of recovered, viable parasites directly after transfection.

To test the performance regarding integration success of the transfected plasmid, we selected the programs U-033, X-001, and X-013. For this experiment, we linearized the plasmid by digestion with *Not*I before electroporation. The linearized plasmid is supposed to be integrated into the β-tubulin gene via homologous recombination. We quantified the transfection efficiency via the outgrowth ratio. This was determined by seeding parasites 24 hours after transfection into 96-well plates in different densities under selection pressure of 100 µg/ml G418. The plates were incubated at 27°C for until a stable culture had grown. The outgrowth ratio was defined as the number of wells with parasites divided by the total number of inoculated wells and the number of parasites inoculated per well. Furthermore, we tested the outgrown parasites for eGFP positivity with flow cytometry, and for presence of the resistance gene with PCR. Not all outgrown parasites were positive in flow cytometry and/or PCR. But, in general, the different read-outs led to similar efficiencies (Table 4).

	Survival (%)	Outgrowth	Flow cytometry	PCR
X-001	28.1	-5.04	-5.93	-5.76
U-033	13.3	-5.71	-5.81	-5.95
X-013	35.0	-5.36	-5.54	-5.66

Table 4. Efficiency of stable transfection. Outgrowth, flow cytometry, and PCR are given as the log10 of the efficiency

In conclusion, the differences between the tested X-, Z-, and U-programs in overall efficiency are comparably small. Program U-033 is generally the most efficient for transient transfection as well as stable transfection, even though it has a relatively small survival rate of the electroporated trypanosomes. Depending on the purpose of the transfection, this difference might justify the decision between U-033 and any of the well-performing X- or Z- programs.

Flow cytometry and epifluorescence to test transfection success of the plasmid pTRIX2-eGFP

The levels of cytosolic eGFP obtained by expression of pTcRG were too low for detection in the high-content fluorescence microscope. With 300 ms of exposure time, most of the parasite signal was below 3x the background level, which is the minimum recommended signal-to-noise ratio for high-content quantification. We therefore decided to try eGFP expression from the ribosomal locus using the plasmid pTRIX2-eGFP for transfection of 10^8 epimastigotes at the end of the exponential growth phase (Fesser et al., 2020).

The transfection success was assessed with respect to eGFP expression levels by flow cytometry, and with respect to subcellular and stage-specific expression by epifluorescence. Clone 12 (G12) was selected according to its eGFP expression level, infectivity, and growth profile. In flow cytometry, the geometric mean of the transfectants was approx. 650 RLU, which is 60-fold above wildtype autofluorescence (Figure 8 B). Approx. 99% of the transfectants were detected as eGFP-positive. Transfectant epimastigotes expressed eGFP cytosolically and in the flagellum (Figure 3, Figure 8 C). While the replicating stages, epimastigotes and amastigotes, expressed eGFP at very high levels,

the infective (metacyclic) trypomastigotes were barely brighter than autofluorescent wildtype parasites (Figure 8 C - F).

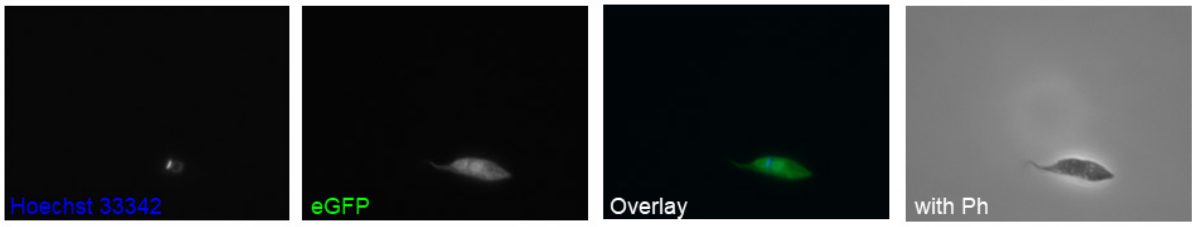

Figure 3 Epifluorescent images of transfectants in epimastigotes

Flow cytometry and high-content microscopy to test pTRIX2-eGFP transgene stability

In a reporter strain for use in *in vitro* assays, the genomic stability of the transgene reporter needs to be tested in the absence of antibiotic, as transgene instability can occur due to the genomic plasticity of *T. cruzi* and selection possibilities are limited in co-culture with mammalian cells. In epimastigotes, transgene stability can easily be measured by flow cytometry; in amastigotes, fluorescence microscopy is a better tool. Another option (not used in the frame of this work) to measure genetic stability is quantitative PCR (qPCR).

The genetic stability of eGFP in the ribosomal locus of our STIB980 parasite line was quantified in epimastigotes as the percentage of eGFP-expressing parasites cultivated over 5 months without G418 compared to epimastigotes cultivated at 500 µg/ml GFP (Fesser et al., 2020)). The percentage of eGFP-expressing epimastigotes was measured with flow cytometry. The eGFP gene was found to be stably maintained and expressed in epimastigotes (Supp. Fig 1 C, Supp. Tab. 1).

Testing the stability of eGFP expression of amastigotes was more difficult, because I first had to establish a way to quantify the ratio of eGFP-expressing parasites. Flow cytometry could not be used, because we lacked a proper protocol to isolate amastigotes from host cells. There are several published protocols for amastigote isolation (Dumoulin & Burleigh, 2018), but we were not able to establish one in our lab. Therefore, I used the automated analysis of high-content microscopy images to quantify eGFP-expressing parasites in the mammalian stages (Fesser et al., 2020)).

Expanded peritoneal mouse macrophages (ePMM) were infected with culture derived trypomastigotes from either the 2nd or the 18th passage after introduction to the trypomastigote-amastigote lytic cycle. I detected parasites by nuclear staining and then determined whether they colocalized with an area of green-fluorescence.

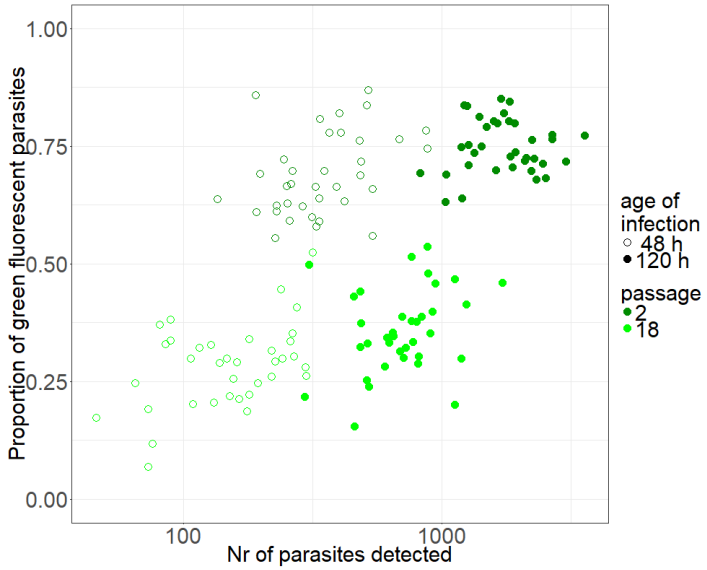

Figure 4 Proportion of amastigotes detected as eGFP-expressing, depending on the number of passages in the amastigote-trypomastigote lytic cycle and the number of parasites detected over age of expression and number of passages

The proportion of eGFP-expressing parasites correlated negatively with the number of passages, and positively with the number of detected parasites (Figure 4). Within each passage, the ratio of eGFP-expressing parasites increased only slightly with the number of detected parasites. This increase was stronger for the later passage. The parasite numbers were clearly dependent on the time since infection, but also differed between the passages. The latter might be explained by differences in infectivity or technical variability during the infection. In general, a substantial proportion of the parasites ceased to express eGFP over passaging in the amastigote-trypomastigote lytic cycle. The ratio of eGFP-expressing parasites dropped from a median of 74% in parasites of passage 2 to a median of 35% in parasites of passage 18 (Fesser et al., 2020), Supp. Fig. 1 D).

However, even the median ratio in passage 2 with 74% is relatively low. Partly, this points out how difficult it is to create a good analysis module with high sensitivity and specificity. Reduced sensitivity is problematic, because true eGFP expressors are taken out of the equation. Closely clustering parasites often detected as one host cell nucleus were one of the major sensitivity issues. This is more severe at later timepoints of infection. The number of detected host cells strongly correlated with the number of detected parasites (data not shown here). Counterintuitively, more host cells were detected longer after infection. This also points towards misclassification of clustered parasites as host cell nuclei. However, this does not really explain the observed low eGFP expression ratios, as at the later timepoints, the ratios were rather higher than lower. Closely clustered parasites are more likely amastigotes. As amastigotes are more likely to express eGFP in contrast to trypomastigotes, the misclassification of amastigotes as host nuclei further skews the ratio of eGFP-expressing parasites towards lower numbers. The misclassification of closely clustered parasites as host nuclei leads to a lower sensitivity and therefore affects the results of the image analysis.

The specificity is mostly reduced by the misclassification of artefacts as parasite nuclei, which will artificially increase the non-fluorescent parasite counts. As the parasite kinetoplasts are quite small (not much bigger than 1 pixel), background noise and other artefacts can easily be misclassified.
From our high-content results, we assume that part of the low ratios of eGFP-expressing amastigotes were mostly due to the analysis module and part to biological non-expression. However, the drop in ratio of eGFP-expressing parasites over passages seems to be real. This indicates that eGFP in our transgenic parasite line is not genetically stable in the amastigote-trypomastigote lytic cycle.

To further quantify the maintenance of the eGFP gene, qPCR with the fluorescence gene and a house-keeping gene could be done on extracted RNA and extracted genomic DNA (gDNA). While quantitative reverse-transcription PCR (qRT-PCR) gives an impression on the bulk transcription level of the fluorescence gene, qPCR on gDNA quantifies the ratio of the parasites that still contain the fluorescence gene in their genome. If 100% of the parasites contain the gene in the genome, the Ct-value should be in a similar range for the house-keeping gene and the fluorescence gene (assuming a perfect efficiency, the Ct-value of a diploid housekeeping gene would be 1 unit smaller than the Ct-value of the transgene). In case of genomic loss, the Ct value of the housekeeping gene should be substantially lower than the Ct-value of the fluorescence gene. This way, qPCR could be used to quantify genomic stability, especially for transgenes, which are not otherwise quantifiable.

Transgenes can be genetically instable due to transgene toxicity and exhaust of amino acids. The selective disadvantage of transgene expression depends on the expression level. With the pTRIX2-eGFP construct, eGFP is under the control of the ribosomal promoter and therefore very highly expressed. This is reflected in very bright parasites, amastigotes as well as epimastigotes. Additionally, we had selected for high expression levels by using high G418 concentrations. Overall, it is likely that the high expression levels favor loss of the transgene. However, this does not explain the specific loss in amastigotes in contrast to the stability in epimastigotes. One hypothesis for the reduced stability of eGFP expression in the mammalian stages is exacerbation of oxidative stress by the chromophore of eGFP. The mammalian stages are probably exposed to more oxidative stress than axenically cultivated epimastigotes. After invasion, trypomastigotes are enveloped in an acidified, lysosome-like compartment (Andrade & Andrews, 2005), where they suffer oxidative stress. After they have escaped to the cytosol, they differentiate into the proliferative amastigotes. In the cytosol, the oxidative stress might be higher than in axenic medium, yet lower than in the lysosome. The postulated higher oxidative stress for intracellular parasites could be exacerbated by the chromophore of eGFP resulting in higher stress and reduced infectivity and/or replication of eGFP-expressing parasites. This would explain the relatively quick drop in the ratio of eGFP-expressing parasites after introduction to the mammalian lytic cycle.

As the mammalian stages need to be co-cultured with mammalian cells, selection in those stages is precluded by the sensitivity of the host cells to the selection antibiotics. Usually, the host cells are more susceptible to the selection antibiotics than wildtype *T. cruzi* parasites. We cannot mitigate host cell sensitivity by expressing the resistance gene in the host cell, as most resistance genes used for selection encode for enzymes that inactivate the antibiotic by covalent modification. Therefore, resistance gene expression by the host cell would also lead to reduced exposure for the parasite. One possible option is to expose trypomastigotes for a couple of hours to the antibiotic and wash them before infection. We saw that short exposure of trypomastigotes can increase the proportion of eGFP-expressing parasites (data not shown). To our knowledge, trypomastigote exposure is the only feasible way to select transgenic parasites in the amastigote-trypomastigote lytic cycle. An alternative is to not select the amastigote and trypomastigote parasites and use them only for one experiment.

Overall, this experiment undermines the importance of the demonstration of genomic stability of a transgene and also the importance of appropriate quantification methodology.

High-content assays to test drug sensitivities of the wildtype and transgenic assay strain

For further characterization of the eGFP-expressing parasite line *T. cruzi* STIB980-G12, we tested whether there is a difference in drug sensitivity of the mammalian stages between transfectant and wildtype. For this, we used a high-content assay design. We infected ePMM with tissue-culture derived trypomastigotes. After 24 h, we washed the plates and added drugs in three-fold serial dilution. The parasites were incubated for 96 h with the respective drugs. Then, the plates were fixed and stained with Draq5 (life technologies). After keeping the plates for 24 h at 4°C, the plates were imaged on the Cy5 channel of the high-content microscope. Draq5 stains nucleic acids, resulting in a very bright nucleus and a darker cytoplasm, which is still brighter than the background signal. In contrast to Hoechst (life technologies), this enables us to directly determine the host cell borders. Therefore, intracellular parasites and infected host cells can be determined without any additional staining of the cytoplasm.

We determined the number of host cells, ratio of infected host cells, total number of intracellular amastigotes, and number of amastigotes per infected host cell. Using an interpolation method (Huber & Koella, 1993), we determined the EC50 values for the ratio of infected cells and number of parasites per infected host cell. Additionally, we determined the cytotoxicity, i.e. the reduction in number of host cells in the uninfected control. The ratio of infected cells, number of amastigotes per host cell, and number of host cells in dependence of drug concentration are depicted in Figure 5.

The EC50 values are displayed in Table 5. There was little difference between the wildtype and the transfectant parasite line. The differences between the parasite lines were in a similar range as the

differences between the technical replicates. The EC50 values calculated based on the ratio of infected cells were comparable to those calculated on the basis of number of parasites per infected cell.

Waltherione G was tested in a range of 41 to 10,000 ng/ml. In this range, we could determine only cytotoxicity. Even at the lowest concentration, the ratio of infected cells was below 50% of the ratio of infected cells in the untreated, infected control. The same was true for the number of parasites per infected cells. Nifurtimox was tested in a range of 410 – 100,000 ng/ml. The EC50 values for nifurtimox were in the range of the lowest concentration tested. Therefore, the EC50 could not always be determined. For the other drugs, EC50 values could be determined and are similar for the wildtype and the eGFP-expressing parasite line.

The cytotoxicity can be determined for most drugs in most replicates, meaning that the EC50 values of most drugs are lower than the highest tested concentration. Wells with less than 50% of host cells compared to the uninfected, untreated control were excluded from the determination of EC50 values against *T. cruzi*. Especially the ratio of infected cells can be skewed for cytotoxic agents, as infected host cells can exhibit a different sensitivity to the drug than uninfected host cells.

The selectivity index is the ratio between the EC50 of the parasites to the EC50 of the host cells. Both, when looking at the ratio of infected cells as when looking at the number of parasites per infected cell, the selectivity index is over 10 for most drugs.

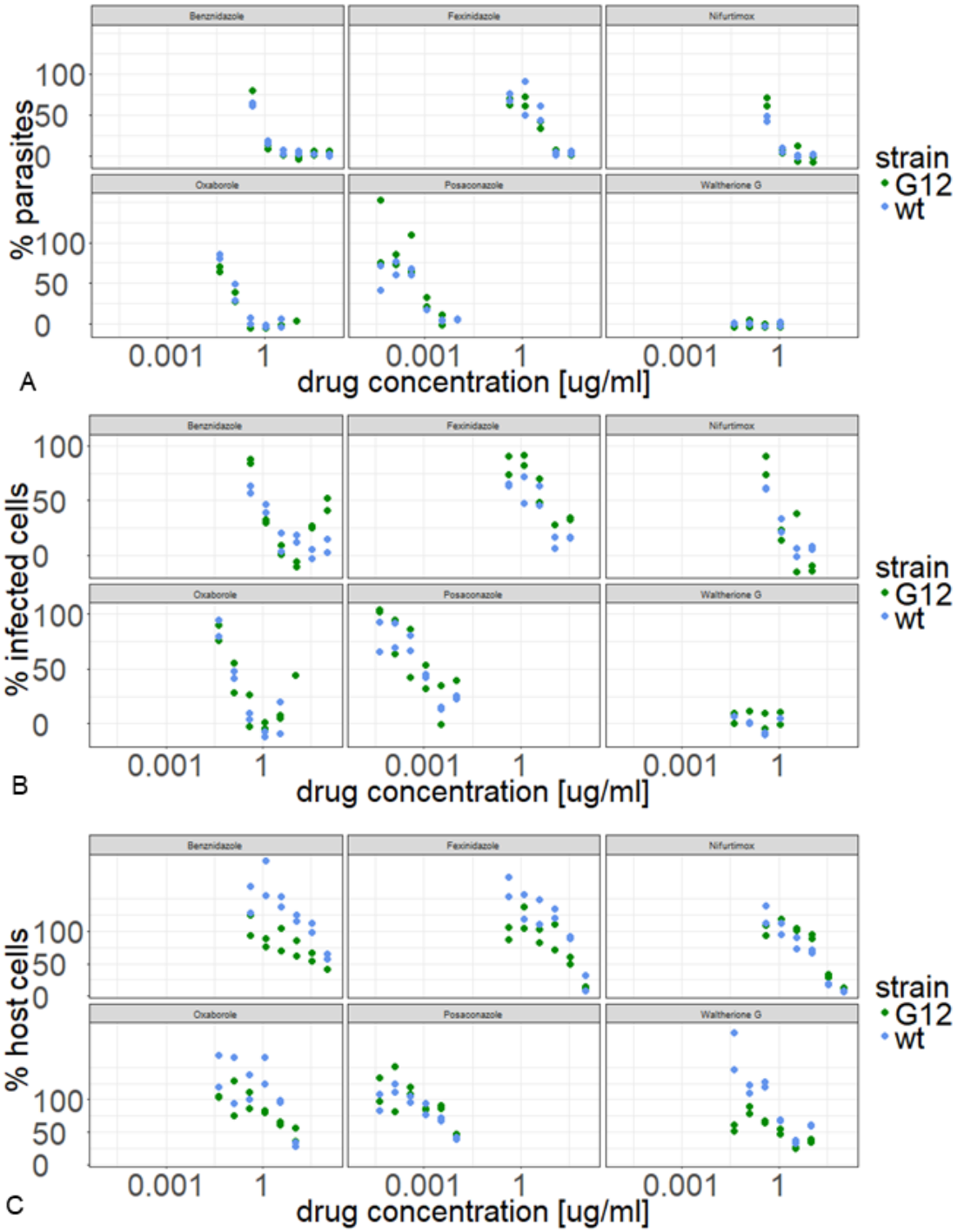

Figure 5 Relative amastiogte numbers (A), ratio of infected host cells (B), and host cell numbers (C) after treatment with the respective drug concentrations

	(A) Infection rate		(B) Intracellular Amastigotes		(C) Cytotoxicity	
EC50 [ng/ml]	wt	G12	wt	G12	wt	G12
Benznidazole	730	840	570	660	>100,000	43’000
	760	830	520	540	>100,000	65’000
Fexinidazole	950	5’500	1’200	2’200	57’000	31’000
	5’000	3’400	4’500	2’300	69’000	41’000
Waltherione G	< 41	< 41	< 41	< 41	>10,000-	910
	< 41	< 41	< 41	< 41	>10,000	1’300
Oxaborole	110	82	120	68	7’500	5’700
	101	140	81	72	6’900	>10,000
Nifurtimox	610	720	<410	570	17’000	23’000
	540	670	<410	500	16’000	23’000
Posaconazole	0.88	0.23	0.55	0.53	73	0.0
	0.82	1.20	0.47	0.85	6.3	9.0

Table 5 Drug sensitivity of the mammalian stages. The results are from two technical replicates for each parasite line.

Conclusion

Aiming to provide a new assay strain to the toolbox of antichagasic drug discovery, I started by demonstrating that our strain *T. cruzi* STIB980 belongs to the DTU TcI. I determined which antibiotics would be most useful for selection of transgenic derivative with respect to the wildtype sensitivity. Additionally, I established an optimal transfection protocol for use in our laboratory. Success of transfection can be determined on the genomic level with PCR and Southern blot. I determined phenotypic transfection success and the genetic stability by flow cytometry (for epimastigotes), by epifluorescence microscopy (applicable to most stages), and high-content microscopy (for amastigotes). To rule out effects of the transgenes on drug sensitivity, I compared wildtype and transfectant sensitivity of amastigotes with a high-content assay protocol. The eGFP-expressing clone *T. cruzi* STIB980-G12 has a strong expression of fluorescence and a comparable drug sensitivity profile to untransfected *T. cruzi* STIB980. The eGFP transgene is stable in epimastigotes but not in amastigotes, underlining the importance of testing genetic stability of transgenes in the different life-cycle stages.

Methods

Parasite and cell cultivation

Host cells

MEF (mouse embryonic fibroblasts) were cultivated in RPMI supplemented with 10% heat-inactivated fetal calf serum (iFCS) at 37°C, 5% CO_2 and >95% humidity. MEF were sub-cultured once per week at a ratio of 1:10 after 5 min treatment with trypsin.

Parasites

T. cruzi STIB980 clone 1 was obtained from A. Osuna in 1983. *T. cruzi* epimastigotes were maintained in supplemented liver infusion tryptose (LIT) (2 or 20 µg/ml hemin, 10% iFCS, (Fernandes & Castellani, 1966)) at 27°C. They were diluted weekly to keep them in the log growth phase. Epimastiogte cultures were kept for 3 - 4 weeks in the same medium in order to stimulate metacyclogenesis. Health of the culture with epimastigotes and metacyclic trypomastigotes was controlled microscopically. About 10^8 parasites from a healthy, predominantly metacyclic culture were taken to infect MEF for 48 hours. The mammalian cycle of amastigotes and trypomastigotes was maintained by infecting MEF weekly with a multiplicity of infection (MOI) of 1:1.

Macrophage isolation

Peritoneal mouse macrophages were obtained from female CD1 mice (30-35g). A 2% (w/v) starch solution in distilled water was injected i.p., and macrophages were harvested 24 h later by peritoneal lavage with RPMI medium containing 1% MäserMix (Maser, Grether-Buhler, Kaminsky, & Brun, 2002). After centrifugation at 460 rcf at 4°C for 15 min, the supernatant was removed, and the pellet was resuspended in RPMI medium containing 1% MäserMix, 10% iFCS and 15% medium conditioned by LADMAC cells (ATCC® CRL2420™). Medium conditioned by LADMAC cells contains the growth factor colony stimulating factor 1 (CSF1). The ePMM were kept in this medium at 37°C for 3-4 days and then detached with 5 min trypsin treatment and cell scrapers. The number of cells was estimated by counting with a Neubauer hemocytometer using light microscopy (×40 magnification).

Establishing clonal parasite cultures

The gilded paper clip method was used for cloning (Figure 2 A). A midlog epimastigote culture was diluted to 5×10^4 parasites/ml. The outer wells of a 96-well plate were filled with 100 µl sterile water. As preparation, 15 µl of conditioned LIT (LIT supplemented with 10% of filtered post-culture medium and 20% of iFCS) were filled into one corner of the other wells, so that some space of the well remained dry. Using a gold-plated paper clip, a micro-drop (approximately 0.1 µl) was transferred from the

diluted parasite suspension to the dry space of the well. Two people analyzed the well under an inverted microscope, whether it contained only one parasite. Wells containing only one parasite were supplemented with 35 µl of conditioned LIT. The plates were incubated at 27°C and assessed regularly for parasite growth. After phenotypic characterization concerning growth rate, eGFP expression, and infectivity, the outgrown clones were cultivated as described above.

Molecular Methods

Isolation of gDNA

We used several methods to isolate gDNA according to the required sensitivity and specificity. For quick detection of transgenes by PCR, we used a quick isolation method. For more uses that required a higher purity, we isolated the DNA with phenol-chloroform. Later, we also used the DNeasy blood and tissue kit (QIAGEN).

For the quick isolation methods, a dense culture of (approx. 10^7) parasites were pelleted at 1800 rcf for 10 minutes and washed in 1 ml NTE (10 mM Tris-HCl, 1 mM EDTA, 100 mM NaCl). They were pelleted again at 15700 rcf for 1 minute and resuspended in 100 µl TE (10 mM Tris-HCl, 1 mM EDTA) pH 8.0. For lysis, 1 µl of 10% SDS was added and incubated at 55°C for 10 minutes. Proteins and cell debris were precipitated by the addition of 30 µl 5M potassium acetate and incubation on ice for 5 minutes followed by 5 minutes full-speed centrifugation at 4°C. The supernatant was transferred to a new tube and the DNA was precipitated by the addition of 2 volumes of cold 100% ethanol, short incubation on ice and 5 minutes full speed centrifugation at 4°C. The DNA was washed in 70% ethanol and resuspended in 20 µl DNAse-free water.

For the phenol-chloroform isolation, approx. 10^8 parasites were pelleted at 1800 rcf for 10 minutes and washed in 1 ml NTE. The parasites were pelleted again at 2300 rcf for 10 minutes and resuspended in 500 µl NTE. To lyse the parasites, 25 µl SDS 10% were added. The lysate was treated with 50 µl RNase A (10 mg/ml) and incubated for 2 hours at 37°C. After addition of 25 µl Pronase (20 mg/ml), the mixture was incubated over night at 37°C. To remove cellular debris, 500 µl water-saturated phenol were added. For mixing, the tube was inverted several times. Phase separation was achieved by centrifugation at 16100 rcf for 5 minutes. All subsequent centrifugation steps were carried out this way. The upper – aqueous – phase containing the DNA was transferred to a new tube. Next, 500 µl chloroform:isoamyl alcohol (24:1) were added, mixed, and centrifuged. The upper phase was again transferred to a new tube. The DNA was precipitated by the addition of 1 ml cold 100% ethanol and centrifugation. The pellet was washed with 1 ml of cold 70% ethanol and centrifuged again. The supernatant was discarded. The pellet was air dried and resuspended in 80 µl DNase-free water.

Genotyping

We performed genotyping according to the method of Messenger et al (Messenger et al., 2015). For genotyping, we isolated gDNA with the phenol-chloroform extraction method. Three PCR were performed (Table 6), one for G6PI (glucose-6-phosphate isomerase), one for LSU (large ribosomal subunit) and one for HSP60 (heat-shock protein 60). The PCR products from G6PI and HSP60 were digested with *Hha*I and *Eco*RV, respectively. The profiles were compared with the profiles of control DNA samples donated by Dr. M. Lewis, LSHTM.

target	Primer	.	annealing - step 1	annealing - step 2
LSU	D71	AAGGTGCGTCGACAGTGTGG	60°C (1 min, 27 cycles)	-
	D72	TTTTCAGAATGGCCGAACAGT		
HSP60	HSP60_for	GTGGTATGGGTGACATGTAC	72°C (30 s, 4 cycles)	60°C (30 s, 28 cycles)
	HSP60_rev	CGAGCAGCAGAGCGAAACAT		
G6PI	GPI_for	GGCATGTGAAGCTTTGAGGCCTTTTTCAG	64°C (30 s, 4 cycles)	60°C (30 s, 28 cycles)
	GPI_rev	TGTAAGGGCCCAGTGAGAGCGTTCGTTGAATAGC		

Table 6 Drug sensitivity of the mammalian stages. The results are from two technical replicates for each parasite line.

Plasmid manipulations

The plasmid pTcRG (Figure 6 A) was obtained from Prof. Dr. S. Teixeira, Federal University of Minas Gerais, Brazil. The circular plasmid was used for transient transfection. To test stable transfection efficiency, the plasmid pTcRG was linearized with *Not*I-HF (NEB).

The plasmid pTRIX2-eGFP was derived from the pTRIX-REh9 (Lewis et al., 2014) The red-shifted luciferase gene was replaced by *eGFP* gene amplified from the plasmid pTc-iTrBG (Figure 6 B) using the *Xho*I and *Bam*HI restriction sites of pTRIX2. For the final transfection, 2.5 µg pTRIX2-eGFP plasmid (Figure 8 A) were linearized with *Asc*I and *Sac*I (NEB, Ipswich, MA, USA).

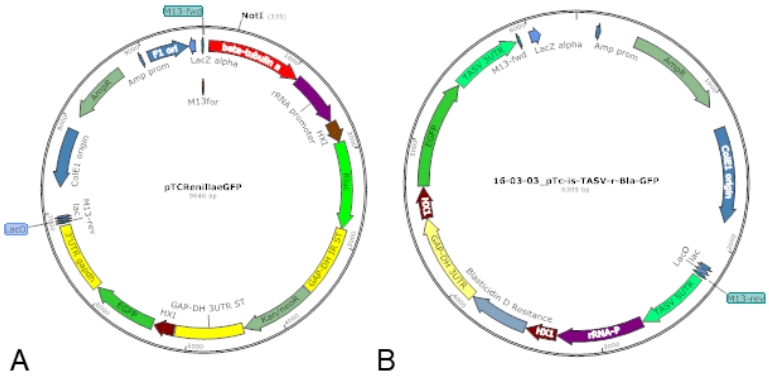

Figure 6 Plasmids used for this work. A pTcRG pTCRenillaeGFP, B pTciTrBG pTc-is-TASV-r-Bla-GFP

Genetic manipulation of parasites

Testing transfection efficiency

In order to test for transfection efficiency, 10^7 epimastigotes from a mid-log growth phase were centrifuges and resuspended in 100 µl of TbBSF buffer (Burkard et al., 2007) containing 10 µg of circular (for transient efficiency) or linearized (for stable efficiency) pTcRG plasmid or no DNA. The parasites were electroporated using different programs of the nucleofector device (Lonza). Parasites were contained in a 0.2 mm cuvette (BioRad). After electroporation, parasites were transferred to 10 ml LIT with a fine-tipped pasteur pipette. Directly after the transfer, the parasites were counted to determine the proportion of surviving parasites.

The parasites transfected with circular plasmid were incubated for 24 hours and then tested with flow cytometry for eGFP expression.

The parasites transfected with linearized plasmid were incubated for 24 hours before the addition of G418. To determine the efficiency of stable integration, the parasites were counted and plated in different densities in 48 wells per density. We quantified, the number of wells, in which parasites grew after 3 weeks of drug pressure with G418.

Transfection of epimastigote Trypanosoma cruzi

As learned at the LSTHM, I transfected a dense epimastigote culture at the end of the log growth phase (starting to form rosettes, 10^8 epimastigotes) with the 2.5 µg pTRIX2-eGFP plasmid (Figure 8 A) linearized with *Asc*I and *Sac*I (NEB, Ipswich, MA, USA). The fragments were separated on a long 0.8% agarose gel in 1x TBA on a long run to ensure separation of the digested fragment from the undigested plasmid. The 7.8 kb fragment, the construct, was cut from the gel and purified using the NucleoSpin Plasmid kit (Macherey-Nagel). Twenty-four hours after transfection, the parasites were diluted 1:10 in medium containing 100 µg/ml G418. In order to determine the transfection efficiency, a fourfold dilution series was done from the 1:10 parasite line in a 48 well plate. Parasites were checked on a regular basis, at least weekly, for dying of wildtype parasites in response to G418 and outgrowth of transfectants. The selected epimastigotes were cloned by limiting dilution. Clone 12 (G12) was selected according to its eGFP expression level, infectivity and growth profile. Transgenic epimastigotes were kept at 500 µg/ml G418.

PCR for detection of pTcRG transfection success

Genomic DNA was isolated from 100-500 µl of parasite culture (of limiting dilution for testing stable transfection), according to the observed density, by using the quick gDNA protocol mentioned above. I did two PCR using FIREPol on all samples. One PCR using a primer pair designed to detect GAP-DH in qPCRs (GAP-DH_for & GAP-DH_rev) in order to detect, whether enough DNA was in the sample to obtain a PCR product at all. In the second PCR, I used a primer pair to amplify the neomycin resistance gene (mR_Neo_for & mR_Neo_rev).

Phenotypic methods

Drug sensitivity assay with epimastigotes

To test for antibiotic sensitivity, in each well, 100 µl epimastigotes with the densities of 5×10^6/ml, (A) 1×10^5/ml (B), and 2×10^4/ml (C) were incubated with drugs in threefold serial dilution with 11 dilution steps. After 69 h (A) or 165 h (B, C) incubation at 27°C, 10 µl of resazurin solution (12.5 mg in 100 ml water) were added to each well. After another 3 h of incubation, the plates were read with the SpectraMAX GeminiXS fluorescence reader (Molecular Devices). EC50 values were determined in R version 3.5.1 (R Core Team, 2018) using the “drc” package (Ritz, Baty, Streibig, & Gerhard, 2015).

Flow cytometry

For flow cytometry, 10^5 epimastigotes were fixed with 10% formalin for 15 min and then analyzed for the green fluorescence levels (FL1) at the BD FACSCalibur (Becton Dickinson and Company, Franklin Lakes, NJ, USA). The threshold for eGFP expression was set, so that only the 0.4% most green autofluorescent wildtype parasites from the control were determined to be eGFP-expressing. The proportion of eGFP-expressing cells was therefore the proportion of parasites exhibiting a higher fluorescence level than the threshold.

Fluorescence microscopy

Parasites (epimastigotes, trypomastigotes) were fixed to a glass slide (Menzel Superfrost Plus). They were allowed to sink for 15 min, then washed with PBS and fixed with 10% formalin. The slides were fixed with 10% formalin for 15 min. All samples were embedded in Vectashield with DAPI (Vector Laboratories, Peterborough, United Kingdom) and covered with a 1.5 AutomatStar coverslip (DURA group). Samples were imaged using the Leica DM 5000B microscope with a Sola FISH 365 LED light source. Images were taken on the 20x and 63x objectives with phase contrast and DIC, respectively. Fluorescence images were taken by using the A4 (Excitation 377/50 nm, Emission 447/60 nm) and L5 (Excitation 470/40 nm, Emission 525/50 nm) filter cubes.

High-content microscopy

ImageXpress Micro XLS (Molecular Devices) was used. Fluorescent imaging was done using following filter cubes: eGFP (300 ms), DAPI (50 ms), and Cy5 (300ms). Phase-contrast images were taken on the transmitted light channel (TL10, 10% illumination). All images were taken using a 20x Zeiss objective.

Image analysis

Image analysis was performed on the MetaXpress 6 software. On fixed images, host nuclei and parasite kinetoplast DNA were detected. The parasites mitochondrial DNA (kinetoplast DNA) is very AT-rich and is therefore stained stronger by minor-groove binding stains such as Hoechst 33342 (Wheeler, Gull, & Gluenz, 2012). Round objects of the size 5-30 µm and a fluorescence difference of 5000 were detected as host cell nuclei. Parasite kinetoplast DNA was detected by applying a TopHat filter with 10 pixels diameter as round objects of 1.5 -15 µm sizes and a fluorescence difference of 200, which did not coincide with host cell nuclei. Parasite kinetoplast DNA in an area, where the green fluorescence level was lower than an adaptive threshold of 2000, was called eGFP-negative parasites. The remaining parasites were denoted eGFP-positive parasites.

High-content assay

Assay design

For the standard assay, 10^4 ePMM were seeded into the central wells of a black 96-well plate (Greiner, uClear, black, REF 655090, Lot E1803364) in 100 µl of RPMI medium containing 1% MäserMix, 10% FCS and 15% RPMI containing LAD-Mac growth factors per well. The border wells were filled with 100 µl of water. After 48 hours, the ePMM were infected with 10^4 trypomastigotes from either the wildtype or the eGFP-expressing parasite line. After 24 hours, the remaining trypomastigotes were washed off twice with 200 µl RPMI per well. The infected ePMM were kept in 100 µl RPMI containing 1% MäserMix and 10% iFCS. Drugs were added in three-fold serial dilution 24 hours post-infection. 96 hours after addition of drugs, the plates were fixed with 10% formalin for 15 min at room temperature. Afterwards the plates were stained with 50 µl of 5 µM Draq5 (Merck) per well for 30 min at room temperature in the dark. The plates were stored at 4°C for at least 24 hours and then imaged using the ImageXpress Micros XLS with the Cy5 filter cube for 300 ms per image on 9 sites per well. Assays were performed with two technical and two biological replicates.

Image analysis

Image analysis was performed on the MetaXpress 6 software. On fixed images from the Cy5 channel, host nuclei, host cytoplasm and parasites were detected. Objects of the size 5-20 µm and a fluorescence difference of 6000 above local background were detected as host cell nuclei. They had cytoplasm as a positive marker as objects of the size 5 – 20 µm and a fluorescence difference of 1500

above local background. Border objects were removed. Parasites were detected as granularity objects of the size of 1 – 5 µm and a fluorescence difference of 2000 above local background. Granularity objects coinciding with host cell nuclei were removed. All parasites in non-border cytoplasm were counted as amastigotes. All cells containing at least one parasite were counted as infected cells.

Statistical analysis and graphical depiction

Statistical analysis and graphs were done in R version 3.5.1 (R Core Team, 2018) using the packages "tidyverse" (Wickham, 2017) and "readxl" (Wickham & Bryan, 2018).

Acknowledgements

I wish to thank the Swiss National Science Foundation, the Nikolaus und Bertha Burckhardt-Bürgin-Stiftung and the Freiwillige Akademische Gesellschaft for financial support.

I am thankful to Prof. Dr. Pascal Mäser and Dr. Marcel Kaiser for supervision. I am grateful to M. Cal, C. Kunz and Dr. R. Schmidt for training in parasite cultivation and molecular biology.

I thank R. Rocchetti for isolation of ePMM.

I thank Prof. Dr. Antonio Osuna for the kind provision of the *T. cruzi* strain.

I thank Dr. M. Lewis for gDNA of *T. cruzi* reference strains and recommendations concerning genotyping.

I thank Prof. Dr. S. Teixeira for providing the plasmid pTcRG.

I thank Prof. Dr. J. Kelly and Dr. M. Taylor for providing the plasmid pTRIX2-RE9h. I am grateful to Dr. F. Olmo for training me in transfecting *T. cruzi*.

I kindly thank Prof. Dr. Till Voss and his group for letting us use the high-content microscope.

The genome of *Trypanosoma cruzi* STIB980

Introduction

The genome of *Trypanosoma cruzi*, the causative agent of Chagas' disease, is complex due to its extraordinarily high proportion of repeat-rich sequences. About 50% of the genome content were estimated to be repetitive (El-Sayed, Myler, Bartholomeu, et al., 2005). This is in stark contrast to *Trypanosoma brucei* and the *Leishmania spp.*, which have a repetitive genome content of about 25% and 20%, respectively (Reis-Cunha & Bartholomeu, 2019). The repetitive elements of the *T. cruzi* genome seem to be multigene families, transposable elements, and tandem repeats (Berna et al., 2018). Due to its extensively repetitive nature, the *T. cruzi* genome - investigated by shot-gun Sanger sequencing - was not fully assembled at the time of publication of the TriTryp genomes, i.e. the genomes of *T. brucei*, *Leishmania major* and *T. cruzi*, CL Brener strain (Berriman et al., 2005; El-Sayed, Myler, Bartholomeu, et al., 2005; El-Sayed, Myler, Blandin, et al., 2005; Ivens et al., 2005). It took further attempts to assemble the *T. cruzi* CL Brener genome on chromosome level (Weatherly, Boehlke, & Tarleton, 2009). Chromosome-level assembly was achieved with the help of TriTryp synteny maps and BAC libraries (Weatherly et al., 2009). The assembly was additionally hampered by the fact that *T. cruzi* CL Brener, as a DTU TcVI strain, is of hybrid nature, with two distinct sets of chromosomes. One is derived from the parental DTU TcII and the other from the parental DTU TcIII. The two haplotypes were separated by comparing them to sequences from the *T. cruzi* Esmeraldo strain (DTU TcII, (El-Sayed, Myler, Bartholomeu, et al., 2005)). Therefore, the publically available CL Brener genome - so far the reference genome for *T. cruzi* - consists of three datasets: An Esmeraldo-like chromosome set, a NonEsmeraldo-like chromosome set, and contigs that could not be assigned to either of the subsets. To obtain a chromosome-level assembly, N-filled gaps were accepted. In the release 37 of TriTrypDB (Available at: https://tritrypdb.org/common/downloads/release-37/), approximately 1'700 gaps filled with 4'700'000 and 6'700'000 letters N were still present in either of the chromosome sets.

The repetitive nature of the *T. cruzi* genome makes this parasite a poster child in the advent of long-read sequencing technologies. In 2018, the first two assemblies employing the Pacific Biosciences single molecule real-time (SMRT) sequencing technology were published (Berna et al., 2018); one from the Dm28c strain (DTU TcI) and one from the TCC strain (DTU TcVI). The authors succeeded to decompress collapsed repeated sequences and to assemble both genomes on haplotype level. Additionally, the authors identified the compartmentalized nature of the *T. cruzi* genome. According to their analyses, the *T. cruzi* genome consists of core compartments separated by interruptive compartments. The core compartment consisting of conserved genes, which are in synteny not only between *T. cruzi* strains but also with *T. brucei* and *Leishmania spp.* sequences. In contrast, the interruptive compartments are mostly comprised of species-specific multigene families. The number of genes of these multigene families varies between *T. cruzi* strains and even between haplotypes. Differences in size of the interruptive compartments between haplotypes can explain the differences

in size between homologous chromosomes (Souza et al., 2011). In contrast to *T. brucei*, where the variability is mostly found within the sub-telomerically located variable surface glycoprotein genes and expression-site associated genes (ESAGs), the *T. cruzi* disruptive compartments can be found throughout the genome (Berna et al., 2018). These observations underline the importance of sequencing individual *T. cruzi* strains, as the copy numbers even of genes annotated as single copy can vary between strains, which will jeopardize reverse genetic approaches such as knock-out experiments. This also further underlines the value of long-read sequencing technologies. PacBio-sequenced genomes of several other strains were published and compared (Callejas-Hernandez, Girones, & Fresno, 2018; Callejas-Hernandez, Rastrojo, Poveda, Girones, & Fresno, 2018). Recently, the first *T. cruzi* genome sequenced with Oxford Nanopore technology and assembled in hybrid assembly with Illumina reads was published (Diaz-Viraque et al., 2019). Here, we present the sequencing and assembly of the *T. cruzi* STIB980 genome with the combination of Illumina and Nanopore sequencing. With the increasing use of *T. cruzi* STIB980 for *in vitro* assays, target deconvolution and drug resistance studies, knowledge of its genome is of paramount importance to make the strain amenable to genetic engineering.

The genome of *Trypanosoma cruzi* STIB980: Using high-coverage short-read sequencing to polish a long-read assembly of genomic and mitochondrial DNA

Manuscript for submission in Microbial Resource Announcements

Anna F. Fesser[1,2], Marcel Kaiser[1,2], Pascal Mäser*[1,2], Remo S. Schmidt[1,2,†]

[1]Molecular Parasitology and Infection Biology, Swiss Tropical & Public Health Institute, Switzerland

[2]University of Basel, Basel, Switzerland

[†]Present Address: Agroscope, Schwarzenburgstrasse 161, Bern, Switzerland

[*]corresponding author: Pascal Mäser

E-mail pascal.maeser@swisstph.ch

Abstract

Trypanosoma cruzi is the causative agent of Chagas' disease. We report the draft genome sequence of the Trypanosoma cruzi strain STIB980 (DTU TcI), comprising 492 contigs and having a genome size of 28.2 Mbp. This genome demonstrates the usefulness of long-read sequence technologies for genomes with repetitive regions.

Announcement

The genome of *Trypanosoma cruzi*, the causative agent of Chagas' disease, is complex due to its extraordinarily high proportion of repeat-rich sequences. About 50% of the genome content were estimated to be repetitive (El-Sayed, Myler, Bartholomeu, et al., 2005). This is in stark contrast to *Trypanosoma brucei* and the *Leishmania* spp., whose repetitive genome content amounts to 25% and 20%, respectively (Reis-Cunha & Bartholomeu, 2019) (Reis-Cunha & Bartholomeu, 2019). Most of the repetitive elements of the *T. cruzi* genome seem to be multigene families, transposable elements, and tandem repeats (Berna et al., 2018). This extensive repetitive nature complicates the assembly of the genome using short-read sequencing approaches. Kinetoplastids like *T. cruzi*, *T. brucei* and *Leishmania* spp. are characterized by their single mitochondrion (the kinetoplast). The mitochondrial genome (kinetoplast DNA, kDNA) is organized in circular format: The maxicircles harbor the mitochondrial genes in a cryptic manner (Westenberger et al., 2006), whereas the minicircles harbor templates for RNA editing (Junqueira, Degrave, & Brandão, 2005), crucial for decryption of the maxicircles' information.

Genomic DNA was extracted from *T. cruzi* strain STIB980 epimastigotes (DTU TcI; obtained from Prof. Dr. A. Osuna, Universidad de Granada, Granada, Spain). Epimastigotes were cultivated in liver infusion tryptose (LIT) medium (Fernandes & Castellani, 1966) supplemented with 10% heat-inactivated fetal calf serum and 2 µg/ml hemin at 28°C. The DNA from 10^7 epimastigotes was isolated with phe nol-chloroform-isoamyl alcohol extraction, followed by ethanol precipitation or collecting the precipitated DNA with a glass hook for Illumina sequencing and Nanopore sequencing, respectively.

Short-read sequencing was done using an Illumina HiSeq 2500 sequencer with 125bp paired-end reads and the PCR-free KAPA HyperPrep kit for library preparation (Illumina). Long-read sequencing used the MinION platform and the Ligation Sequencing kit 108 (SQK-LSK108, Oxford Nanopore Technology) for library preparation. Basecalling was carried out using Albacore.

Illumina and Nanopore sequencing produced 67'187'531 reads and 250'013 reads, respectively. Quality control was done with the FastQC software (Babraham Bioinformatics - FastQC A Quality Control tool for High Throughput Sequence Data., version 0.11.3, available at:

http://www.bioinformatics.babraham.ac.uk/projects/fastqc/). The reads were categorized into nuclear genome, maxicircle (we assembled only a single contig), minicircles and sequences of unknown origin according to their size and GC content (Figure 7). The majority of the reads were categorized as minicircles, with a GC content between 30% and 40% and a length of approx. 1.4 Mb.

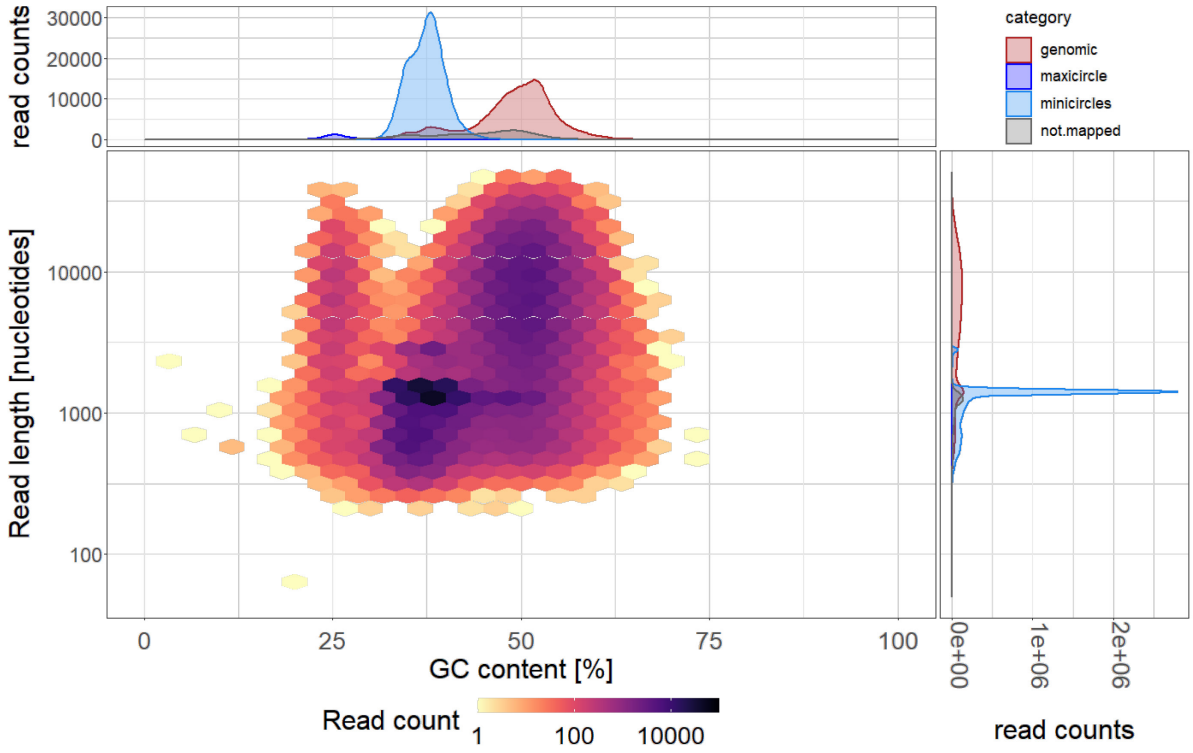

Figure 7 Distribution of Nanopore reads of STIB980 according to GC content and read length

The pore-chopped (Wick, Judd, Gorrie, & Holt, 2017) Nanopore reads were assembled using Canu (version 1.7, (Koren et al., 2017)) with an expected genome size of 53 Mb. Illumina polishing of the Canu-assembled Nanopore reads was performed using Pilon (version 1.22, (Walker et al., 2014)). The assembly resulted in a 492 contigs with a haploid genome size of 28.2 Mb (Table 7).

	total size of assembly	**n contigs**	**N50**	**largest contig**	**smallest contig**
total	28'220'043	492	158'042	715'804	1'001
nuclear	27'888'483	397	165'577	715'804	1'660
minicircles	248'782	91	2'699	10'035	1'264
maxicircle	68'708	1			
unknown	14'070	3	*3'090*	9'979	1'001

Table 7 Summary statistics of separated assemblies

Gene annotation was performed on Companion using *T. brucei* TREU927 (Steinbiss et al., 2016) as reference. Pseudo chromosome contiguation was selected with a minimum required match length of 500 bp and similarity of 85%. Of 8826 genes annotated, 8662 as coding genes (1498 with function), and 164 as non-coding. Of the 2015 pseudogenes, 1498 were annotated with function. To identify additional genes, gene prediction was performed using GLIMMER (Salzberg, Delcher, Kasif, & White,

1998) with the standard codon table. The genome of *T. cruzi* Dm28c (Berna et al., 2018) served as training set. This resulted in 10043 open-reading frames (ORFs) with a median length of 1077 bp. The amino acid sequences were aligned on the SwissProt database (Bairoch, 2000) using BLASTP (Altschul, Gish, Miller, Myers, & Lipman, 1990) with an e-value of 10^{-8}. Of the 3505 annotated genes, 399 genes had a high similarity to *T. cruzi* genes.

Acknowledgement

Library preparation and sequencing on the Illumina platform was performed at the Quantative Genomics Facility Basel (GFB) of the ETH Zürich. Computational work was mostly done on the high-perfomance computing clusters of sciCORE (http://scicore.unibas.ch/) scientific computing center at University of Basel.

We wish to thank Prof. Dr. A. Osuna for the kind provision of the strain.

We wish to thank Prof. Dr. R. Neher and Dr. N. Noll from the Biozentrum, University of Basel, for providing us with the Nanopore library preparation kit and all the input around Nanopore sequencing.

We wish to thank Dr. T. Otto for input on genome assembly.

Non-invasive monitoring of drug action: a new live *in vitro* assay design for Chagas' disease drug discovery

Published in PLoS Negl Trop Dis: https://doi.org/10.1371/journal.pntd.0008487

Anna F. Fesser[1,2], Olivier Braissant[3], Francisco Olmo[4], John M. Kelly[4], Pascal Mäser*[1,2], Marcel Kaiser[1,2]

[1]Molecular Parasitology and Infection Biology, Swiss Tropical & Public Health Institute, Switzerland

[2]University of Basel, Basel, Switzerland

[3]Department of Biomedical Engineer, University of Basel, Basel, Switzerland

[4]London School of Hygiene and Tropical Medicine, London, United Kingdom

*corresponding author: Pascal Mäser

E-mail pascal.maeser@swisstph.ch

Abstract

New assay designs are needed to improve the predictive value of the *Trypanosoma cruzi in vitro* tests used as part of the Chagas' disease drug development pipeline. Here, we employed a green fluorescent protein (eGFP)-expressing parasite line and live high-content imaging to monitor the growth of *T. cruzi* amastigotes in mouse embryonic fibroblasts. A novel assay design allowed us to follow parasite numbers over 6 days, in four-hour intervals, while occupying the microscope for only 24 hours per biological replicate. Dose-response curves were calculated for each time point after addition of test compounds, revealing how EC50 values first decreased over the time of drug exposure, and then leveled off. However, we observed that parasite numbers could vary, even in the untreated controls, and at different sites in the same well, which caused variability in the EC50 values. To overcome this, we established that fold change in parasite number per hour is a more robust and informative measure of drug activity. This was calculated based on an exponential growth model for every biological sample. The net fold change per hour is the result of parasite replication, differentiation, and death. The calculation of this fold change enabled us to determine the tipping point of drug action, i.e. the time point when the death rate of the parasites exceeded the growth rate and the fold change dropped below 1, depending on the drug concentration and exposure time. This revealed specific pharmacodynamic profiles of the benchmark drugs benznidazole and posaconazole.

Author Summary

Chagas' disease, caused by *Trypanosoma cruzi,* is a chronic debilitating infection occurring mostly in Latin America. There is an urgent need for new, well tolerated drugs. However, the latest therapeutic candidates have yielded disappointing outcomes in clinical trials, despite promising preclinical results. This demands new and more predictive *in vitro* assays. To address this, we have developed an assay design that enables the growth of *T. cruzi* intracellular forms to be monitored in real time, under drug pressure, for 6 days post-infection. This allowed us to establish the tipping point of drug action, when the death rate of the parasites exceeded the growth rate. The resulting pharmacodynamics profiles can provide robust and informative details on anti-chagasic candidates, as demonstrated for the benchmark drugs benznidazole and posaconazole.

Introduction

About 8 million people globally are infected with *Trypanosoma cruzi*, the causative agent of Chagas' disease (Stanaway & Roth, 2015). The progression of Chagas' disease is divided into three phases: an acute, a chronic indeterminate and, in about 30% of the infected people, a symptomatic chronic phase. This last phase can begin decades after infection and is marked by severe cardiac or digestive symptoms. There are only two drugs registered for Chagas' disease, benznidazole and nifurtimox, and these suffer from severe side effects and variable efficacy (Molina et al., 2014). Therefore, new treatment options are needed urgently.

Azoles like posaconzale and E1224, a prodrug of ravuconazole, were the most advanced drug candidates. However, in clinical trial, 80% of the posaconazole-treated patients relapsed within the 20 month follow-up after treatment, in contrast to 6% of the benznidazole-treated patients (Molina et al., 2014). As a result, the research community was forced to rethink the pre-clinical drug discovery pipeline for Chagas' disease (Chatelain, 2015; Keenan & Chaplin, 2015). In particular, the design of *T. cruzi in vitro* assays had to be revisited to render them more predictive for the situation *in vivo*. A number of parameters were proposed for optimization: the choice of strains (Moraes et al., 2014; Zingales et al., 2014), the life-cycle stages (Francisco, Jayawardhana, Lewis, Taylor, & Kelly, 2017), the treatment regimens (G. Yang, Lee, Ioset, & No, 2017), and assay designs that assessed drug cidality. Tremendous progress has been made, especially in the area of high-content imaging technology for phenotypic assays (Alonso-Padilla et al., 2015; Alonso-Padilla & Rodriguez, 2014; De Rycker et al., 2016; Engel et al., 2010; Moraes et al., 2014; Neitz et al., 2015; Nohara et al., 2010; G. Yang et al., 2017). New wash-out designs were also introduced to assess reversibility and cidality of drug action (Cal et al., 2016; MacLean et al., 2018). In combination with the development of more sensitive animal models (Canavaci et al., 2010; Henriques, Henriques-Pons, Meuser-Batista, Ribeiro, & de Souza, 2014; Lewis, Francisco, Taylor, & Kelly, 2015), this permitted a focus on pharmacokinetic (PK) and pharmacodynamic (PD) parameters. PK-PD modeling allows treatment regimens to be modified for optimal exposure of the target organism to the drug candidate (Hodel, Kay, & Hastings, 2016; Meyer, Meyers, & Shapiro, 2019; ter Kuile, White, Holloway, Pasvol, & Krishna, 1993). It also helps to define benchmark PK-PD parameters of the target product profile for drug candidates.

While there has been progress in modeling drug candidate PK profiles (Perin et al., 2017), the PD profile of a drug remains more difficult to determine. Two major aspects of PD need to be considered: time-to-kill and the question of whether drug action is concentration-driven or time-driven. Isothermal microcalorimetry has been used to determine time-to-kill for various pathogens, including African trypanosomes and *Plasmodium falciparum* (Gysin et al., 2018; Wenzler et al., 2012). However, isothermal microcalorimetry cannot be used for intracellular amastigotes, the disease-relevant stage of *T. cruzi*, as it is impossible to differentiate the heatflow of the parasite from that of

the host cell. Time-to-kill can also be determined by setting more than one temporal endpoint in an assay, which can mean that one plate per time point has to be assessed (De Rycker et al., 2016; MacLean et al., 2018). An efficient method to determine pharmacodynamic parameters still needs to be found.

Here, we describe a new *in vitro* live-imaging assay design and novel analysis methodology, which enables time-to-kill to be determined and identifies whether drug action is time- or concentration-driven.

Methods

Parasite and Cell cultivation

Mouse embryonic fibroblasts (MEF) were cultivated in RPMI supplemented with 10% FCS at 37°C, 5% CO_2 and >95% humidity. MEF were sub-cultured once per week at a ratio of 1:10 after 5 min treatment with trypsin. *T. cruzi* STIB980 clone 1 (DTU TcI) was obtained from A. Osuna in 1983. Epimastigotes were maintained at 27°C in liver infusion tryptose (LIT) medium (Fernandes & Castellani, 1966) supplemented with 20 µg/ml hemin and 10% FCS. Cultures were diluted weekly to maintain exponential growth. To stimulate metacyclogenesis, epimastiogte cultures were kept in the same medium for 3 - 4 weeks. About 10^7 parasites from a predominantly metacyclic culture were taken to infect MEF for 48 h, and the cycle of amastigotes and trypomastigotes was maintained by infecting MEF weekly with an MOI of 1:1. eGFP-expressing parasites were kept for maximum of 4 weeks in the mammalian cycle.

Transfection

Exponentially growing *T. cruzi* epimastigotes were synchronized for 24 h with 20 mM of hydroxyurea (Sigma) (Olmo, Costa, Mann, Taylor, & Kelly, 2018). Following hydroxyurea removal by washing twice with PBS, 10^7 epimastigotes were electroporated with 2.5 µg of pTRIX2-eGFP plasmid (Figure 8 A) linearized with *Asc*I and *Sac*I (New England Biolabs). The plasmid had been derived from pTRIX-REh9 (Lewis et al., 2014). We used the Amaxa Nucleofector (programme X-014) with buffer Tb-BSF (Pacheco-Lugo et al., 2017), conditions we had found to be optimal for *T. cruzi*. 24 h after transfection, the parasites were diluted 1:10 in medium containing 100 µg/ml G418 (Invivogen). Epimastigotes were cloned by limiting dilution. Clones were selected according to their eGFP expression level, infectivity and growth profile. Transgenic epimastigote cultures were maintained in the presence of 500 µg/ml G418.

Flow cytometry

10^5 epimastigotes in a small volume (approx. 100 µl) were fixed by the addition of the same volume of 10% formalin for 15 min at room temperature. After fixation, the volume was adjusted to 1.5 ml with PBS. Then, the parasites were analyzed for the levels of green fluorescence (FL1; excitation 488/10 nm and emission 530/30 nm) on a BD FACSCalibur (Becton Dickinson and Company) gating approximately from 100 to 2000 on the FSC and the SSC channel.

Fluorescence microscopy

Epimastigote or trypomastigote parasites were deposited on a glass slide (Menzel Superfrost Plus), allowed to settle for 15 min, then washed with PBS and fixed with 10% formalin. For amastigotes, 10^4 MEF per well were seeded on 16-well LabTek chamber glass slides (LabTek). After 24 h, 48 h, and 72 h, the MEF were infected with 10^5 trypomastigotes per well. The slides were fixed with 10% formalin for 15 min. All samples were embedded in Vectashield with DAPI (Vector Laboratories) and covered with a 1.5 AutomatStar coverslip (DURA group). Samples were imaged using the Leica DM 5000B microscope with a Sola FISH 365 LED light source. Images were taken with a 10x ocular, plus a 20x or 63x objective, with phase contrast and DIC, respectively. Fluorescence images were taken by using the filter cubes A4 (excitation 377/50 nm, emission 447/60 nm) or L5 (excitation 470/40 nm, emission 525/50 nm).

Macrophage isolation

Peritoneal mouse macrophages were obtained from female CD1 mice (30 – 35 g body weight) as follows: 2 ml of a 2% (wt/vol) starch solution in distilled water were injected i.p., and macrophages were harvested 24 h later by peritoneal lavage with RPMI medium containing 1% anticontamination cocktail (100 µl in 10 ml, (Maser et al., 2002)). After centrifugation at 460 g at 4 °C for 15 min, the supernatant was removed, and the pellet was resuspended in RPMI medium containing 1% anticontamination cocktail, 10% heat-inactivated fetal calf serum (iFCS) and 15% RPMI containing LADMAC (ATCC CRL2420) growth factors. The expanded peritoneal mouse macrophages (ePMM) were kept in this medium at 37 °C for 3-4 days and then detached with 5 min trypsin treatment and cell scrapers. The cells were counted with a Neubauer hemocytometer.

High-content microscopy

All assays were performed on an ImageXpress Micro XLS (Molecular Devices) high-content microscope. Fluorescent imaging was done using the following filter cubes: eGFP (300 ms exposure), DAPI (50 ms exposure), and Cy5 (300 ms exposure). Phase-contrast images were taken on the transmitted light

channel (TL10, 10% illumination). All images were taken using a 20x Zeiss objective and a cooled CCD camera with (6.45 µm x 6.45 µm pixel size, 1392 x 1040 pixel resolution).

Live high-content assay

For the live high content assay, 10^4 ePMM were seeded into the central wells of a black 96-well plate in 100 µl of RPMI medium supplemented with 1% anticontamination cocktail (Maser et al., 2002), 10% iFCS and 15% RPMI containing LADMAC growth factors. The border wells were filled with 100 µl water. Every 24 h a new set of wells was infected with 3×10^4/well culture-derived trypomastigotes leading to an MOI of 3 parasites to 1 host cell. This had previously been tested to lead to an optimized detection of parasites per host cells with a geometric mean of 1.1 parasites per host cells [95% confidence interval from 0.82 to 1.4]. 24 h post-infection (hpi), the remaining extracellular trypomastigotes were washed off twice with 200 µl supplemented RPMI and the infected host cells were further cultivated in 100 µl RPMI, with serial dilution of drugs. On the sixth day of infection, the plate was covered with translucent PCR film (Eppendorf AG) and placed into the ImageXpress Micro XLS microscope into an environmental chamber with 37°C, humidity, and no additional CO_2. After 1 h acclimatization, the focus plane was determined. On 9 sites per well, images were taken every 4 h using the eGFP filter set (300 ms exposure) and transmitted light with 10% illumination (300 ms exposure).

After live imaging, all supernatant was removed and the cells were fixed with 10% formalin for 15 min at room temperature and stained with 100 µg/ml Hoechst 33342 (Merck) for 30 min in the dark at room temperature. The plate was stored at 4 °C until it was imaged with the ImageXpress using transmitted light with 10% illumination (300 ms exposure), the eGFP (300 ms exposure) and the DAPI (50 ms exposure) filter set on 9 sites per well.

Image analysis

Image analyses were performed on the MetaXpress 6 software. For live imaging, green fluorescent parasites were quantified from the eGFP channel. The TopHat filter was applied with 10 pixel diameter. Round objects of size 1-10 µm and a fluorescence difference of over 1000 were designated as parasites (from the filtered image). For imaging of fixed cells, host nuclei and parasite kinetoplasts were counted. Parasites' mitochondrial DNA (kinetoplast DNA, kDNA) is AT-rich and was therefore stained more strongly using minor-groove binding stains such as Hoechst 33342 (Wheeler et al., 2012). Round objects of size 5 – 30 µm with a fluorescence difference of over 1000 were designated as host cell nuclei.

Parasite kDNA was detected by applying a TopHat filter with 10 pixels diameter as round objects of 1-10 µm and a fluorescence difference of over 1000, which did not coincide with host cell

nuclei. Parasite kDNA in an area where the green fluorescence difference was lower than 1000 were defined as eGFP-negative parasites. The remaining parasites were denoted eGFP-positive parasites.

Statistical analyses

Statistical analyses were performed in R version 3.5.1 (R Core Team, 2018) using the packages "tidyverse" (Wickham, 2017), "readxl" (Wickham & Bryan, 2018), and "viridis" (Garnier, 2018). Scripts for different analysis steps are available under GitHub (https://github.com/fesser-af/NiMDA). The dose-response relationship for each time point of drug exposure was quantified by a four-parameter log-logistic model (Equation 1) using the package "drc" (Ritz et al., 2015) in R. When a dose-response model with an upper plateau (d) of 100 % and lower plateau of 0 % could be determined, it was chosen preferentially.

$$rel.growth = c + \frac{d - c}{1 + e^{b\left(ln\left(\frac{x}{f}\right)\right)}}$$

Equation 1 Dose-response model. The four-parameters of this model to determine the relative growth at a given concentration (x) were the upper plateau (d), the lower plateau (c), the hill slope (b), and the inflection point (f). The inflection point (f) corresponds to the half maximal effective concentration (EC50). The base of the exponential is e (Euler's number).

Exponential models of change in parasite numbers (Equation 2) were determined for each site in R. Exponential multiplication was assumed to dominate the replication period.

$$P(t) = P(0) * (e^c)^t$$

Equation 2 Exponential model for change in parasite numbers. $P(t)$is the number of detected parasites at a certain time after infection (in h), $P(0)$ is the hypothetical number of parasites at this site assuming an exponential growth over the whole range of the time after infection, e^c describes the fold change in parasite numbers per h, t is the time of infection of interest (in h)

Results

Transfected *T. cruzi* expressing eGFP in the replicating life-cycle stages

To enable fluorescence-based live imaging, *T. cruzi* STIB980 epimastigotes were transfected with a linearized plasmid containing the *eGFP* gene (enhanced green fluorescent protein) under control of the rRNA promoter (Figure 8 A), which was designed to integrate into the spacer region within the genomic rRNA locus. Fluorescent metacyclic, amastigote, and trypomastigote forms were derived from the transfected and cloned epimastigote transformants as described (Methods). eGFP expression was detected in the replicating stages of the transfected parasite line by flow cytometry and epifluorescence microscopy (Figure 8 B - F). As quantified by flow cytometry, the green fluorescence levels (excitation 488 nm, emission 522 nm) in epimastigote forms were about 100 times higher than the autofluorescence levels of non-transfected cells (Figure 8 B). Epifluorescence imaging showed an even distribution of eGFP throughout the cytosol in epimastigotes and amastigotes, the two replicating stages (Figure 8 C and E, respectively). Green fluorescence could also be detected in the flagellum of epimastigotes and the short flagellum of amastigotes. In contrast, in the non-replicating stages, the metacyclic trypomastigotes and trypomastigotes (Figure 8 D and F, respectively), green fluorescence was barely distinguishable from the autofluorescence of the non-transfected parent. While the epimastigote replication rate of the transgenic *T. cruzi* line was nearly unaltered (Supp. Fig. 1A), the infectivity of the transgenic trypomastigotes was slightly lower than that of the wildtype trypomastigotes (Supp. Fig. 1B).

When cultivated for approx. 4 months in the absence of antibiotic selection, the ratio of the transgenic *T. cruzi* amastigotes still expressed eGFP at a detectable level was reduced to approx. half of a recently introduced population (Supp. Fig. 1D). When epimastigote forms of the transgenic *T. cruzi* line were cultivated without antibiotics for six months, about 96% still expressed eGFP (Supp. Fig. 1C, Supp. Tab. 1). For this reason, amastigote cultures were only maintained for 4 weeks after they had been derived from epimastigotes.

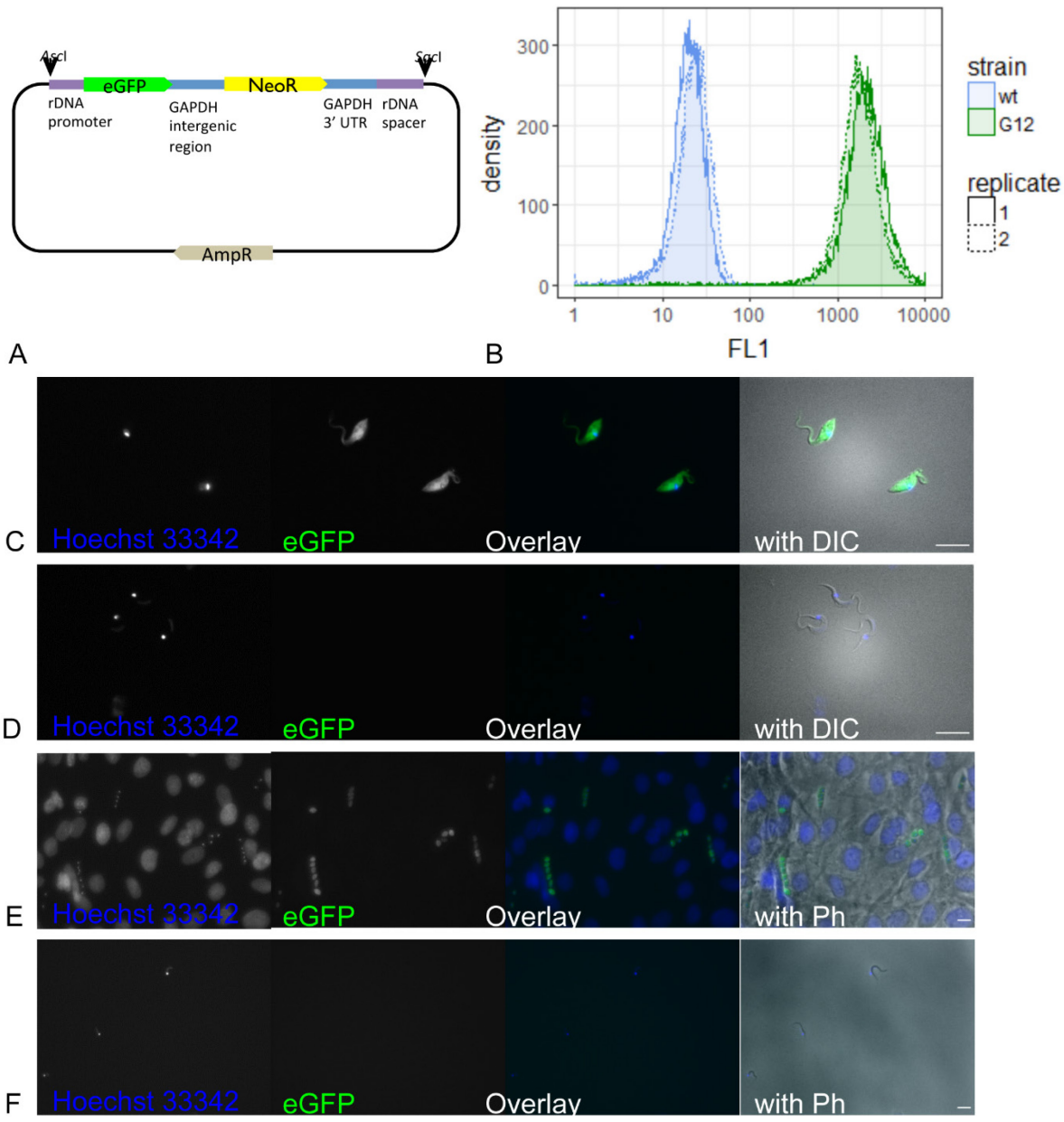

Figure 8 **Transgenic parasites transfected with pTRIX2-eGFP.** (A) The plasmid pTRIX2-eGFP was constructed by inserting the enhanced green fluorescent protein gene into the *T. cruzi* rDNA targeting plasmid pTRIX2-RE9h (Lewis et al., 2014). (B) Fluorescence levels of transfectant (G12) and wildtype (wt) epimastigotes were measured with flow cytometry. Epifluorescent images of transfectants in epimastigotes (C), metacyclic trypomastigotes (D), amastigotes in MEF (E), and trypomastigotes (F). Epimastigotes and metacyclic trypomastigotes were imaged with 630x magnification for 200 ms on DIC, 100 ms with the A4 filter cube (Hoechst 33342), and 300 ms with the L5 filter cube (GFP). Amastigote-infected MEF and trypomastigotes were imaged with 400x magnification for 50 ms with phase-contrast, 50 ms with the A4 filter cube (Hoechst 33342), and 815 ms with the L5 filter cube (GFP). Scale bars represent 10 µm.

A new assay design for live monitoring of drug action

We have devised a new plate design combined with a special imaging scheme that enables observation of parasite development over 6 days, with only 24 h of user time on the high-content microscope (Figure 9). The mammalian cells were cultured in 96-well plates, but were not all infected with *T. cruzi* at the same time (Figure 9 B). Instead, every 24 h, a new row of 10 wells was infected with an MOI of 3:1 (Figure 9). 24 h post infection (hpi), the wells were washed thoroughly to remove extracellular parasites. Then, 7 wells were treated with a 3-fold serial dilution of test compound, while the remaining wells were left untreated. Thus in every row on the plate, the parasites had the same period of infection and the same period of drug exposure. In every column, the parasites were exposed to the same drug concentration. By day 6, when all the rows were used up, the infection period covered 1 to 6 days and drug treatment from 0 to 5 days. The plate was then placed into the microscope for automated live imaging over 24 h. Every 4 h, images were taken from 9 sites per well on the eGFP channel for parasite quantification as well as with transmitted light for quality control. After 24 h, the plate was fixed with 10% formalin and stained with Hoechst 33342. All 9 sites per well were imaged once again on the DAPI channel, eGFP channel, and with transmitted light. The DNA stain enabled the number of host cells to be determined by nuclei count (5 – 30 µm round objects), with the number of parasites inferred from counting their kinetoplasts (1 – 10 µm round objects). The parasite kinetoplast is brighter than the parasite nucleus, because the AT-rich kinetoplast DNA binds Hoechst preferentially (Wheeler et al., 2012).

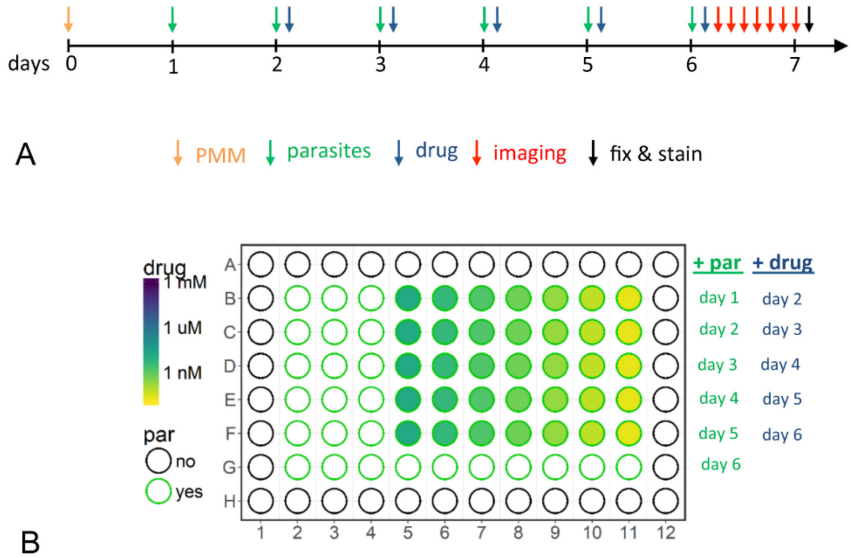

Figure 9 **Assay design.** The timeline of the experimental set-up (A) and plate design (B). On a 96 well plate, a new set of wells containing expanded peritoneal mouse macrophages (ePMM) was infected every 24 h. Extracellular parasites were removed 24 h hpi and drugs were added in 3-fold serial dilution. On day 6, after addition of parasites and drugs (either benznidazole or posaconazole), the plate was imaged on 9 sites per well over 24 h every 4 h (live imaging). After 24 h live imaging, the plate was fixed and stained with Hoechst 33342 and imaged again (fixed imaging). Green fluorescent parasites per image were detected for all images (from live and fixed imaging) of the green fluorescent channel. Kinetoplasts per image were detected on images of the DAPI channel (fixed imaging).

High-content imaging reveals the high degree of variability in untreated cultures

All assays were performed as biological triplicates, which resulted in a total of 27,540 fluorescent microscopy images per drug tested. On every image of the eGFP channel, the number of green fluorescent parasites was determined; on the DAPI channel images of fixed cells, the numbers of host nuclei and parasites (on basis of kDNA) were also determined.

Parasite numbers per image were driven by the time post infection, drug concentration, and the drug exposure time (Figure 10). There was a high degree of variability: between the days of infection (rows on the plate), between replicate wells in the same row, and even between different sites in the same well. Nevertheless, there were common trends in the dynamics of infection (Figure 10 A and B). In the untreated control cultures, the increase in parasite numbers over the period of infection (6 days) could be separated into three phases. During the first 24 h, the increase was usually the most pronounced, but also displayed the highest variance, consistent with settling of parasites into the focal plane and the differentiation of trypomastigotes, that barely expressed eGFP, to amastigotes that express eGFP. During days 2 to 4, parasite numbers, as determined by green fluorescence, continued to increase, consistent with amastigote replication, but began to level off towards day 4 (Figure 10 A). On days 5 and 6, parasite numbers inferred from the green fluorescent channel increased only slightly, if at all (Figure 10 A). Around day 4, differentiation to trypomastigotes dominated the development in parasite numbers over amastigote replication. Fixation of cells allowed a direct comparison between the parasite numbers determined by green fluorescence and those determined from DNA-staining of the kinetoplast (Figure 10 A and B and Supp. Fig 2). The latter method returned higher numbers. Parasites detected as kDNA on the DAPI channel, but not on the eGFP channel, could be either trypomastigotes that did not express eGFP, dead parasites whose kinetoplast was still intact, or revertants that no longer expressed the *eGFP* gene. During the middle phase (day 3 post infection), the proportion of parasites detected on the green fluorescent channel to parasites detected on the DAPI channel was 0.95. This suggests that the plateauing of eGFP-positive parasites at later time points was due to the transformation of intracellular amastigotes to trypomastigotes and not to a loss of the *eGFP* gene.

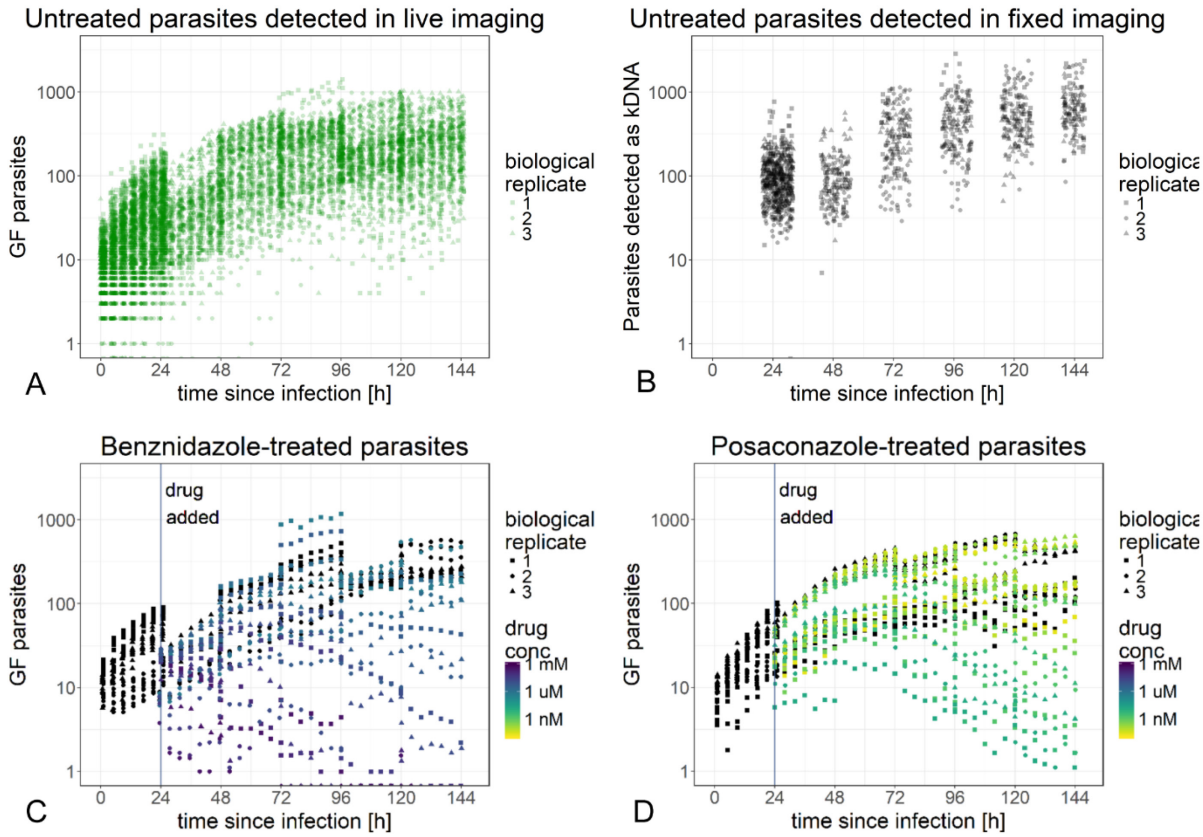

Figure 10 **Parasite numbers over time after infection and drug exposure.** The assay design was used to monitor the development of parasite numbers for posaconazole and benznidazole treated parasites. Number of untreated parasites per image over time after infection are depicted from live (A) and fixed (B) imaging with detection as green fluorescent parasites or as kinetoplasts, respectively. Mean number of treated parasites per image per well is depicted for benznidazole (C) and posaconazole (C) in live imaging detected as green fluorescent parasites. Untreated controls are depicted in black (C, D).

In our experience, ePMM are the best suited for long-term, high-content experiment in respect to their longevity and parasite detection rates on the DAPI channel (Cal et al., 2016). But even with ePMM, the host cell numbers (per image) were decreasing slightly, yet significantly, over the course of the imaging period of a biological replicate batch (from the first plate of a batch (benznidazole) to the last plate of a batch (posaconazole), a total of 5 days, Supp. Fig 3A). This led to a slight increase of the parasite to host cell ratio in older host cells (Supp. Fig. 3B). The host cells were unevenly distributed over a well, which additionally could have influenced the variability in parasite numbers. The host cells were relatively tolerant to benznidazole and posaconazole, with EC50 values of >345 µM and >143 nM, respectively (Supp. Fig. 4).

The decrease in EC50 values over time of drug exposure is a characteristic feature of a drug

For each time point of drug exposure, the growth relative to the untreated control at the same stage of infection depends on the drug concentration. A four-parameter log-logistic model was used to determine this relationship and the half maximal effective concentration (EC50, Figure 11 A and B).

The predictions of the dose-response models in comparison to the counted parasite numbers over time are shown in Supp. Fig. 5.

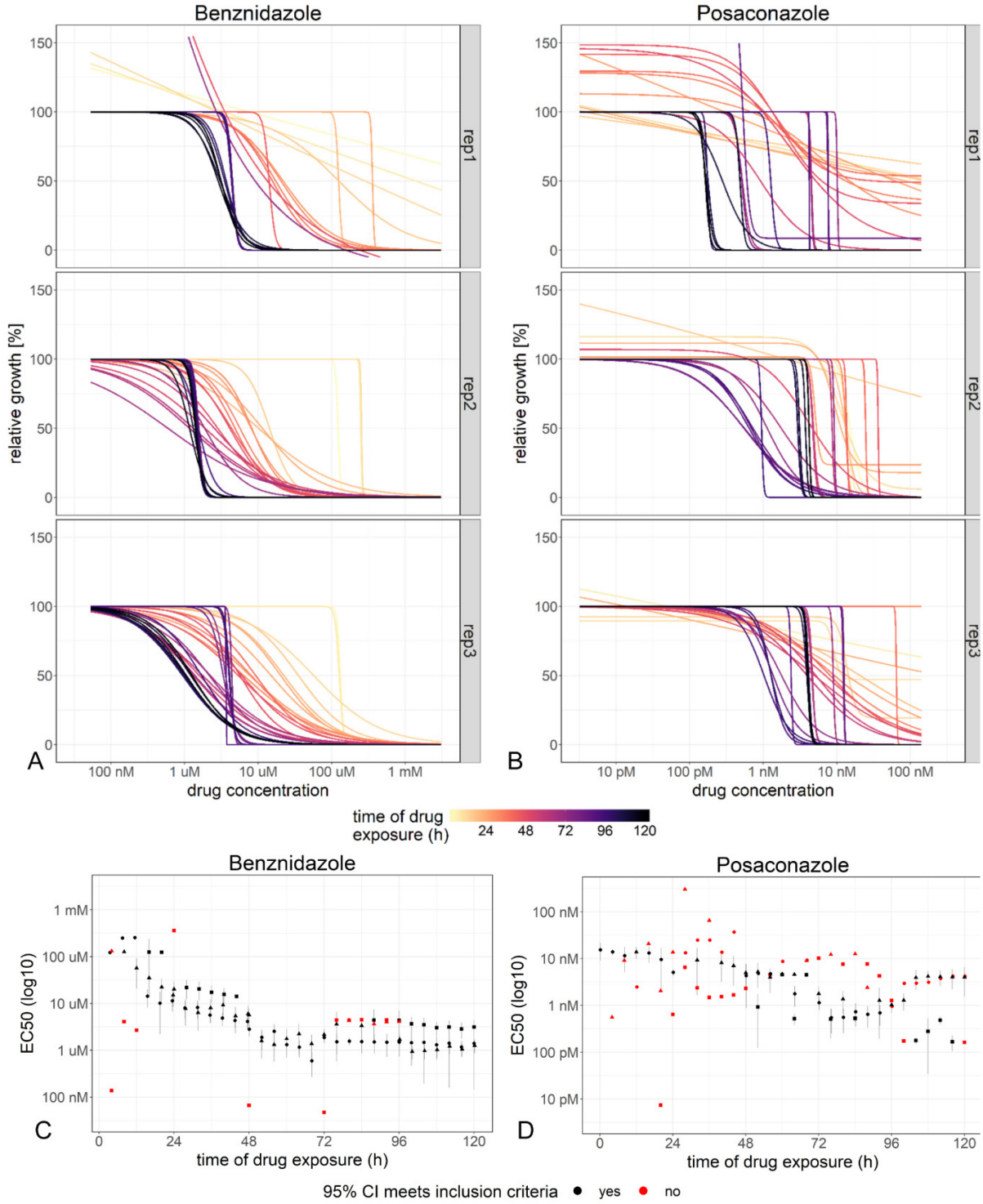

Figure 11 **Development of the concentration of half-maximal effect (EC50) over time of drug exposure.** Dose-response curves were estimated for each time point after drug exposure by modelling growth relative to the same-aged untreated control using the "drc" package in R for benznidazole-(A) and posaconazole-treated (B) parasites. The resulting estimates of the EC50 are plotted over time of drug exposure (C, D). For several time points the 95% confidence interval of the EC50 value did not meet the inclusion criteria, i.e. upper and lower limits less than tenfold higher or lower than the EC50 value.

Over the time of drug exposure, the EC50 values decreased until they reached a stable minimum (Figure 11 C and D). How soon the final EC50 value was reached, was as characteristic for a drug as the final EC50 value itself. For benznidazole, the EC50 value decreased from a median value of 15 µM (with 95% confidence intervals ranging from 6.7 µM to 29 µM) after 24 h of drug exposure to 1.7 µM (with 95% confidence intervals ranging from 0.66 µM to 2.7 µM) after 52 h of drug exposure. Afterwards, the majority of the EC50 values remained in this range. In contrast, for posaconazole, during the first 48 h, only 12 EC50 values could reliably be determined with a median of 9.4 nM (95% confidence intervals ranging from 0.88 nM to 22 nM). 52 h after drug exposure, an EC50 value could be determined in all replicates for the first time with a median value of 4.8 nM (95% confidence intervals ranging from 0.12 nM to 8.0 nM). Afterwards, the majority of the EC50 values remained in this range.

The EC50 values in these experiments were highly variable, even between biological replicates. At some time points, the EC50 values could not be determined with a reasonable 95% confidence interval. This is consistent with the fact that the parasite numbers have a high variability even in the untreated culture. Thus, classical end-point read-outs such as EC50 may not be the most suitable method for quantifying drug action with live imaging. We therefore aimed for a more robust read-out.

The change in parasite numbers at each site can be quantified in an exponential model

At every imaged site, the same set of host cells was observed over the 24 h period of imaging. Therefore, for each site, the change in parasite numbers between time points in this 24 h interval (as exemplified in Figure 12 A) only depended on the age of infection, the drug concentration, and the time of drug exposure. We determined an exponential model for parasite numbers over time at every imaged site (Methods, Equation 2).

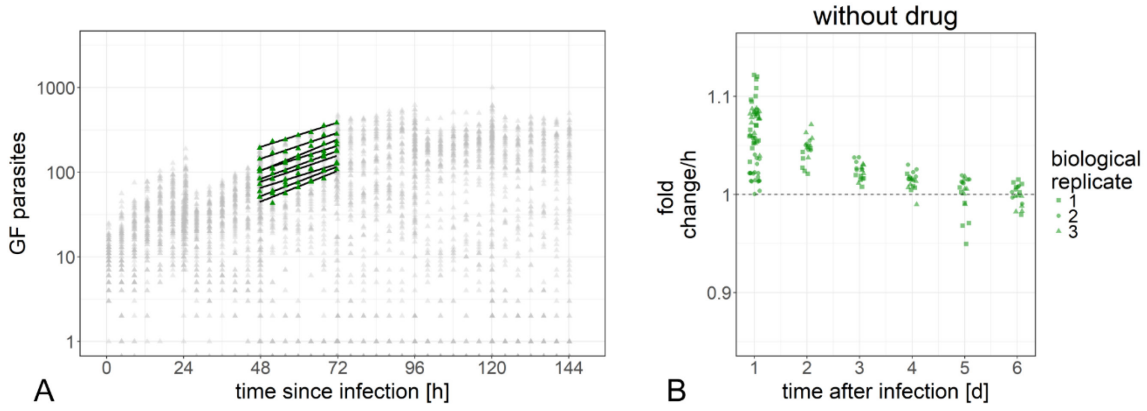

Figure 12 **Exponential model of the development of parasite numbers over time.** Numbers of green fluorescent parasites from one plate are plotted over time after infection (A). The parasite numbers obtained at the seven time points from the 9 sites in one well from this plate are highlighted in green as an example. The exponential models (Methods) determined for every site of this well are plotted for illustration. The variable "fold change per h" of those exponential models for every site of all plates changes between days after infection (B).

This exponential model of change in parasite numbers has two parameters: the offset P(0) and the slope c (Equation 2). In the logarithmized version of the equation, the slope c can be negative, zero

or positive, corresponding to declining, stagnating and growing parasite numbers, respectively. The slope c is a net result of replication rate, differentiation rate, and parasite reduction rate. The offset (basal parasite number, P(0)) is an extrapolation of the number of parasites in the monitored region at the time of infection.

Most of the observed variability in parasite numbers was captured by the variability in P(0), which already differed between different sites of one well. This was to be expected since the numbers of infected host cells are not evenly distributed over the whole well, and some infected host cells would have been infected by more than one parasite.

While the extrapolated basal parasite number P(0) was very variable, the fold change in parasite numbers (i.e. the exponential of the slope, e^c) was more robust, especially between days 2 – 4. In addition, the fold change is more informative as it directly reflects the difference between replicating and dying amastigotes (at least in the early phase, when the amastigotes do not differentiate to trypomastigotes; Figure 12 B). For these reasons, we used the fold change of parasite numbers over time of drug exposure to characterize drug action. In particular, we focused on the tipping point of drug action, i.e. the time point when the death rate of the parasites exceeded the growth rate, and the fold change dropped below 1.

The tipping point of drug action is a sensitive and robust readout

The fold change in parasite numbers in drug-treated cultures was calculated based on the exponential model of parasite replication. Initially, the parasites continue to replicate, although often more slowly than in the untreated control. After some time of drug exposure, at certain concentrations, parasite numbers start to decrease, i.e. parasites are dying. Once most parasites are killed, the parasite numbers will not decrease further and the fold change will approximate to 1. If the fold change exceeds 1 again, this might indicate that surviving parasites are replicating, or reflect an issue with drug stability. Certain drugs might be cytostatic at some concentrations. In this case, the net fold change would be stable at approx. 1 over the whole period of drug exposure.

The tipping point was defined as the time point immediately after the net fold change dropped below 1. The tipping point of drug action is both time- and concentration-dependent. Figure 13 shows the fold change in parasite numbers for each concentration and for every day post drug exposure. For each replicate and each drug concentration, the tipping point, i.e. the day when the fold change in parasite number has significantly dropped below 1 (95 % confidence interval excluding 1), is marked.

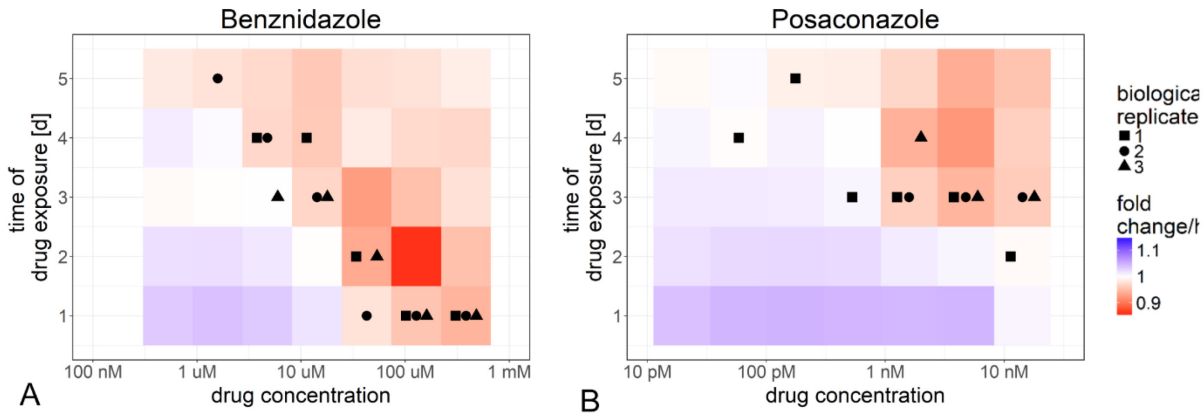

Figure 13 **The fold change in parasite numbers of drug-treated parasites depends on drug concentration and time of drug exposure.** The fold change in parasite numbers was obtained by exponential models of change in parasite numbers for every site (Methods). The fold change in parasite numbers depended on the concentration and time of exposure with benznidazole (A) and posaconazole (B). The first day of drug exposure, at which the fold change was significantly below 1, is indicated for every replicate.

In the benznidazole-treated wells, parasite numbers started to decrease within the first 24 h of drug treatment at the highest concentrations. After 48 h, parasite numbers reached 0 for the highest concentration. In the posaconazole-treated wells, parasite numbers continued to increase for at least 2 days. For benznidazole, there was a correlation between drug concentration and the tipping point of drug action (Figure 13 A). In contrast, in most cases, the posaconazole-treated parasites only started dying during the third day of drug exposure, even at the highest concentration (Figure 13 B). In summary, calculating the tipping points allowed the measurement of time- and concentration-dependence of drug action against intracellular *T. cruzi* amastigotes, and illustrated potential shortcomings of posaconazole as compared to benznidazole.

Discussion

The target candidate profile for Chagas disease is very demanding. A successful preclinical candidate needs to demonstrate high activity against a broad range of *T. cruzi* strains from all DTUs (Zingales et al., 2014). The activity needs to be selective (i.e. a high selectivity index) and trypanocidal, i.e. leading to irreversible clearance of parasites. Preferably, this activity is achieved quickly. Due to the diversity of aspects in activity, there is no single one assay design to test for all requirements. A hit from a predictive primary assay will have to pass through a panel of secondary assays. The LacZ assay (Alonso-Padilla & Rodriguez, 2014; Buckner et al., 1996) with its high throughput capacity is an attractive primary assay. Several secondary assays have been established in the last few years, in particular wash-out assay designs (Cal et al., 2016; MacLean et al., 2018; Sykes & Avery, 2015) and formats like the clonal outgrowth assay (Shah-Simpson, Pereira, Dumoulin, Caradonna, & Burleigh, 2016) to measure irreversible cidality. High-content microscopy has led to great innovation in kinetoplastid drug discovery (Alonso-Padilla et al., 2015; Alonso-Padilla & Rodriguez, 2014; De Rycker et al., 2016; Engel et al., 2010; Moraes et al., 2014; Neitz et al., 2015; Nohara et al., 2010; Yazdanparast et al., 2014). It combines the high throughput capacity of systems such as the LacZ assay (Alonso-Padilla & Rodriguez, 2014; Buckner et al., 1996) with detailed information on the numbers of parasites and host cells. Nuclear staining as a read-out allows high-throughput *in vitro* assays to be undertaken with a broad panel of strains (Moraes et al., 2014). Furthermore, high-content assays with nuclear staining allow for a direct determination of selectivity indexes. However, the use of nuclear staining generally requires fixation of the cells, precluding live imaging over several days to observe the time-course of drug action. Live imaging can be more easily done with fluorescent *T. cruzi* reporter lines.

We established an eGFP expressing parasite line for use in live imaging assays. This parasite line expresses eGPF in high levels from the ribosomal locus, but only in the replicating life-cycle stages. This is in line with the observation that the reduction of transcription in the non-replicating (metacyclic) trypomastigote stage is particularly pronounced for ribosomal loci (Elias, Marques-Porto, Freymuller, & Schenkman, 2001).

The new assay design presented here enables the monitoring of *T. cruzi* amastigote replication for 6 days post-infection, and drug action over 5 days of exposure, in four-hourly intervals. Nine sites per well can be monitored separately. This not only creates a wealth of data – it also reveals a high degree of variability in *T. cruzi* numbers, not only between different wells and different days of infection, but also between different sites in the same well, infected on the same day. This complicated the EC50 determination at each time point.

In contrast, the fold change per h in the number of parasites over the period of 24 h after drug incubation is a sensitive and robust measure of pharmacodynamics. The fold change on a specific day of infection was very reproducible within wells, between wells, and between days of infection. The

fold change is influenced by the drug concentration and the time of drug exposure. For each drug concentration, we can determine the day of drug exposure at which the net fold change per h drops significantly below one. At this tipping point, the death rate of the parasites exceeds the growth rate. The graphical representation of the fold change per h of parasite numbers in relation to drug concentration and exposure time clearly depicts the different pharmacodynamics of benznidazole and posaconazole. For benznidazole, the time-to-kill decreased roughly exponentially with increasing drug concentration. In contrast, even at the highest concentrations of posaconazole tested, the net killing only started after 3 days of drug exposure.

The concept of monitoring growth of intracellular *T. cruzi* via rates (i.e. fold change) and determining the tipping point of drug action provides a novel pharmacodynamic parameter to determine time-to-kill that can be applied to any assay design employing repetitive imaging of the same site. The fold change in parasite numbers can readily be incorporated to PK-PD modelling, as mathematical modelling requires rates. We propose to introduce the concentration-dependency of the tipping point of drug action as a novel measure to benchmark drug candidates for Chagas' disease *in vitro*.

Acknowledgement

Isolation and expansion of peritoneal macrophages was performed by Romina Rocchetti. Monica Cal provided cell and parasite culture support and support with high-content microscopy. Dr. Remo Schmidt supported the molecular biology and basic statistical analyses. We kindly thank Prof. Dr. Till Voss and his group for letting us use the high-content microscope. Special thanks to him and Dr. Nicolas Brancucci for fruitful discussions on high-content use. We thank Prof. Dr. Antonio Osuna for the kind provision of the *T. cruzi* strain. We thank Prof. Dr. Joachim Clos for the kind provision with the LADMAC cells. This work would not have been possible without the financial support of the Swiss National Science Foundation, the Nikolaus und Bertha Burckhardt-Bürgin-Stiftung, and the Freiwillige Akademische Gesellschaft. Olivier Braissant's work is supported by the Merian Iselin Stiftung

Supporting information

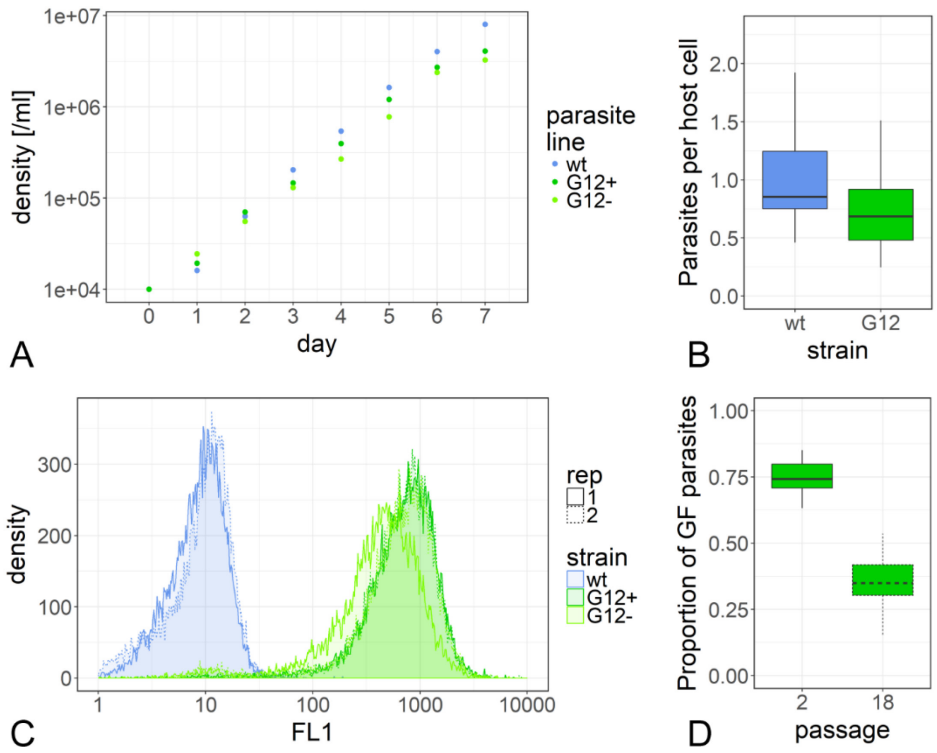

Supp. Fig 1. **Epimastigote replication (A), trypomastigote infectivity (B), transgene expression stability in epimastigotes (C) and amastigotes (D) of the transgenic parasite line.** Epimastigote density (A) was quantified daily after inoculum of 10^4 epimastigotes/ml using the Neubauer chamber. Wt denotes the STIB980 wildtype, G12+ the eGFP-expressing STIB980 line cultivated constantly in 500 µg/ml G418, and G12- the eGFP-expressing STIB980 line cultivated for 5 months without any antibiotic selection pressure. (B) Infectivity was measured using high-content microscopy of Hoechst-stained ePMM infected with the MOI 5:1 for 48 h. (C) Phenotypic transgene stability was measured in epimastigotes by flow cytometry in two replicates. The geometric mean of the fluorescence level of the parasite population and the proportion of green fluorescent parasites were determined (Supp. Tab.1). (D) In amastigotes, phenotypic transgene stability was measured by simultaneous comparison of ePMM infected for 5 days with a MOI 5:1 using trypomastigotes, which have either been passaged weekly 2 or 18 times in a Mef culture.

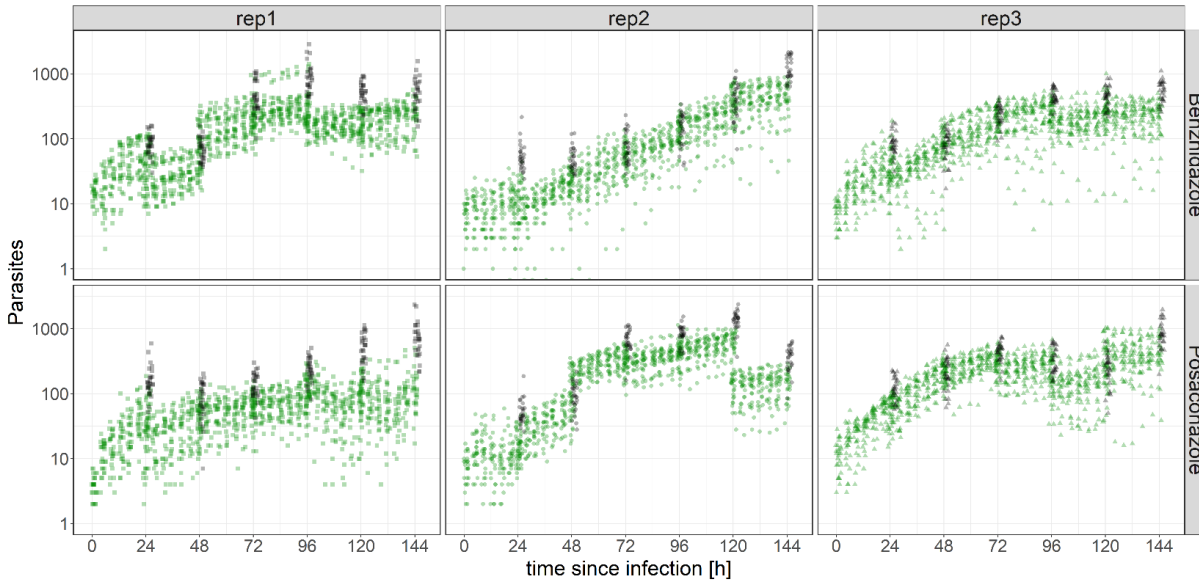

Supp. Fig 2. **Development of parasite numbers over time for all replicates separately.** Parasite numbers per image from untreated wells of all biological replicates from live imaging (green, detected as eGFP positive parasites) and fixed imaging (black, detected as kinetoplasts).

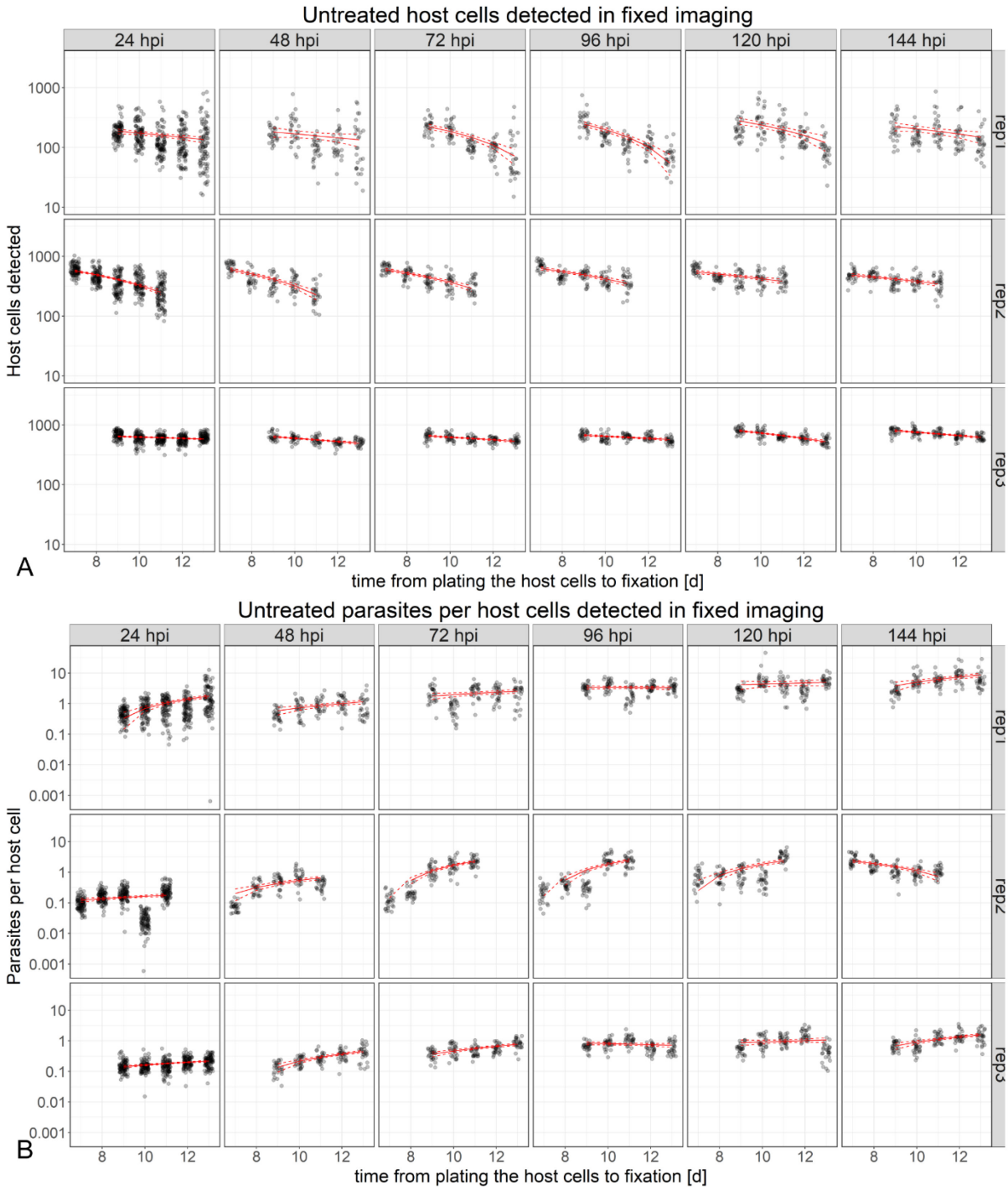

Supp. Fig 3. **Development of host cell numbers over time for all replicates.** Host cell numbers per image (A) and parasites per host cell numbers per image (B) from untreated wells of all biological replicates from fixed imaging (black, parasites detected as kinetoplasts) in relation to time passed between plating the host cells and fixing the plate. Linear models of the correlation and their 95% interval are plotted in red.

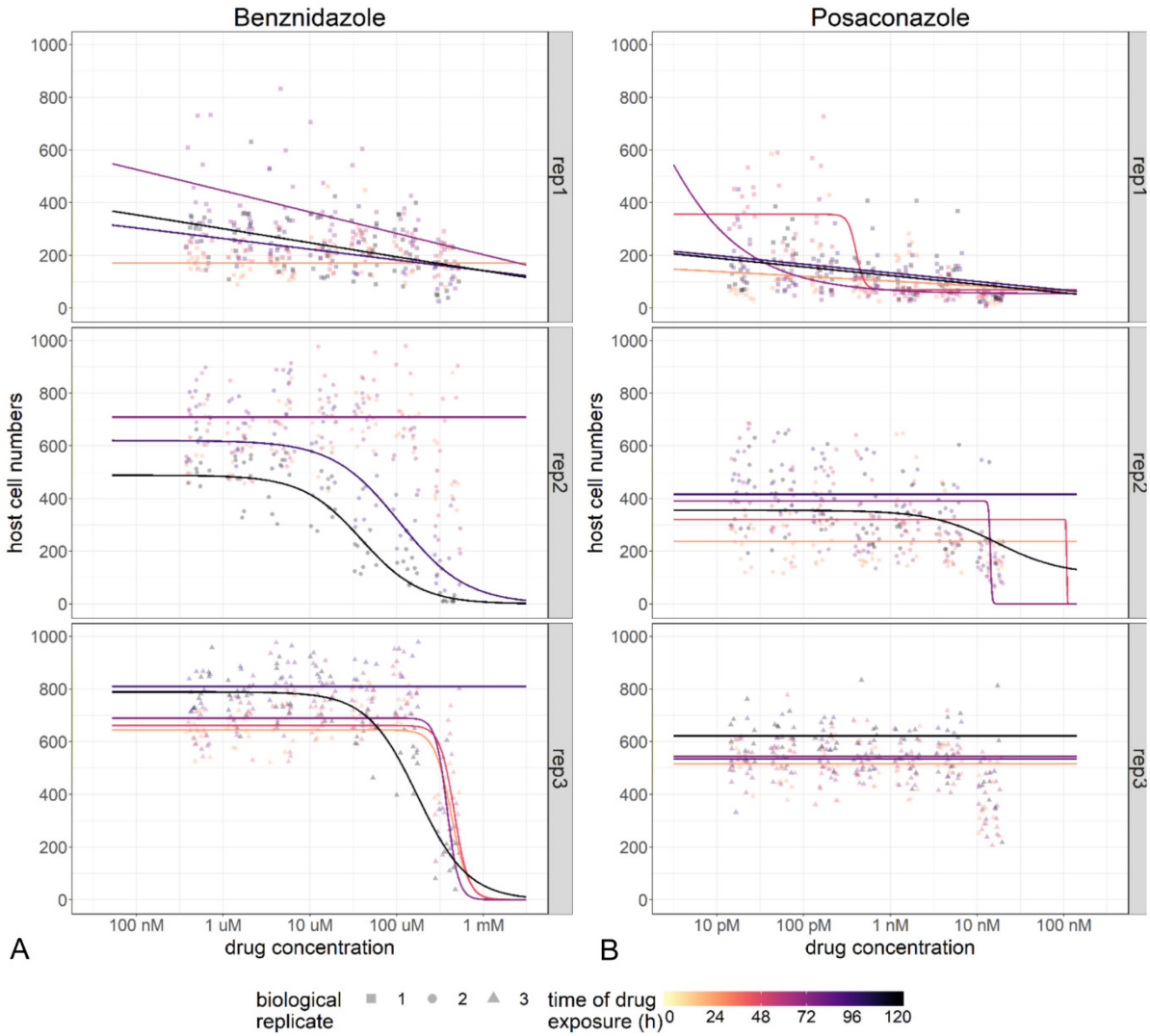

Supp. Fig 4. **Development of host cell numbers over time and drug exposure.** Host cell numbers per image at the given drug concentrations (of benznidazole (A), and posaconazole (B)) and the respective dose-response curves estimated using Equation 1 with the R package "drc" for all time points, at which a dose-response curve could be estimated.

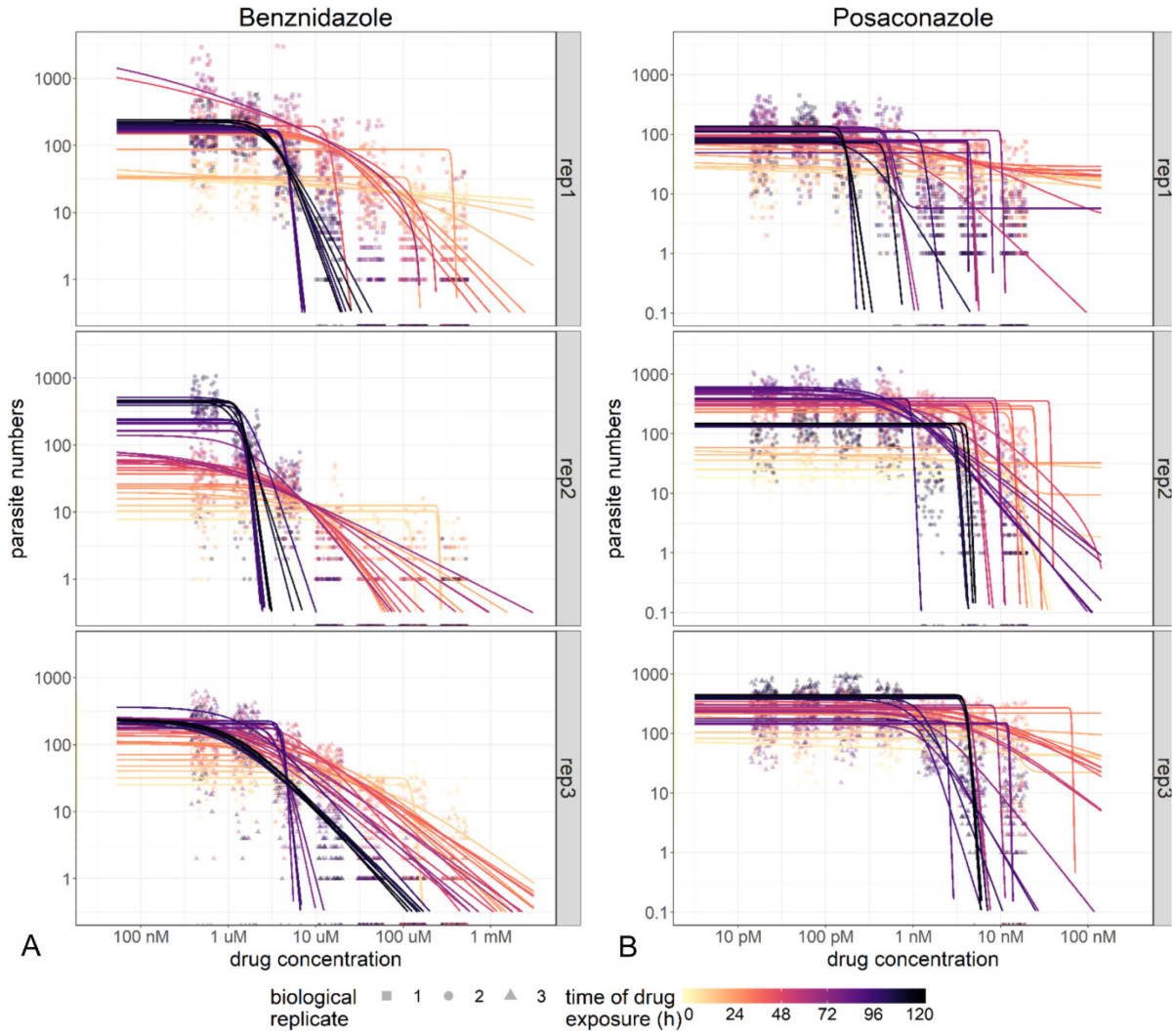

Supp. Fig 5. **Development of parasite numbers over time and drug exposure.** Parasite numbers per image (detected as green fluorescent parasites in the live imaging) at the given drug concentrations (of benznidazole (A), and posaconazole (B)) and the respective dose-response curves estimated using Equation 1 with the R package “drc” for all imaged time points. The y-axis in logarithmic scale to illustrate the parasite development over time.

Supp. Tab. 1. **Stability of transgene expression in *T. cruzi* epimastigotes.**

Phenotypic transgene stability was measured in epimastigotes by flow cytometry in two replicates. The geometric mean of the fluorescence level of the parasite population and the proportion of green fluorescent parasites were determined. Wt denotes the *T. cruzi* STIB980 wildtype, G12+ the eGFP-expressing STIB980 line cultivated constantly in 500 µg/ml G418, and G12- the eGFP-expressing STIB980 line cultivated for 5 months without any antibiotic selection pressure.

	RFU (geometric mean)		**% Green fluorescent parasites**	
	Replicate 1	**Replicate 2**	**Replicate 1**	**Replicate 2**
wt	8.3	8.6	0.110	0.367
G12+	640.0	670.0	98.9	98.3
G12-	580.0	790.0	96.4	96.1

Discussion and Outlook

The scope of the project

This project contributed to *in vitro* drug discovery for Chagas' disease in our group and in general. We established the methodology for molecular genetics of *Trypanosoma cruzi* and performed whole genome sequencing of *T. cruzi* strain STIB980. With those tools established, we generated a eGFP-expressing *T. cruzi* parasite line. And with this parasite line, I developed a live *in vitro* assay design resulting in a novel analysis pipeline and a novel read-out to monitor pharmacodynamics.

Etablishing tools for molecular genetics in *Trypanosoma cruzi*

Genotyping of *Trypanosoma cruzi* STIB980

The genetic make-up of *T. cruzi* parasites is thought to influence the disease phenotype and drug sensitivity (Zingales et al., 2014). Therefore, it is recommended to test drug candidates to a variety of *T. cruzi* strains (Zingales et al., 2014). In this context, it was important to genotype the *T. cruzi* strain which we sought to establish as an assay strain for live imaging. Genotyping according to Messenger et al. (2015) revealed that the strain belongs to distinct typing unit (DTU) TcI and had been wrongly annotated as Y strain. This result highlights the importance of genotyping when working with strains from old collections. DTU TcI is important for cardiac symptoms in humans (Zingales et al., 2012). In humans, DTU TcI is predominentally distributed North of the Amazon basin (Izeta-Alberdi et al., 2016). Belonging to the clinically relevant DTU TcI, our selected *T. cruzi* strain is a good choice for drug testing.

However, it is not clear whether drug sensitivity really is a DTU-specific trait. It seems very likely that drug sensitivity varies as much between strains within one DTU as between different DTUs (Moraes et al., 2014). Therefore, it would have been desirable to determine the exact origin of the strain. However, the glucose-6-phosphate isomerase (G6PI) sequence, which is an isoenzymic marker of *T. cruzi* (Broutin, Tarrieu, Tibayrenc, Oury, & Barnabe, 2006), of our strain showed SNPs in comparison to the G6PI sequences of *T. cruzi* Sylvio and *T. cruzi* Dm28c, the DTU TcI reference strains, for which we had genomic DNA available. We could therefore only conclude that our strain is neither Sylvio nor Dm28c. Thus, we named it according to our internal system: *T. cruzi* STIB980. We determined the drug sensitivity profiles of *T. cruzi* STIB980 epimastigotes and amastigotes against benchmark drugs.

If we want to establish *T. cruzi* STIB980 as a reference strain for drug discovery, it will need features that make it useful. For this purpose, we wanted to establish the expression of at least one reporter gene. The most useful reporter for high-content assays and in vivo studies would be the Luciferase-Neon fusion protein from the London School of Hygiene and Tropical Medicine (Costa et al., 2018). If the strain is to be used for screening, establishing *LacZ* expression would be useful as well (Buckner et al., 1996). Both plasmids were kindly donated by the respective research groups.

Therefore, we plan to establish those reporter genes in *T. cruzi* STIB980. Whatever the transgene, a careful phenotypical characterization of the transfectants needs to be warranted.
One established feature that is certainly useful is the genome sequence of *T. cruzi* STIB980, assembled from Nanopore sequencing with SNP correction by Illumina reads.

The genome sequence of *Trypanosoma cruzi* STIB980

The genome sequence of *T. cruzi* STIB980 will support mode-of-action studies and the genetic manipulation of the parasite line. For mode-of-action studies, transcriptomics of resistant parasite lines or of drug-exposed parasites are planned. For the correct mapping of Illumina reads, the corresponding genome sequence will be very useful. The genome sequence is also useful for the genetic manipulation of *T. cruzi* STIB980. The exact sequence of a strain is essential for correct primer design. Furthermore, the genome sequence can help when fragments for homologous recombination should be ordered commercially.

In general, the genome assembly obtained with the programs Canu and Pilon is satisfying for these purposes. In my opinion, *T. cruzi* defies the relevance of chromosome level assembly. The chromosome numbers vary between *T. cruzi* strains and the chromosome sizes vary between homologous chromosomes (Souza et al., 2011). The *T. cruzi* CL Brener reference sequence is assembled to chromosomes, but at the prize of enormous stretches of gaps filled with the letter N. A small number of large contigs may be more useful.

For our purposes, we wanted to make sure that the core compartment of the *T. cruzi* STIB890 genome was assembled correctly. The disruptive compartment is defined as the non-syntenic regions of the genome composed mainly of the multigene families of the trans-sialidases (TS), mucin-associated surface proteins (MASP), and mucins (Berna et al., 2018). Due to its repetitive nature, the disruptive compartment is intrinsically more difficult to assemble. While Berna et al. have reported the successful resolution of previously collapsed sequences of the disruptive compartment (Berna et al., 2018), this might remain a unique case until long-read sequencing is firmly established in kinetoplastid research. The highly repetitive nature of the disruptive compartment might contribute to genomic plasticity in *T. cruzi*. Genomic plasticity still remains to be studied in more detail; nevertheless, it can be assumed that the genomic plasticity increases the likelihood of loss of transgenes.

Transgene expression levels and stage-specificity

The eGFP-transfected derivative of *T. cruzi* STIB980 expressed the green fluorescence only in the replicating stages. As eGFP was expressed from the ribosomal locus, it was expressed at high levels in the replicating stages. In contrast, the (metacyclic) trypomastigotes barely expressed green fluorescence. This was not surprising, as expression in general, and specifically from the ribosomal

locus, is drastically reduced in trypomastigotes (Elias et al., 2001). This phenomenon had been observed before (Kessler et al., 2013). Therefore, Costa et al., using the pTRIX2-LucNeon to integrate the fused reporter into the ribosomal locus, specifically tested for green fluorescence in the trypomastigote stages with confocal microscopy (Costa et al., 2018). They were able to detect green fluorescence. However, they did not compare the fluorescence levels to those of the replicative stages.

Kessler et al. propose to make use of this stage-specificity for *in vitro* assays, to specifically test for compounds killing the replicating stages. However, I will argue later that inhibition of replication is not necessarily the most suitable read-out in Chagas' disease drug discovery.

We have also tried to establish a stage-specific reporter parasite line. In a first attempt, we tried to replace stage-specific surface genes with a fluorescent reporter, i.e. one *amastin* gene (TcCLB.509965.390) and one trypomastigote, alanine, serine and valine rich protein (*TASV*, TcCLB.509147.40, (Garcia et al., 2010)) gene for amastigote-specific and trypomastigote-specific expression, respectively. Both constructs contained a ribosomal promoter and a resistance gene with the *gyceraldehyde 3-phosphate dehydrogenase* (*GAPDH)* 3'UTR, followed by the respective reporter gene under the control of the stage-specific 3'UTR. The integration sites were the 5' and 3' UTRs of the respective stage-specific genes that we wanted to replace.

However, we only managed to establish a parasite line resistant to the selection antibiotic (phleomycin) for the amastigote-specific transfection. For the trypomastigote-specific construct containing the blasticidin resistance, we could not find a discriminative concentration that only killed the wildtype, parental line. We discontinued this project due to time constraints. However, this observation indicates that the expression levels of the resistance genes might have been influenced by a positional effect in the genome. Both constructs were targeting surface proteins. Both amastin and TASV are members of multigene families and therefore likely to be located in the disruptive compartment of the genome. There might be differences in chromatin-composition between the disruptive compartment and the core compartment. The differential expression of surface proteins from multigene families has not been comprehensively studied. Hypothetically, proteins from multigene families might be expressed all at once at extremely low individual abundance. This might indicate a low expression of the individual genes. Another option is that some of the multigene family members are silenced, which would presumably be conferred by heterochromatin, while others are expressed strongly. These questions are not easily answered, as the multigene family members often have only minor differences. Therefore, even the detection of differential expression is really difficult. One study looked at differential expression of MASPs in clonal lines of *T. cruzi* epimastigotes and trypomastigotes (Seco-Hidalgo, De Pablos, & Osuna, 2015). They found different expression patterns in different clones, indicating that there is silencing of some of the multigene family members. The 3'UTR of at least one amastin was shown to confer detectable levels of amastigote-specific reporter

gene expression (Araujo et al., 2011), so it is indeed involved in stage-specific gene expression. In summary, gene expression in *T. cruzi* is regulated not only be the UTRs but also by the location of the gene in the genome.

Parasite sensitivity towards selection markers

Our experience with the stage-specific fluorescent reporters has demonstrated that wildtype sensitivity is not the only factor playing into the choice of antibiotics for selection of transfectants. It is likely that the expression of the blasticidin resistance gene from a trypomastigote-specific locus, which is probably in the disruptive compartment, even under the control of the ribosomal promoter was too low to allow outgrowth of transgenic parasites.

Transgene stability in *Trypanosoma cruzi*

The genetic stability of the eGFP-expressing parasite line was tested phenotypically by flow cytometry in epimastigotes and by high-content microscopy in amastigotes. For transgenes that encode a fluorescent protein, phenotypic testing of the stability is easily feasible with flow cytometry or fluorescence microscopy. It is reasonable to test for the phenotype rather than the genotype. For a useful reporter line, the expression levels of the transgene are more important than its mere presence in the genome. Therefore, phenotypic testing is necessary and relevant. This is straightforward in *T. cruzi* epimastigotes, because in epimastigotes the parasite numbers can easily be determined. Therefore, the phenotypic read-out can be correlated with parasite numbers. In the amastigote stage this is more complicated, as the numbers of amastigotes depend on invasion capacity and replication rate. For this reason, in amastigotes, transgene stability is best determined as genetic stability using qPCR on genomic DNA, comparing transgene abundance with the abundance of a single-copy house-keeping gene.

The requirements for *in vitro* assay design for Chagas' disease

The goal of *in vitro* drug discovery is to find a compound that affects the livelihood of all parasite forms occurring in a patient to a point of no return on the road to parasite death as quickly as possible, at the lowest possible concentration. The concentration of the compound needs to be so low that the patient's cells do not get affected for the duration of the treatment.

The role of replication during *in vitro* assays for Chagas' disease

The majority of the current *in vitro* assays measures endpoint numbers of cells starting from a small inoculum. This favors the detection of inhibitors of replication, e.g. static compounds in addition to

cidal ones. In my opinion, a long drug exposure time in assays is unfavorable for two reasons. One, long drug exposure is a very rare phenomenon *in vivo* due to the pharmacokinetic profile of most compounds. Two, a long drug exposure also means a high degree of replication in the untreated control. Therefore, the measured effect is mostly inhibition of replication. An effect of 50% inhibition of replication is the same as inhibiting one duplication event, e.g, applying a static compound at a 100% effect concentration for one doubling time. Therefore, I would propose drug exposure in a time-window of 1-3 doubling times only. However, this would require the addition of the drug at a later stage in the amastigote life cycle, so that the untreated control give signals that are high enough to discriminate between true and stochastic effects. All this applies for total parasite numbers as well as number of parasites per infected cell.

When the measured effect is the reduction of infected cells, this is a different matter. In a short assay covering only one lytic cycle – not including trypomastigogenesis and reinfection -- a reduction in the proportion of infected cells is always a hint towards cidal compounds. However, when the duration of the assay is longer than a lytic cycle, the proportion of infected cells is the sum of the effects on amastigote replication, trypomastigogenesis, invasion capacity and cidality. These contributions are difficult to disentangle.

Parameters to be optimized in assay design for Chagas' disease

A test compound can affect the parasite in many ways. First of all, and desirably, it can affect amastigote and trypomastigote viability. Less desirably, it can induce "dormant" stages with reduced metabolism and drug sensitivity. Furthermore, a compound can effect invasion capacity, amastigogenesis, replication rate, and trypomastigogenesis. Additionally, a compound could hypothetically boost the cell's (and potentially the body's) defense against the parasite. The primary goal, however, in *in vitro* testing is to find a compound that is cidal against amastigotes, preferably also against trypomastigotes and dormant stages. This leads to the question, how to design an assay, in which the major effect measured is the cidality against amastigotes.

Apart from the measured effects, the discriminatory power of an assay is an important consideration for assay design. This discriminatory power is driven by effect size and the variability of the read-out. The discriminatory power of an assay has been captured by the z-score (Zhang, Chung, & Oldenburg, 1999). In order to increase discriminatory power, one can either increase effect size or decrease variability. Increasing effect size usually means to increase the number of parasites and the proportion of infected cells in the untreated control.

The parameters at hand to focus on measuring cidality against amastigotes and to increase discriminatory power are the total assay duration, the multiplicity of infection, the time of infection,

the duration of exposure, the timing of drug exposure, choice of host cells, the choice of the strain, and the choice of read-outs.

Assay duration obviously depends on the choice of host cells and the choice of the parasite strain. The choice of host cells can influence the assay duration by host cell viability and replication rate. The infectivity, stress resistance and replication rate of the parasite strain can influence the choice of assay duration. A critical question is whether reinfection is wanted during the assay. While reinfection will increase total parasite numbers and the proportion of infected cells in the untreated control, it also expands the measured effects to effects on trypomastigogenesis, invasion capacity, and amastigogenesis.

The multiplicity of infection (MOI) is chosen to maximize the proportion of infected cells and the total number of parasites at read-out in the untreated control. However, a high MOI can potentially shorten the time until trypomastigogenesis and, therefore, reinfection (Abuin et al., 1999). This might decrease the health and therefore total number of host cells, leading to artefacts. The choice of MOI has to be optimized for every combination of parasite strain and host cell type.

The time of infection is the time from inoculation of the host cell cultures with extracellular trypomastigotes until they are washed off. A long time of infection leads to a high proportion of infected cells and high number of parasites at the time of read-out. However, a shorter time of infection might increase the synchronicity of the culture. The time of infection is also subject to practicability in a routine screening setting; e.g. 24 hours of infection might be easier to manage than 12 hours of infection. In addition, shortening the time of infection will likely require a higher MOI to obtain the same proportion of infected cells and number of parasites.

The duration of drug exposure should always be long enough to be able to observe the wanted effects. This also means, that short drug exposure would favor fast-acting compounds. The untreated control continuously grows during the time of drug exposure; parasites will replicate and reinfect. Thus, with an increase in time of exposure, the measured drug effect will consist more of an effect on replication and on invasion and differentiation, in contrast to cidality.

Together with the duration of drug exposure, also the timing of drug exposure needs to be considered. This also will determine which effects are captured in the assay. If the test compound is added before or with the trypomastigotes, effects on invasion capacity and amastigogenesis will also be measured. The earlier a test compound is added, the stronger its effect on replication is favored over its cidality. A late addition of the test compound favors cidal compounds over static compounds, while still enabling high total numbers of parasites and therefore a high discriminatory power of the assay.

The choice of the host cell has a biological component and an assay design component. In general, *T. cruzi* seems to be extremely promiscuous, allowing a broad spectrum of potential host cells

in the assay design. However, the assay should be representative of the situation *in vivo*. Yet, the parasite's host cell preference inside a mammalian host is disputed (Brener & Chiari, 1965; de Diego, Palau, Gamallo, & Penin, 1998; Lewis et al., 2014; Lewis & Kelly, 2016; Vago et al., 1996) and not well understood. There seems to be a strain-dependence for tropism, and the organ preference might also vary between different host species (Flores-Lopez & Machado, 2015). One frequently mentioned host cell type are muscle cells. This might have been an argument for the choice of L6 rat myoblasts in our standard assay design. Yet, especially since the advent of high-content imaging, non-dividing host cells are preferred. Using non-dividing cells precludes the measure of effect on host cell replication. Additionally, non-dividing host cells do not overgrow the well. Overgrown host cells negatively impact both sensitivity and specificity of image-based quantification. An additional aspect for image-based assays is the quality of host cell attachment. Finally, host cell viability and fitness throughout the assay duration needs to be guaranteed.

The choice of the *T. cruzi* strain is an important parameter that is regularly discussed. Assay strains should preferably be representative of the real life situation, i.e. similar to the major strains circulating in in endemic regions. In general, stress-resistant parasites might be preferable. Rather sooner than later, test compounds should be tested against a broad variety of strains (Zingales et al., 2014). This has become more feasible with the advent of high-content imaging and the use of nuclear staining rather than reporter genes (Moraes et al., 2014). Nevertheless, parameters such as MOI and assay duration need to be optimised for every tested strain separately.

Two major read-outs are being used to determine the effectivity of a test compound: proportion of infected host cells and total number of (intracellular) parasites. The number of host cells is easily determined in high-content imaging by the use of nuclear stains. To determine the proportion of infected cells, the host cell cytoplasm needs to be determined. This can be done with a separate stain for the cytoplasm, e.g. phalloidin for F-actin, or with Draq5, which strongly stains the nucleus and the cytoplasm more weakly. However, Draq5 has issues of sensitivity and specificity, as it also decreases the signal-to-noise ratio for the parasite DNA detection. Parasites can be detected by DNA staining, either via the nuclear DNA or via the kDNA. Additionally, fluorescent protein-expressing parasites can be used. Another option is to stain the parasites with antibodies, in particular with stage-specific antibodies to obtain information on the life-cycle stages. Also, transfectants expressing a reporter gene from the ribosomal locus only in replicating stages have been proposed for stage-specific assays (Kessler et al., 2013). However, this needs to be considered carefully, as the absence of fluorescent parasites could indicate parasite death, differentiation, shut-down of metabolism, or mere loss of the transgene. Therefore, I would prefer to not use a ribosomal expressor for a stage-specific read-out.

Another relevant read-out concerns the recently demonstrated dormant stages of *T. cruzi* (Sanchez-Valdez et al., 2018). So far, these have been demonstrated by the retention of a fluorescent stain in the cytoplasm (in contrast to dilution of the stain in dividing cells) or by the absence of a nuclear marker of division (Sanchez-Valdez et al., 2018). However, the dormant stages need to be studied more extensively before they can be included into an *in vitro* assay as a read-out.

The *in vitro* assay pipeline for Chagas' disease

There is not a single *in vitro* assay that can determine all the desired effects of a test compound on the parasites. Therefore, the hits from high-throughput screening campaign are usually handed over to a whole panel of secondary assays. Currently, *in vitro* drug discovery often starts with image-based high-throughput screening of chemically diverse libraries (Alonso-Padilla et al., 2015; De Rycker et al., 2016; Ekins et al., 2015; Engel et al., 2010; McKerrow et al., 2009; Moon et al., 2014; Neitz et al., 2015; Pena et al., 2015; Sykes & Avery, 2015). The hits are then confirmed by other assay types such as LacZ reporter assays (Buckner et al., 1996; Neitz et al., 2015). Hits of high activity and selectivity should then be tested *in vitro* on a variety of strains (Moraes et al., 2014; Zingales et al., 2014). Total clearance using highly sensitive assays and reversibility by wash-out assays determine the degree of cidality of a test compound (Cal et al., 2016). An interesting design to test for cidality is also the clonal outgrowth assay (Dumoulin & Burleigh, 2018). Time frames of action of a test compound can be explored by existing assay design (De Rycker et al., 2016). Our live assay design with some adaptation for practicability could become a highly informative secondary assay for time-to-kill. Finally, testing against trypomastigotes carries the hope that the test compound might be active against parasites with low metabolic activity and therefore cidal against all parasite forms.

I personally would propose a slight change in the design of screening assays. The current screening design seems to favor static compounds over cidal compounds. To turn this skew to cidal compounds, I would propose drug exposure only for the last 24 hours of the assay. Additionally, I would propose a rather short assay duration, preventing reinfection. To obtain a high proportion of infected cells and high number of parasites at read-out, I propose to use a high MOI.

A novel *in vitro* assay read-out for Chagas' disease drug discovery established

High-content assays for Chagas' disease drug discovery

High-content microscopy has led to great innovation in kinetoplastid drug discovery (Alonso-Padilla et al., 2015; Alonso-Padilla & Rodriguez, 2014; De Rycker et al., 2016; Engel et al., 2010; Moraes et al., 2014; Neitz et al., 2015; Nohara et al., 2010; Yazdanparast et al., 2014). Among the specific advantages of image-based drug assays are the increased number of read-outs, a higher throughput, the possibility

to test wildtype parasite lines and the possibility to test living cultures. High-content imaging facilitates new read-outs, e.g. differentiation between intracellular and extracellular parasites, number of surviving host cells, and the differentiation between infected and uninfected host cells. In contrast to indirect estimates on parasite numbers from the colorimetric or fluorimetric methods as the CPRG- (Buckner et al., 1996) or resazurin-based assays, direct counts of parasite numbers are obtained in image-based assays. Furthermore, the number of host cells can be determined within the same assay. This way, the selectivity index can be determined in a single assay and trypanocidal compounds can directly be differentiated from cytotoxic compounds. Additionally, intracellular parasites can be distinguished from extracellular parasites and uninfected host cells from infected cells. These read-outs had been possible before the introduction of high-content imaging, but they would have required manual read-out of either Giemsa- or DNA-stained slides and therefore much more person-time. Automatic algorithm-based quantification enormously increased the through-put. Finally, as several sites in one well are imaged, an uncertainty estimate for the read-out values can be obtained and a flavor of the high variability underlying the replication of *T. cruzi*.

Another advantage is the possibility to do drug testing on wildtype parasite lines. When fixed samples are imaged, usually the parasites and host cells are stained, with nucleic acid stains, antibodies or other staining techniques. Therefore, transgenic parasite lines are not required for fixed imaging. This opens the possibility to test a wider variety of strains (Moraes et al., 2014). Additionally, there is no need for speculation about the effect of the introduction of genetic material, especially of drug resistance cassettes, on drug susceptibility.

While fixation enables the use of wildtype parasite lines, live imaging enables continuous read-outs. Without fixation, the samples can be imaged at several timepoints over the span of the infection cycle. However, live imaging requires fluorescent parasite lines. Live imaging has the potential to catch information on the dynamics of drug action. Furthermore, wash-out assays can be performed with the same sample at several timepoints, e.g. once per week over several weeks, reducing the demand in material and the variability between the timepoints. The limit for assay duration is mainly the viability of the host cells. The final timepoint can be determined ad hoc.

The facilitation of new read-outs, together with the potential of testing wildtype lines or repeated live imaging, are the central, but not the only advantages of high-content, image-based assays for Chagas' disease drug discovery. However, there are many challenging aspects about high-content assays concerning the image-analysis algorithm, live imaging, data management, and variability.

The established image-analysis algorithms are a powerful tool to increase the speed of quantification, but they require expert users. Often the user has to face a trade-off between sensitivity and specificity. Several aspects play into sensitivity. With a low signal-to-noise ratio, some parasite

might not be detected leading to false negative results. Correct quantification of intracellular parasites such as *T. cruzi* and *Leishmania spp.* is difficult. Two adjacent parasites might be counted as one. Especially when the parasite load is very high, many closely clustered parasites can be erroneously counted as host cell nuclei in nucleic acid based staining. These aspects of sensitivity require some caution in statements about absence of parasites, and therefore in the deployment of high-content imaging for cidality assays. The specificity can be compromised by false detection due to background signals and artifacts. To balance between sensitivity and specificity requires experience of the user.

While live imaging opens new opportunities to observe the dynamic aspects of drug action, it also requires transgenic parasite lines. The generation of transgenic parasite lines is cumbersome and limits these opportunities. During live imaging, phototoxicity should not be neglected.

As the name says, high-content imaging produces a lot of data. This requires good data management and an appropriate data storage plan. While estimators of uncertainty are important, this uncertainty also requires more statistical expertise to handle. The complexity of image-analysis algorithms, live imaging, data management, and variability require pre-considerations and experience from the user.

Overall, numerous publications in the recent years have proven that the opportunities of high-content imaging for drug discovery outweigh the challenges.

Variability in *Trypanosoma cruzi* replication during *in vitro* assays for Chagas' disease

At first, the recorded variability from the *in vitro* monitoring of *T. cruzi* replication was overwhelming. Concentrating on the fold-change as a read-out parameter showed that the replication rate in the untreated controls is statistically robust, but time-dependent. This time-dependence of the fold-change is very likely due to trypomastigogenesis. Differentiation to the trypomastigote stage happens at the same time for all amastigotes inside one host cell, however at different timepoints for amastigotes in different cells. The molecular nature of the trigger(s) is not known. Before amastigotes differentiate to trypomastigotes, they stop replicating. So, with the start of trypomastigogenesis, the replication rate starts to drop. Additionally, as trypomastigotes express very low levels of eGFP, with the start of trypomastigogenesis, the parasites start disappearing. In total, this leads to a decrease in the measured net fold-change. However, as the parasite quantifications from the fixed images showed, the general trend of increase in parasite numbers continues.

Other sources of variability are differences in parasite numbers between different sites within one well, differences in pipetting (seen between different wells of one row), differences between days of infection (seen in wells from different rows) and differences between plates. We started to parse out these sources of variability with the help of Bayesian modelling. However, so far, we were not able to obtain monomodal results for all parameters. In a next step, we will review our assumptions and

the included parameters in order to find out whether it is possible to get unambiguous parameter values, or whether some parameters continue to have multiple solutions.

Read-outs in the new assay design

The variety of read-outs could even have been further increased by recording more data on the host cells. In the images of fixed cells, we quantified the host cells using Hoechst for nuclear staining. However, the fixed images did not fully overlap with the images from live imaging. Therefore, we could not use site-specific host cell numbers to normalize the parasite numbers, which might have reduced the within-well variability. However, as the within-well variability was so high, a full overlap between fixed and live images would have been required to confidently use it for normalization. For further application, it could be interesting to test whether Hoechst staining and imaging is cytotoxic over 24 hours with 4 hour-intervals. If not, this would enable normalization per host cell and also show direct effects of the test compound on the host cell.

Another option, at least for fixed imaging, is the staining with Draq5. As Draq5 weakly stains the cytoplasm, it also enables the determination of intracellular parasites and infected host cells. Furthermore, cells at the image border can be removed, which otherwise can be a source for bias. As longer wavelengths are used to image Draq5-stained samples, there might be less cytotoxicity involved. However, I had decided against this, because in my experience, sensitivity and specificity for parasite detection was decreased when using Draq5 compared to Hoechst, as the difference in intensity between parasite DNA and cytoplasm was reduced.

One interesting option is staining the cytoplasm (specifically the actin filaments) of the host cell with fluorophore-labelled phalloidin. This also enables the detection of intracellular parasites and infected host cells, without decreasing sensitivity or specificity of the parasite DNA detection. However, imaging the phalloidin-stained cytoplasm would increase the number of channels in use and therefore, the requirements for imaging time and for storage of the images. Nevertheless, the addition of a cytoplasmic marker and with it of further read-outs is worth considering for future assays.

Time-to-kill as a read-out for Chagas' disease drug discovery

Describing the effect of a drug as the fold-change in parasite numbers over time is a novel approach to characterize drug action. It is a legitimate measure, because the model is developed over biologically very closely related data points. Focusing on the fold-change reduces the influence of the inter-day and intra-well variability, as most of this variability is due to different starting points of parasite numbers. Displaying the fold-change over drug concentration and time of drug exposure, we could show how many days that it takes a drug to start killing parasites at a given concentration in a statistically sound way. Additionally, the essence of the pharmacodynamic profile of a drug can be seen

in one glance. The time-window could be further reduced by building the model with less timepoints for shorter periods, e.g. three timepoints (8 hour observation window), leading to more fine-scaled answers.

A slight change in assay design will reduce variability and improve feasibility

The setup of this assay can be optimized concerning labor-intensity, microscope occupancy and variability. Taking as many plates as days of planned observation, all plates could be infected at the same time with a fluorescent parasite line. After 24 hours, the remaining trypomastigotes can be washed off and drug can be added. After addition of drug, the first plate can be imaged. Every 24 hours, a new plate can be imaged, until all plates have been imaged. The first 24 hours can be spared, because in this period, the major effects that can be observed are the settling down of the trypomastigotes, the infection of the host cells, and amastigogenesis, which carries no additional information. Using the same plate design as before, six drugs can be tested using five plates and occupying the microscope for five days, which would be one day less for six drugs than with the previous assay design. In this new approach fewer control wells are needed. Therefore, the plate setup could be changed to harbor 9 drugs with six concentrations or 6 drugs with nine concentrations. This would further reduce the required microscope occupancy. Additional advantages are a reduction in hands-on time and potentially a reduction in variability. With this setup, infection and drug addition is done only once and not every 24 hours, which will substantially reduce the lab time required for infection and drug addition. The only remaining user time is to start the microscope every 24 hours. With this reduction in handling, the whole layer of variability introduced by different days of infection would be dropped, hopefully leading to reduced variability in the results.

This new assay setup would not only decrease the variability and user time, but also allow for additional changes. The observation period is now fully driven by the interest of the investigator and not by the available number of wells on the plate. If desired, the effects could be observed for ten days after drug addition. But the observation period could also be shortened to 72 or 96 hours, as a promising candidate compound should actually kill the parasite rather rapidly. Another interesting setup would be the wash-out of drugs 24 hours after addition to test for reversibility of drug action.

Conclusion

In the course of this PhD project, we have explored many aspects of genetic manipulation of *T. cruzi*, including genotyping of our lab strain, the genome sequence of *T. cruzi* STIB980, and aspects around transgene expression levels, selection antibiotics and transgene stability in different life-cycle stages of *T. cruzi*. I hope these experiences are a solid foundation for the future experiments of Sabina Beilstein, who started to work on characterizing the mode-of-action of waltheriones using *T. cruzi* STIB980.

Additionally, I explored the role of parasite replication in the context of assay design for Chagas' disease drug discovery. This led me to consider all parameters of assay design. The non-invasive monitoring of drug action established with the eGFP-expressing parasite *T. cruzi* STIB980 delivered a novel read-out, which characterizes a drug in respect of pharmacodynamics. With slight changes in assay design, this assay will be more practicable, which will enrich the drug discovery pipeline for Chagas' disease and promote the development of new drugs required so urgently.

Acknowledgements

This work would not have been possible without the contribution of countless people and institutions. **Therefore, I am grateful:**

To the Swiss National Science Foundation for providing salary, travel costs and lab consumables.
To the Nikolaus und Bertha Burckhardt-Bürgin-Stiftung for enabling me to finish this project.
To the Freiwillige Akademische Gesellschaft for supporting my living expenses in the last months of the project.

To Prof. Dr. Nicolas Fasel for being my co-referee. Thank you for all your input in the meetings and taking the time for the thesis and defense. Thanks you for calling my attention to transgene stability and for encouraging me to dive deeper into the analysis of the seemingly unsurmountable variability.

To Pascal and your unshakable optimism and believe in my abilities. I am fascinated by your broad interests and very deep knowledge. Thank you for all you surprising ideas and constant support. Thank you for leading the Parasite Chemotherapy unit and giving me the opportunity for this project.
To Marcel and your steady support. You managed the variety of ideas, which Pascal and I provided. You always listened, when things overwhelmed me. You endured my protests. You questioned my wild plans. But, you accepted me taking yet another class of statistics.
To the Parasite Chemotherapy Unit. I still mean it, when I say, that you're my favorite lab!
To Monica. You first taught me, how to deal with trypanosomes. Then you taught me how to deal with humans. Thank you for managing this lab. Thank you for your friendship.
To Remo with your deep knowledge, fast thinking, and never ending kindness. You are my guru, when it comes to molecular biology, chemistry and graphical design.
To Natalie. You always listened to my joy and more often to my complaints. You taught me loads. About lab and about live. If not in vivo, via WhatsApp. I will miss your companionship.
To Sonja. Thank you for hugs and deep talk. Thank you for your support.
To Romina for countless Asian lunch sessions on SciFi, fantasy and cosplay.
To Kirsten for hugs, laughter and willpower.
To Chri for all you taught me about trypanosomes, chemistry and molecular biology.

To all the MSc students for your friendship. Thanks to you, my internal calendar does not count
the year, in which I tried to construct stage-specific plasmids,
the year, in which the stage-specific plasmids failed to express at all,
the year, in which the eGFP line lost its transgene,
the year, in which the high-content microscope failed regularly, and
the year, in which I fought variability.
But instead, for my it's
the year of my own master,
the year of Marina's and Suvitha's master,
the year of Michaela's and Amélie's master,
the year of Silvan's and Annabelle's master, and
the year of Dennis' master.
Thank you, each of you is special to me.
To Halim, Mélanie, Nina, and Mahmoud for the companionship. It was a great time with you.
To Sabina for bravely taking up the mess I'm gonna leave. Thanks for continuing, what I tried to start. It was a relieve to know, that my work was not in vain. And it is so good to leave it in competent hands.

To all my collaborators.
To Till. Thanks that I could occupy the high-content microscope for that long-stretched periods.
To Niggi, Eva and other people from GRU. Thanks for be supportive, when I again blocked the high-content microscope. Thanks for all the input and advice. Thanks for discussions about science and life.
To the DNDi. Thank you for your input and your important work!
To the people from LSHTM. For all the plasmids, I could reuse.
To John for all I learned from you.
To Paco for teaching me, how to transfect.
To Michael for the DNA and input on genotyping.
To Martin for your knowledge on *T. cruzi* molecular biology.
To the whole London group. I enjoyed the time in London and admire your work.
To Santuza Teixeira for kindly providing me with the plasmids pTcRG and an amastigote-specific plasmid
To Olivier for your input with statistics of growth dynamics.
To Antonio Osuna for the *T. cruzi* lab strain.
To Joachim Clos for the LADMac cells.
To Mike for support with the high-content microscope.
To Oliver for attempting to introduce me to the wonders of Bayesian statistics.

To the Biostatistics unit for sharing office heat and Eulerhof lunch breaks. Thanks for also sharing life.

To my MSc colleagues. A special shout-out to those who dared to continue at Swiss TPH: Manuela, Anneth, Jennifer, Eva, Nadja, Jerry.

To the MolImmu unit for hosting me in your lab. For MolBio and centrifuges. And for harboring my office chaos corner.

To all the coffee breakers, Fabi and Tierry, the malaria people …

To Mari and all the other visiting scientists. You enriched our unit.

To the technical service, the animal caretakers, Yvette and Anna. I cannot imagine, what our institute would look like, if you weren't doing your great work. Thank you!

To all the friends I found at the institute. It's a great place to be. And attracts great people.

I would also not have been able to finish this project, if it weren't for the life outside work.

Therefore, I am deeply grateful for friends and family.

To the Stadtposaunenchor Basel for introducing me to the trombone, Old music, the Münster tower and Basel culture.

To Phonlage61. Finally, playing tuba again. Thanks for the cool music and good talks.

To vineyard Basel, the church which supported my beliefs and unbeliefs. Thanks to the friends I found there: Anne, you really inspire me. And hey, thanks for your support. Christine, you're amazing.

To all my flatmates. You made Basel a home.

To all my friends, mostly afar. There is no words for what you mean to me. Support, inspiration and joy will have to suffice.

To my family.

To Julia. Thanks for your friendship. I admire you and always enjoy seeing you grow up.

To my parents. Seems that you listened to Goethe's advice. I grew deep roots and strong wings thanks to you. Ain't only biology, that without you none of what I've done would be possible.

You mostly are responsible, that I can say:

I am a very privileged person. I am grateful to this. However, I'd like to share. And even this I learned from you.

THANK YOU!

References

Abuin, G., Freitas-Junior, L. H., Colli, W., Alves, M. J., & Schenkman, S. (1999). Expression of trans-sialidase and 85-kDa glycoprotein genes in Trypanosoma cruzi is differentially regulated at the post-transcriptional level by labile protein factors. *J Biol Chem, 274*(19), 13041-13047. doi:10.1074/jbc.274.19.13041

Alexander, A. D., Villalta, F., & Lima, M. F. (2003). Transforming growth factor alpha binds to Trypanosoma cruzi amastigotes to induce signaling and cellular proliferation. *Infect Immun, 71*(7), 4201-4205. doi:10.1128/iai.71.7.4201-4205.2003

Alonso-Padilla, J., Cotillo, I., Presa, J. L., Cantizani, J., Pena, I., Bardera, A. I., . . . Rodriguez, A. (2015). Automated high-content assay for compounds selectively toxic to Trypanosoma cruzi in a myoblastic cell line. *PLoS Negl Trop Dis, 9*(1), e0003493. doi:10.1371/journal.pntd.0003493

Alonso-Padilla, J., & Rodriguez, A. (2014). High throughput screening for anti-Trypanosoma cruzi drug discovery. *PLoS Negl Trop Dis, 8*(12), e3259. doi:10.1371/journal.pntd.0003259

Alsford, S., Kawahara, T., Glover, L., & Horn, D. (2005). Tagging a T. brucei RRNA locus improves stable transfection efficiency and circumvents inducible expression position effects. *Mol Biochem Parasitol, 144*(2), 142-148. doi:10.1016/j.molbiopara.2005.08.009

Altschul, S. F., Gish, W., Miller, W., Myers, E. W., & Lipman, D. J. (1990). Basic local alignment search tool. *J Mol Biol, 215*(3), 403-410. doi:10.1016/s0022-2836(05)80360-2

Analytics, C. Web of Science. Retrieved from https://apps.webofknowledge.com/

Andrade, L. O., & Andrews, N. W. (2005). The Trypanosoma cruzi-host-cell interplay: location, invasion, retention. *Nat Rev Microbiol, 3*(10), 819-823. doi:10.1038/nrmicro1249

Andreoli, W. K., Taniwaki, N. N., & Mortara, R. A. (2006). Survival of Trypanosoma cruzi metacyclic trypomastigotes within Coxiella burnetii vacuoles: differentiation and replication within an acidic milieu. *Microbes Infect, 8*(1), 172-182. doi:10.1016/j.micinf.2005.06.013

Araujo, P. R., Burle-Caldas, G. A., Silva-Pereira, R. A., Bartholomeu, D. C., Darocha, W. D., & Teixeira, S. M. (2011). Development of a dual reporter system to identify regulatory cis-acting elements in untranslated regions of Trypanosoma cruzi mRNAs. *Parasitol Int, 60*(2), 161-169. doi:10.1016/j.parint.2011.01.006

Atwood, J. A., 3rd, Weatherly, D. B., Minning, T. A., Bundy, B., Cavola, C., Opperdoes, F. R., . . . Tarleton, R. L. (2005). The Trypanosoma cruzi proteome. *Science, 309*(5733), 473-476. doi:10.1126/science.1110289

Bairoch, A. (2000). The SWISS-PROT protein sequence database and its supplement TrEMBL in 2000. *Nucleic Acids Research, 28*(1), 45-48. doi:10.1093/nar/28.1.45

Balcazar, D. E., Vanrell, M. C., Romano, P. S., Pereira, C. A., Goldbaum, F. A., Bonomi, H. R., & Carrillo, C. (2017). The superfamily keeps growing: Identification in trypanosomatids of RibJ, the first riboflavin transporter family in protists. *PLoS Negl Trop Dis, 11*(4), e0005513. doi:10.1371/journal.pntd.0005513

Behbehani, K. (1973). Developmental cycles of Trypanosoma (Schizotrypanum) cruzi (Chagas, 1909) in mouse peritoneal macrophages in vitro. *Parasitology, 66*(2), 343-353. doi:10.1017/s0031182000045273

Berna, L., Rodriguez, M., Chiribao, M. L., Parodi-Talice, A., Pita, S., Rijo, G., . . . Robello, C. (2018). Expanding an expanded genome: long-read sequencing of Trypanosoma cruzi. *Microb Genom, 4*(5). doi:10.1099/mgen.0.000177

Berriman, M., Ghedin, E., Hertz-Fowler, C., Blandin, G., Renauld, H., Bartholomeu, D. C., . . . El-Sayed, N. M. (2005). The genome of the African trypanosome Trypanosoma brucei. *Science, 309*(5733), 416-422. doi:10.1126/science.1112642

Brener, Z., & Chiari, E. (1965). Aspects of Early Growth of Different Trypanosoma cruzi Strains in Culture Medium. *The Journal of Parasitology, 51*(6), 922-926. doi:10.2307/3275869

Broutin, H., Tarrieu, F., Tibayrenc, M., Oury, B., & Barnabe, C. (2006). Phylogenetic analysis of the glucose-6-phosphate isomerase gene in Trypanosoma cruzi. *Exp Parasitol, 113*(1), 1-7. doi:10.1016/j.exppara.2005.11.014

Buckner, F. S., Verlinde, C. L., La Flamme, A. C., & Van Voorhis, W. C. (1996). Efficient technique for screening drugs for activity against Trypanosoma cruzi using parasites expressing beta-galactosidase. *Antimicrob Agents Chemother, 40*(11), 2592-2597.

Burkard, G., Fragoso, C. M., & Roditi, I. (2007). Highly efficient stable transformation of bloodstream forms of Trypanosoma brucei. *Mol Biochem Parasitol, 153*(2), 220-223. doi:10.1016/j.molbiopara.2007.02.008

Cal, M., Ioset, J. R., Fugi, M. A., Maser, P., & Kaiser, M. (2016). Assessing anti-T. cruzi candidates in vitro for sterile cidality. *Int J Parasitol Drugs Drug Resist, 6*(3), 165-170. doi:10.1016/j.ijpddr.2016.08.003

Callejas-Hernandez, F., Girones, N., & Fresno, M. (2018). Genome Sequence of Trypanosoma cruzi Strain Bug2148. *Genome Announc, 6*(3). doi:10.1128/genomeA.01497-17

Callejas-Hernandez, F., Rastrojo, A., Poveda, C., Girones, N., & Fresno, M. (2018). Genomic assemblies of newly sequenced Trypanosoma cruzi strains reveal new genomic expansion and greater complexity. *Sci Rep, 8*(1), 14631. doi:10.1038/s41598-018-32877-2

Canavaci, A. M., Bustamante, J. M., Padilla, A. M., Perez Brandan, C. M., Simpson, L. J., Xu, D., . . . Tarleton, R. L. (2010). In vitro and in vivo high-throughput assays for the testing of anti-Trypanosoma cruzi compounds. *PLoS Negl Trop Dis, 4*(7), e740. doi:10.1371/journal.pntd.0000740

Caradonna, K. L., Engel, J. C., Jacobi, D., Lee, C. H., & Burleigh, B. A. (2013). Host metabolism regulates intracellular growth of Trypanosoma cruzi. *Cell Host Microbe, 13*(1), 108-117. doi:10.1016/j.chom.2012.11.011

Cazzulo, J. J., & Frasch, A. C. (1992). SAPA/trans-sialidase and cruzipain: two antigens from Trypanosoma cruzi contain immunodominant but enzymatically inactive domains. *Faseb j, 6*(14), 3259-3264.

Chatelain, E. (2015). Chagas disease drug discovery: toward a new era. *J Biomol Screen, 20*(1), 22-35. doi:10.1177/1087057114550585

Claser, C., Curcio, M., de Mello, S. M., Silveira, E. V., Monteiro, H. P., & Rodrigues, M. M. (2008). Silencing cytokeratin 18 gene inhibits intracellular replication of Trypanosoma cruzi in HeLa cells but not binding and invasion of trypanosomes. *BMC Cell Biol, 9*, 68. doi:10.1186/1471-2121-9-68

Coimbra, V. C., Yamamoto, D., Khusal, K. G., Atayde, V. D., Fernandes, M. C., Mortara, R. A., . . . Rabinovitch, M. (2007). Enucleated L929 cells support invasion, differentiation, and multiplication of Trypanosoma cruzi parasites. *Infect Immun, 75*(8), 3700-3706. doi:10.1128/iai.00194-07

Costa, F. C., Francisco, A. F., Jayawardhana, S., Calderano, S. G., Lewis, M. D., Olmo, F., . . . Taylor, M. C. (2018). Expanding the toolbox for Trypanosoma cruzi: A parasite line incorporating a bioluminescence-fluorescence dual reporter and streamlined CRISPR/Cas9 functionality for rapid in vivo localisation and phenotyping. *PLoS Negl Trop Dis, 12*(4), e0006388. doi:10.1371/journal.pntd.0006388

Cruz-Bustos, T., Potapenko, E., Storey, M., & Docampo, R. (2018). An Intracellular Ammonium Transporter Is Necessary for Replication, Differentiation, and Resistance to Starvation and Osmotic Stress in Trypanosoma cruzi. *mSphere, 3*(1). doi:10.1128/mSphere.00377-17

Dawidowski, M., Emmanouilidis, L., Kalel, V. C., Tripsianes, K., Schorpp, K., Hadian, K., . . . Popowicz, G. M. (2017). Inhibitors of PEX14 disrupt protein import into glycosomes and kill Trypanosoma parasites. *Science, 355*(6332), 1416-1420. doi:10.1126/science.aal1807

de Diego, J. A., Palau, M. T., Gamallo, C., & Penin, P. (1998). Relationships between histopathological findings and phylogenetic divergence in Trypanosoma cruzi. *Trop Med Int Health, 3*(3), 222-233. doi:10.1111/j.1365-3156.1998.tb00275.x

De Rycker, M., Thomas, J., Riley, J., Brough, S. J., Miles, T. J., & Gray, D. W. (2016). Identification of Trypanocidal Activity for Known Clinical Compounds Using a New Trypanosoma cruzi Hit-Discovery Screening Cascade. *PLoS Negl Trop Dis, 10*(4), e0004584. doi:10.1371/journal.pntd.0004584

Diaz-Viraque, F., Pita, S., Greif, G., de Souza, R. C. M., Iraola, G., & Robello, C. (2019). Nanopore sequencing significantly improves genome assembly of the protozoan parasite Trypanosoma cruzi. *Genome Biol Evol*. doi:10.1093/gbe/evz129

DNDi. (2019). DNDi R&D Portfolio June 2019. Retrieved from https://www.dndi.org/diseases-projects/portfolio/

Doyle, P. S., Zhou, Y. M., Hsieh, I., Greenbaum, D. C., McKerrow, J. H., & Engel, J. C. (2011). The Trypanosoma cruzi protease cruzain mediates immune evasion. *PLoS Pathog, 7*(9), e1002139. doi:10.1371/journal.ppat.1002139

Dumoulin, P. C., & Burleigh, B. A. (2018). Stress-Induced Proliferation and Cell Cycle Plasticity of Intracellular Trypanosoma cruzi Amastigotes. *MBio, 9*(4). doi:10.1128/mBio.00673-18

Dvorak, J. A., & Hyde, T. P. (1973). Trypanosoma cruzi: interaction with vertebrate cells in vitro. 1. Individual interactions at the cellular and subcellular levels. *Exp Parasitol, 34*(2), 268-283.

Dvorak, J. A., & Poore, C. M. (1974). Trypanosoma cruzi: interaction with vertebrate cells in vitro. IV. Environmental temperature effects. *Exp Parasitol, 36*(1), 150-157.

Ekins, S., de Siqueira-Neto, J. L., McCall, L. I., Sarker, M., Yadav, M., Ponder, E. L., . . . Talcott, C. (2015). Machine Learning Models and Pathway Genome Data Base for Trypanosoma cruzi Drug Discovery. *PLoS Negl Trop Dis, 9*(6), e0003878. doi:10.1371/journal.pntd.0003878

El-Sayed, N. M., Myler, P. J., Bartholomeu, D. C., Nilsson, D., Aggarwal, G., Tran, A. N., . . . Andersson, B. (2005). The genome sequence of Trypanosoma cruzi, etiologic agent of Chagas disease. *Science, 309*(5733), 409-415. doi:10.1126/science.1112631

El-Sayed, N. M., Myler, P. J., Blandin, G., Berriman, M., Crabtree, J., Aggarwal, G., . . . Hall, N. (2005). Comparative genomics of trypanosomatid parasitic protozoa. *Science, 309*(5733), 404-409. doi:10.1126/science.1112181

Elias, M. C., Marques-Porto, R., Freymuller, E., & Schenkman, S. (2001). Transcription rate modulation through the Trypanosoma cruzi life cycle occurs in parallel with changes in nuclear organisation. *Mol Biochem Parasitol, 112*(1), 79-90.

EMA. (2018). Fexinidazole Winthrop H-W-2320 [Press release]. Retrieved from https://www.ema.europa.eu/en/fexinidazole-winthrop-h-w-2320

Engel, J. C., Ang, K. K., Chen, S., Arkin, M. R., McKerrow, J. H., & Doyle, P. S. (2010). Image-based high-throughput drug screening targeting the intracellular stage of Trypanosoma cruzi, the agent of Chagas' disease. *Antimicrob Agents Chemother, 54*(8), 3326-3334. doi:10.1128/aac.01777-09

Engel, J. C., & Dvorak, J. A. (1988). Trypanosoma cruzi: cell biological behavior of epimastigote and amastigote forms in axenic culture. *J Protozool, 35*(4), 513-518. Retrieved from https://onlinelibrary.wiley.com/doi/abs/10.1111/j.1550-7408.1988.tb04140.x?sid=nlm%3Apubmed

Ferguson, M. A., Duszenko, M., Lamont, G. S., Overath, P., & Cross, G. A. (1986). Biosynthesis of Trypanosoma brucei variant surface glycoproteins. N-glycosylation and addition of a phosphatidylinositol membrane anchor. *J Biol Chem, 261*(1), 356-362. Retrieved from http://www.jbc.org/content/261/1/356.full.pdf

Fernandes, J. F., & Castellani, O. (1966). Growth characteristics and chemical composition of Trypanosoma cruzi. *Experimental Parasitology, 18*(2), 195-202. doi:https://doi.org/10.1016/0014-4894(66)90016-6

Fesser, A. F., Braissant, O., Olmo, F., Kelly, J. M., Mäser, P., & Kaiser, M. (2020). Non-invasive monitoring of drug action: A new live in vitro assay design for Chagas' disease drug discovery. *PLoS Negl Trop Dis, 14*(7), e0008487. doi:10.1371/journal.pntd.0008487

Flores-Lopez, C. A., & Machado, C. A. (2015). Differences in inferred genome-wide signals of positive selection during the evolution of Trypanosoma cruzi and Leishmania spp. lineages: A result of disparities in host and tissue infection ranges? *Infect Genet Evol, 33*, 37-46. doi:10.1016/j.meegid.2015.04.008

Francisco, A. F., Jayawardhana, S., Lewis, M. D., Taylor, M. C., & Kelly, J. M. (2017). Biological factors that impinge on Chagas disease drug development. *Parasitology, 144*(14), 1871-1880. doi:10.1017/s0031182017001469

Franco, C. H., Alcantara, L. M., Chatelain, E., Freitas-Junior, L., & Moraes, C. B. (2019). Drug Discovery for Chagas Disease: Impact of Different Host Cell Lines on Assay Performance and Hit Compound Selection. *Trop Med Infect Dis, 4*(2). doi:10.3390/tropicalmed4020082

Garcia, E. A., Ziliani, M., Aguero, F., Bernabo, G., Sanchez, D. O., & Tekiel, V. (2010). TcTASV: a novel protein family in trypanosoma cruzi identified from a subtractive trypomastigote cDNA library. *PLoS Negl Trop Dis, 4*(10). doi:10.1371/journal.pntd.0000841

Garg, N., Tarleton, R. L., & Mensa-Wilmot, K. (1997). Proteins with glycosylphosphatidylinositol (GPI) signal sequences have divergent fates during a GPI deficiency. GPIs are essential for nuclear division in Trypanosoma cruzi. *J Biol Chem, 272*(19), 12482-12491. doi:10.1074/jbc.272.19.12482

Garnier, S. (2018). viridis: Default Color Maps from 'matplotlib'. Retrieved from https://CRAN.R-project.org/package=viridis

Gazos-Lopes, F., Martin, J. L., Dumoulin, P. C., & Burleigh, B. A. (2017). Host triacylglycerols shape the lipidome of intracellular trypanosomes and modulate their growth. *PLoS Pathog, 13*(12), e1006800. doi:10.1371/journal.ppat.1006800

Giorgi, M. E., & de Lederkremer, R. M. (2011). Trans-sialidase and mucins of Trypanosoma cruzi: an important interplay for the parasite. *Carbohydr Res, 346*(12), 1389-1393. doi:10.1016/j.carres.2011.04.006

Gonzales-Perdomo, M., de Castro, S. L., Meirelles, M. N., & Goldenberg, S. (1990). Trypanosoma cruzi proliferation and differentiation are blocked by topoisomerase II inhibitors. *Antimicrob Agents Chemother, 34*(9), 1707-1714. doi:10.1128/aac.34.9.1707

Gonzalez, J., Ramalho-Pinto, F. J., Frevert, U., Ghiso, J., Tomlinson, S., Scharfstein, J., . . . Nussenzweig, V. (1996). Proteasome activity is required for the stage-specific transformation of a protozoan parasite. *J Exp Med, 184*(5), 1909-1918. doi:10.1084/jem.184.5.1909

Gysin, M., Braissant, O., Gillingwater, K., Brun, R., Maser, P., & Wenzler, T. (2018). Isothermal microcalorimetry - A quantitative method to monitor Trypanosoma congolense growth and growth inhibition by trypanocidal drugs in real time. *Int J Parasitol Drugs Drug Resist, 8*(2), 159-164. doi:10.1016/j.ijpddr.2018.03.003

Henriques, C., Henriques-Pons, A., Meuser-Batista, M., Ribeiro, A. S., & de Souza, W. (2014). In vivo imaging of mice infected with bioluminescent Trypanosoma cruzi unveils novel sites of infection. *Parasit Vectors, 7*, 89. doi:10.1186/1756-3305-7-89

Herrera, L. J., Brand, S., Santos, A., Nohara, L. L., Harrison, J., Norcross, N. R., . . . Maldonado, R. A. (2016). Validation of N-myristoyltransferase as Potential Chemotherapeutic Target in Mammal-Dwelling Stages of Trypanosoma cruzi. *PLoS Negl Trop Dis, 10*(4), e0004540. doi:10.1371/journal.pntd.0004540

Herwaldt, B. L. (2001). Laboratory-acquired parasitic infections from accidental exposures. *Clin Microbiol Rev, 14*(4), 659-688, table of contents. doi:10.1128/CMR.14.3.659-688.2001

Hodel, E. M., Kay, K., & Hastings, I. M. (2016). Incorporating Stage-Specific Drug Action into Pharmacological Modeling of Antimalarial Drug Treatment. *Antimicrob Agents Chemother, 60*(5), 2747-2756. doi:10.1128/AAC.01172-15

Huber, W., & Koella, J. C. (1993). A comparison of three methods of estimating EC50 in studies of drug resistance of malaria parasites. *Acta Trop, 55*(4), 257-261.

Hutner, S. H., & Bacchi, C. J. (1979). Nutrition of the Kinetoplastida. In W. H. R. Lumsden & D. A. Evans (Eds.), *Biology of the kinetoplastida*. London etc.: Academic Press.

Hyde, T. P., & Dvorak, J. A. (1973). Trypanosoma cruzi: interaction with vertebrate cells in vitro. 2. Quantitative analysis of the penetration phase. *Exp Parasitol, 34*(2), 284-294.

Ivens, A. C., Peacock, C. S., Worthey, E. A., Murphy, L., Aggarwal, G., Berriman, M., . . . Myler, P. J. (2005). The genome of the kinetoplastid parasite, Leishmania major. *Science, 309*(5733), 436-442. doi:10.1126/science.1112680

Izeta-Alberdi, A., Ibarra-Cerdena, C. N., Moo-Llanes, D. A., & Ramsey, J. M. (2016). Geographical, landscape and host associations of Trypanosoma cruzi DTUs and lineages. *Parasit Vectors, 9*(1), 631. doi:10.1186/s13071-016-1918-2

Junqueira, A. C., Degrave, W., & Brandão, A. (2005). Minicircle organization and diversity in Trypanosoma cruzi populations. *Trends Parasitol, 21*(6), 270-272. doi:10.1016/j.pt.2005.04.001

Keenan, M., & Chaplin, J. H. (2015). A new era for chagas disease drug discovery? *Prog Med Chem, 54*, 185-230. doi:10.1016/bs.pmch.2014.12.001

Kessler, R. L., Gradia, D. F., Pontello Rampazzo Rde, C., Lourenco, E. E., Fidencio, N. J., Manhaes, L., . . . Fragoso, S. P. (2013). Stage-regulated GFP Expression in Trypanosoma cruzi: applications from host-parasite interactions to drug screening. *PLoS One, 8*(6), e67441. doi:10.1371/journal.pone.0067441

Kipnis, T. L., Calich, V. L., & da Silva, W. D. (1979). Active entry of bloodstream forms of Trypanosoma cruzi into macrophages. *Parasitology, 78*(1), 89-98.

Koren, S., Walenz, B. P., Berlin, K., Miller, J. R., Bergman, N. H., & Phillippy, A. M. (2017). Canu: scalable and accurate long-read assembly via adaptive k-mer weighting and repeat separation. *Genome Res, 27*(5), 722-736. doi:10.1101/gr.215087.116

Lewis, M. D., Fortes Francisco, A., Taylor, M. C., Burrell-Saward, H., McLatchie, A. P., Miles, M. A., & Kelly, J. M. (2014). Bioluminescence imaging of chronic Trypanosoma cruzi infections reveals tissue-specific parasite dynamics and heart disease in the absence of locally persistent infection. *Cell Microbiol, 16*(9), 1285-1300. doi:10.1111/cmi.12297

Lewis, M. D., Francisco, A. F., Taylor, M. C., & Kelly, J. M. (2015). A new experimental model for assessing drug efficacy against Trypanosoma cruzi infection based on highly sensitive in vivo imaging. *J Biomol Screen, 20*(1), 36-43. doi:10.1177/1087057114552623

Lewis, M. D., & Kelly, J. M. (2016). Putting Infection Dynamics at the Heart of Chagas Disease. *Trends Parasitol, 32*(11), 899-911. doi:10.1016/j.pt.2016.08.009

Li, Y., Shah-Simpson, S., Okrah, K., Belew, A. T., Choi, J., Caradonna, K. L., . . . Burleigh, B. A. (2016). Transcriptome Remodeling in Trypanosoma cruzi and Human Cells during Intracellular Infection. *PLoS Pathog, 12*(4), e1005511. doi:10.1371/journal.ppat.1005511

Lima, M. F., & Villalta, F. (1990). Trypanosoma cruzi receptors for human transferrin and their role. *Mol Biochem Parasitol, 38*(2), 245-252.

Loo, V. G., & Lalonde, R. G. (1984). Role of iron in intracellular growth of Trypanosoma cruzi. *Infect Immun, 45*(3), 726-730.

Lucena, A. C. R., Amorim, J. C., de Paula Lima, C. V., Batista, M., Krieger, M. A., de Godoy, L. M. F., & Marchini, F. K. (2019). Quantitative phosphoproteome and proteome analyses emphasize the influence of phosphorylation events during the nutritional stress of Trypanosoma cruzi: the initial moments of in vitro metacyclogenesis. *Cell Stress Chaperones*. doi:10.1007/s12192-019-01018-7

Lwoff, M. (1951). The Nutrition of Parasitic Flagellates (Trypanosomidae, Trichomonadinae). In A. Lwoff (Ed.), *Biochemistry and Physiology of Protozoa* (pp. 129-176): Academic Press.

MacLean, L. M., Thomas, J., Lewis, M. D., Cotillo, I., Gray, D. W., & De Rycker, M. (2018). Development of Trypanosoma cruzi in vitro assays to identify compounds suitable for progression in Chagas' disease drug discovery. *PLoS Negl Trop Dis, 12*(7), e0006612. doi:10.1371/journal.pntd.0006612

Maser, P., Grether-Buhler, Y., Kaminsky, R., & Brun, R. (2002). An anti-contamination cocktail for the in vitro isolation and cultivation of parasitic protozoa. *Parasitol Res, 88*(2), 172-174.

Matteucci, K. C., Pereira, G. J. S., Weinlich, R., & Bortoluci, K. R. (2019). Frontline Science: Autophagy is a cell autonomous effector mechanism mediated by NLRP3 to control Trypanosoma cruzi infection. *J Leukoc Biol*. doi:10.1002/JLB.HI1118-461R

McKerrow, J. H., Doyle, P. S., Engel, J. C., Podust, L. M., Robertson, S. A., Ferreira, R., . . . Craik, C. S. (2009). Two approaches to discovering and developing new drugs for Chagas disease. *Mem Inst Oswaldo Cruz, 104 Suppl 1*, 263-269. doi:10.1590/s0074-02762009000900034

Melo, R. C., & Machado, C. R. (2001). Trypanosoma cruzi: peripheral blood monocytes and heart macrophages in the resistance to acute experimental infection in rats. *Exp Parasitol, 97*(1), 15-23. doi:10.1006/expr.2000.4576

Merli, M. L., Pagura, L., Hernandez, J., Barison, M. J., Pral, E. M., Silber, A. M., & Cricco, J. A. (2016). The Trypanosoma cruzi Protein TcHTE Is Critical for Heme Uptake. *PLoS Negl Trop Dis, 10*(1), e0004359. doi:10.1371/journal.pntd.0004359

Messenger, L. A., Yeo, M., Lewis, M. D., Llewellyn, M. S., & Miles, M. A. (2015). Molecular genotyping of Trypanosoma cruzi for lineage assignment and population genetics. *Methods Mol Biol, 1201*, 297-337. doi:10.1007/978-1-4939-1438-8_19

Meyer, K. J., Meyers, D. J., & Shapiro, T. A. (2019). Optimal kinetic exposures for classic and candidate antitrypanosomals. *J Antimicrob Chemother*. doi:10.1093/jac/dkz160

Molina, I., Gomez i Prat, J., Salvador, F., Trevino, B., Sulleiro, E., Serre, N., . . . Pahissa, A. (2014). Randomized trial of posaconazole and benznidazole for chronic Chagas' disease. *N Engl J Med, 370*(20), 1899-1908. doi:10.1056/NEJMoa1313122

Moon, S., Siqueira-Neto, J. L., Moraes, C. B., Yang, G., Kang, M., Freitas-Junior, L. H., & Hansen, M. A. (2014). An image-based algorithm for precise and accurate high throughput assessment of drug activity against the human parasite Trypanosoma cruzi. *PLoS One, 9*(2), e87188. doi:10.1371/journal.pone.0087188

Moraes, C. B., Giardini, M. A., Kim, H., Franco, C. H., Araujo-Junior, A. M., Schenkman, S., . . . Freitas-Junior, L. H. (2014). Nitroheterocyclic compounds are more efficacious than CYP51 inhibitors against Trypanosoma cruzi: implications for Chagas disease drug discovery and development. *Sci Rep, 4*, 4703. doi:10.1038/srep04703

Morillo, C. A., Marin-Neto, J. A., Avezum, A., Sosa-Estani, S., Rassi, A., Jr., Rosas, F., . . . Yusuf, S. (2015). Randomized Trial of Benznidazole for Chronic Chagas' Cardiomyopathy. *N Engl J Med, 373*(14), 1295-1306. doi:10.1056/NEJMoa1507574

Mortara, R. A., da Silva, S., Patricio, F. R., Higuchi, M. L., Lopes, E. R., Gabbai, A. A., . . . Ferraz Neto, B. H. (1999). Imaging Trypanosoma cruzi within tissues from chagasic patients using confocal microscopy with monoclonal antibodies. *Parasitol Res, 85*(10), 800-808. doi:10.1007/s004360050636

Nakajima-Shimada, J., Hirota, Y., & Aoki, T. (1996). Inhibition of Trypanosoma cruzi growth in mammalian cells by purine and pyrimidine analogs. *Antimicrob Agents Chemother, 40*(11), 2455-2458. Retrieved from https://aac.asm.org/content/aac/40/11/2455.full.pdf

NCBI. pubmed. Retrieved from https://www.ncbi.nlm.nih.gov/pubmed

Neitz, R. J., Chen, S., Supek, F., Yeh, V., Kellar, D., Gut, J., . . . Siqueira-Neto, J. L. (2015). Lead identification to clinical candidate selection: drugs for Chagas disease. *J Biomol Screen, 20*(1), 101-111. doi:10.1177/1087057114553103

Nohara, L. L., Lema, C., Bader, J. O., Aguilera, R. J., & Almeida, I. C. (2010). High-content imaging for automated determination of host-cell infection rate by the intracellular parasite Trypanosoma cruzi. *Parasitol Int, 59*(4), 565-570. doi:10.1016/j.parint.2010.07.007

Olmo, F., Costa, F. C., Mann, G. S., Taylor, M. C., & Kelly, J. M. (2018). Optimising genetic transformation of Trypanosoma cruzi using hydroxyurea-induced cell-cycle synchronisation. *Mol Biochem Parasitol, 226*, 34-36. doi:10.1016/j.molbiopara.2018.07.002

Osuna, A., Jimenez-Ortiz, A., Mascaro, C., & Alonso, C. (1983). Trypanosoma cruzi: arrested division of amastigote forms in enucleated HeLa cells. *J Parasitol, 69*(3), 629-631.

Pacheco-Lugo, L., Diaz-Olmos, Y., Saenz-Garcia, J., Probst, C. M., & DaRocha, W. D. (2017). Effective gene delivery to Trypanosoma cruzi epimastigotes through nucleofection. *Parasitol Int, 66*(3), 236-239. doi:10.1016/j.parint.2017.01.019

Pena, I., Pilar Manzano, M., Cantizani, J., Kessler, A., Alonso-Padilla, J., Bardera, A. I., . . . Julio Martin, J. (2015). New compound sets identified from high throughput phenotypic screening against three kinetoplastid parasites: an open resource. *Sci Rep, 5*, 8771. doi:10.1038/srep08771

Perin, L., Moreira da Silva, R., Fonseca, K. D., Cardoso, J. M., Mathias, F. A., Reis, L. E., . . . Carneiro, C. M. (2017). Pharmacokinetics and Tissue Distribution of Benznidazole after Oral Administration in Mice. *Antimicrob Agents Chemother, 61*(4). doi:10.1128/aac.02410-16

R Core Team. (2018). R: A Language and Environment for Statistical Computing: R Foundation for Statistical Computing. Retrieved from https://www.R-project.org/

Rassi, A., Jr., Rassi, A., & Marin-Neto, J. A. (2010). Chagas disease. *Lancet, 375*(9723), 1388-1402. doi:10.1016/s0140-6736(10)60061-x

Reis-Cunha, J. L., & Bartholomeu, D. C. (2019). Trypanosoma cruzi Genome Assemblies: Challenges and Milestones of Assembling a Highly Repetitive and Complex Genome. *Methods Mol Biol, 1955*, 1-22. doi:10.1007/978-1-4939-9148-8_1

Ritagliati, C., Villanova, G. V., Alonso, V. L., Zuma, A. A., Cribb, P., Motta, M. C., & Serra, E. C. (2016). Glycosomal bromodomain factor 1 from Trypanosoma cruzi enhances trypomastigote cell infection and intracellular amastigote growth. *Biochem J, 473*(1), 73-85. doi:10.1042/BJ20150986

Ritz, C., Baty, F., Streibig, J. C., & Gerhard, D. (2015). Dose-Response Analysis Using R. *PLoS One, 10*(12), e0146021. doi:10.1371/journal.pone.0146021

Salzberg, S. L., Delcher, A. L., Kasif, S., & White, O. (1998). Microbial gene identification using interpolated Markov models. *Nucleic Acids Res, 26*(2), 544-548. doi:10.1093/nar/26.2.544

Sanchez-Valdez, F. J., Padilla, A., Wang, W., Orr, D., & Tarleton, R. L. (2018). Spontaneous dormancy protects Trypanosoma cruzi during extended drug exposure. *Elife, 7*. doi:10.7554/eLife.34039

Schettino, P. M., Majumder, S., & Kierszenbaum, F. (1995). Regulatory effect of the level of free Ca2+ of the host cell on the capacity of Trypanosoma cruzi to invade and multiply intracellularly. *J Parasitol, 81*(4), 597-602.

Seco-Hidalgo, V., De Pablos, L. M., & Osuna, A. (2015). Transcriptional and phenotypical heterogeneity of Trypanosoma cruzi cell populations. *Open Biol, 5*(12), 150190. doi:10.1098/rsob.150190

Shah-Simpson, S., Lentini, G., Dumoulin, P. C., & Burleigh, B. A. (2017). Modulation of host central carbon metabolism and in situ glucose uptake by intracellular Trypanosoma cruzi amastigotes. *PLoS Pathog, 13*(11), e1006747. doi:10.1371/journal.ppat.1006747

Shah-Simpson, S., Pereira, C. F., Dumoulin, P. C., Caradonna, K. L., & Burleigh, B. A. (2016). Bioenergetic profiling of Trypanosoma cruzi life stages using Seahorse extracellular flux technology. *Mol Biochem Parasitol, 208*(2), 91-95. doi:10.1016/j.molbiopara.2016.07.001

Silber, A. M., Tonelli, R. R., Lopes, C. G., Cunha-e-Silva, N., Torrecilhas, A. C., Schumacher, R. I., . . . Alves, M. J. (2009). Glucose uptake in the mammalian stages of Trypanosoma cruzi. *Mol Biochem Parasitol, 168*(1), 102-108. doi:10.1016/j.molbiopara.2009.07.006

Silva-Dos-Santos, D., Barreto-de-Albuquerque, J., Guerra, B., Moreira, O. C., Berbert, L. R., Ramos, M. T., . . . de Meis, J. (2017). Unraveling Chagas disease transmission through the oral route: Gateways to Trypanosoma cruzi infection and target tissues. *PLoS Negl Trop Dis, 11*(4), e0005507. doi:10.1371/journal.pntd.0005507

Souza, R. T., Lima, F. M., Barros, R. M., Cortez, D. R., Santos, M. F., Cordero, E. M., . . . da Silveira, J. F. (2011). Genome size, karyotype polymorphism and chromosomal evolution in Trypanosoma cruzi. *PLoS One, 6*(8), e23042. doi:10.1371/journal.pone.0023042

Stanaway, J. D., & Roth, G. (2015). The burden of Chagas disease: estimates and challenges. *Glob Heart, 10*(3), 139-144. doi:10.1016/j.gheart.2015.06.001

Steinbiss, S., Silva-Franco, F., Brunk, B., Foth, B., Hertz-Fowler, C., Berriman, M., & Otto, T. D. (2016). Companion: a web server for annotation and analysis of parasite genomes. *Nucleic Acids Res, 44*(W1), W29-34. doi:10.1093/nar/gkw292

Stempin, C. C., Tanos, T. B., Coso, O. A., & Cerban, F. M. (2004). Arginase induction promotes Trypanosoma cruzi intracellular replication in Cruzipain-treated J774 cells through the activation of multiple signaling pathways. *Eur J Immunol, 34*(1), 200-209. doi:10.1002/eji.200324313

Sykes, M. L., & Avery, V. M. (2015). Development and application of a sensitive, phenotypic, high-throughput image-based assay to identify compound activity against Trypanosoma cruzi amastigotes. *Int J Parasitol Drugs Drug Resist, 5*(3), 215-228. doi:10.1016/j.ijpddr.2015.10.001

Takagi, Y., Akutsu, Y., Doi, M., & Furukawa, K. (2019). Utilization of proliferable extracellular amastigotes for transient gene expression, drug sensitivity assay, and CRISPR/Cas9-mediated gene knockout in Trypanosoma cruzi. *PLoS Negl Trop Dis, 13*(1), e0007088. doi:10.1371/journal.pntd.0007088

Tarleton, R. L. (2001). Parasite persistence in the aetiology of Chagas disease. *Int J Parasitol, 31*(5-6), 550-554. Retrieved from https://pdf.sciencedirectassets.com/271903/1-s2.0-S0020751900X00793/1-s2.0-S0020751901001588/main.pdf?X-Amz-Security-Token=AgoJb3JpZ2luX2VjEJ%2F%2F%2F%2F%2F%2F%2F%2F%2F%2FwEaCXVzLWVhc3QtMSJIMEYCIQCkOA1Ys1fSXoiwfFomU1%2BlKRs34sxJDXB8aZBV6BN4%2BgIhAKYi3%2FJja%2FtJ3cIT%2FRDqCqFCIyyQaZeCc3hVqK2QR3tOKtoDCCgQAhoMMDU5MDAzNTQ2ODY1IgyGfd2%2B2BcNZTjd%2F9wqtwM%2BATm6HUR8I5H5vISRGKnGG6JKtCFkfjORUEaPhbl8iYE3Ho3Phh7OH1LWV2bambZQh3heXdOx0CBE5lU9cWdfoB%2FCmYlIIwCaa2bJKiNa17dQzW7NltS9vnjlcm%2BRSXJvll8UPi1KdFXmDyn5Ct7EF4G2vTZMBaSSclFTy6Y3In%2BwPImBuGJqzh6UDViMJZZrCVgFj4jCXMISOsFY4iH0nasG8GShdqPWLFC27sArd254l%2BVh9r%2BjhaVenEZgT7fFAnj%2B0S8BEPf28tvtHKMuHqGRp2gnDC3%2Fg9vSx4nq5X1%2B5ThQbiZfY9OhcA7%2FPlxpZnoJvh5528CAY0I%2Bqk0vU8cSineWXRI%2FbbUIr6urnJNpsu7gJV8w4N77HyDkgF6Xsmmw3ZSzOuUQuKY3i3wzrRPKY512NywdCYtebNQU6dQNNFCMUtY7%2FGrvTfHnTq7BUZjuNQAfXatZYkeNvaKaZusr9XWZaztP6Ih%2Fe3y%2FuBEyUXrEFeTHeNWfAzwQhNFMg11Xe3jiGeltHL7HEu689fA27NrPqik2YWSd2i7mhgaO2ENa0EPkzt4wV6ij9Z5Bop%2FHC3BHMJSnn%2BoFOrMB8BHG8DHFkp2SwXqRCdthHJIJJCOBcHpS7oEQ%2B74TLstbvfVIAI41kPcXZDKMOV9HMZovcV%2FAiXo03SGozq0fiDsT59UR6w%2BPMndfoJ6VOy%2BY6DnLItpppax0e2N%2FbOuHDOmPQ1IVkhUrPlmhmM3hqX%2Bqn4SHodhkMmwib6qtEpK99VR7oOwVyMaTWFfV7KAYRUGdiWaaP%2FLzFyihYMubgz9ElFxrcffBXf5cKvYBVpCxHBQ%3D&X-Amz-Algorithm=AWS4-HMAC-SHA256&X-Amz-Date=20190805T072715Z&X-Amz-SignedHeaders=host&X-Amz-Expires=300&X-Amz-Credential=ASIAQ3PHCVTY4POJISL7%2F20190805%2Fus-east-1%2Fs3%2Faws4_request&X-Amz-Signature=5783a7cc6b73c9632831c38a4a1f8cff2e4ef8a0265f089cf5f3bdd53ee39b86&hash=039df5e05079f12f6903dee0677748e432253f7cd364652adcf8475ee0238759&host=68042c943591013ac2b2430a89b270f6af2c76d8dfd086a07176afe7c76c2c61&pii=S0020751901001588&tid=spdf-c6b9a461-a40a-486e-9ed2-36f8377feb7e&sid=cf80fcf218efa5408d0aab55ed83a327139cgxrqb&type=client

Teixeira, T. L., Cruz, L., Mortara, R. A., & Da Silva, C. V. (2015). Revealing Annexin A2 and ARF-6 enrollment during Trypanosoma cruzi extracellular amastigote-host cell interaction. *Parasit Vectors, 8*, 493. doi:10.1186/s13071-015-1097-6

ter Kuile, F., White, N. J., Holloway, P., Pasvol, G., & Krishna, S. (1993). Plasmodium falciparum: in vitro studies of the pharmacodynamic properties of drugs used for the treatment of severe malaria. *Exp Parasitol, 76*(1), 85-95.

Tomlinson, S., Vandekerckhove, F., Frevert, U., & Nussenzweig, V. (1995). The induction of Trypanosoma cruzi trypomastigote to amastigote transformation by low pH. *Parasitology, 110 (Pt 5)*, 547-554.

Torrico, F., Gascon, J., Ortiz, L., Alonso-Vega, C., Pinazo, M. J., Schijman, A., . . . Ribeiro, I. (2018). Treatment of adult chronic indeterminate Chagas disease with benznidazole and three E1224 dosing regimens: a proof-of-concept, randomised, placebo-controlled trial. *Lancet Infect Dis, 18*(4), 419-430. doi:10.1016/s1473-3099(17)30538-8

Tu, X., & Wang, C. C. (2004). The involvement of two cdc2-related kinases (CRKs) in Trypanosoma brucei cell cycle regulation and the distinctive stage-specific phenotypes caused by CRK3 depletion. *J Biol Chem, 279*(19), 20519-20528. doi:10.1074/jbc.M312862200

Urbina, J. A., Payares, G., Contreras, L. M., Liendo, A., Sanoja, C., Molina, J., . . . Loebenberg, D. (1998). Antiproliferative effects and mechanism of action of SCH 56592 against Trypanosoma (Schizotrypanum) cruzi: in vitro and in vivo studies. *Antimicrob Agents Chemother, 42*(7), 1771-1777. Retrieved from https://www.ncbi.nlm.nih.gov/pmc/articles/PMC105681/pdf/ac001771.pdf

Vago, A. R., Macedo, A. M., Oliveira, R. P., Andrade, L. O., Chiari, E., Galvao, L. M., . . . Pena, S. D. (1996). Kinetoplast DNA signatures of Trypanosoma cruzi strains obtained directly from infected tissues. *Am J Pathol, 149*(6), 2153-2159. Retrieved from https://www.ncbi.nlm.nih.gov/pmc/articles/PMC1865364/pdf/amjpathol00036-0357.pdf

Villalta, F., & Kierszenbaum, F. (1982). Growth of isolated amastigotes of Trypanosoma cruzi in cell-free medium. *J Protozool, 29*(4), 570-576.

Villalta, F., & Kierszenbaum, F. (1984). Enhanced multiplication of intracellular (amastigote) stages of Trypanosoma cruzi in vitro. *J Protozool, 31*(3), 487-489.

Walker, B. J., Abeel, T., Shea, T., Priest, M., Abouelliel, A., Sakthikumar, S., . . . Earl, A. M. (2014). Pilon: An Integrated Tool for Comprehensive Microbial Variant Detection and Genome Assembly Improvement. *PLOS ONE, 9*(11), e112963. doi:10.1371/journal.pone.0112963

Weatherly, D. B., Boehlke, C., & Tarleton, R. L. (2009). Chromosome level assembly of the hybrid Trypanosoma cruzi genome. *BMC Genomics, 10*, 255. doi:10.1186/1471-2164-10-255

Wenzler, T., Steinhuber, A., Wittlin, S., Scheurer, C., Brun, R., & Trampuz, A. (2012). Isothermal microcalorimetry, a new tool to monitor drug action against Trypanosoma brucei and Plasmodium falciparum. *PLoS Negl Trop Dis, 6*(6), e1668. doi:10.1371/journal.pntd.0001668

Westenberger, S. J., Cerqueira, G. C., El-Sayed, N. M., Zingales, B., Campbell, D. A., & Sturm, N. R. (2006). Trypanosoma cruzi mitochondrial maxicircles display species- and strain-specific variation and a conserved element in the non-coding region. *BMC Genomics, 7*(1), 60. doi:10.1186/1471-2164-7-60

Wheeler, R. J., Gull, K., & Gluenz, E. (2012). Detailed interrogation of trypanosome cell biology via differential organelle staining and automated image analysis. *BMC Biol, 10*, 1. doi:10.1186/1741-7007-10-1

WHO. (2012). *Research priorities for Chagas disease, human African trypanosomiasis and leishmaniasis.* Retrieved from https://apps.who.int/iris/bitstream/handle/10665/77472/WHO_TRS_975_eng.pdf?sequence=1

Wick, R. R., Judd, L. M., Gorrie, C. L., & Holt, K. E. (2017). Completing bacterial genome assemblies with multiplex MinION sequencing. *Microb Genom, 3*(10), e000132. doi:10.1099/mgen.0.000132

Wickham, H. (2017). tidyverse: Easily Install and Load the 'Tidyverse'. Retrieved from https://CRAN.R-project.org/package=tidyverse

Wickham, H., & Bryan, J. (2018). readxl: Read Excel Files. Retrieved from https://CRAN.R-project.org/package=readxl

Wilkinson, S. R., Taylor, M. C., Horn, D., Kelly, J. M., & Cheeseman, I. (2008). A mechanism for cross-resistance to nifurtimox and benznidazole in trypanosomes. *Proc Natl Acad Sci U S A, 105*(13), 5022-5027. doi:10.1073/pnas.0711014105

Yakubu, M. A., Basso, B., & Kierszenbaum, F. (1992). DL-alpha-difluoromethylarginine inhibits intracellular Trypanosoma cruzi multiplication by affecting cell division but not trypomastigote-amastigote transformation. *J Parasitol, 78*(3), 414-419.

Yakubu, M. A., Majumder, S., & Kierszenbaum, F. (1993). Inhibition of S-adenosyl-L-methionine (AdoMet) decarboxylase by the decarboxylated AdoMet analog 5'-([(Z)-4-amino-2-butenyl]methylamino)-5'-deoxyadenosine (MDL 73811) decreases the capacities of Trypanosoma cruzi to infect and multiply within a mammalian host cell. *J Parasitol, 79*(4), 525-532.

Yang, G., Lee, N., Ioset, J. R., & No, J. H. (2017). Evaluation of Parameters Impacting Drug Susceptibility in Intracellular Trypanosoma cruzi Assay Protocols. *SLAS Discov, 22*(2), 125-134. doi:10.1177/1087057116673796

Yang, X. J. (2004). Lysine acetylation and the bromodomain: a new partnership for signaling. *Bioessays, 26*(10), 1076-1087. doi:10.1002/bies.20104

Yazdanparast, E., Dos Anjos, A., Garcia, D., Loeuillet, C., Shahbazkia, H. R., & Vergnes, B. (2014). INsPECT, an open-source and versatile software for automated quantification of (Leishmania) intracellular parasites. *PLoS Negl Trop Dis, 8*(5), e2850. doi:10.1371/journal.pntd.0002850

Zhang, J. H., Chung, T. D., & Oldenburg, K. R. (1999). A Simple Statistical Parameter for Use in Evaluation and Validation of High Throughput Screening Assays. *J Biomol Screen, 4*(2), 67-73. doi:10.1177/108705719900400206

Zingales, B. (2018). Trypanosoma cruzi genetic diversity: Something new for something known about Chagas disease manifestations, serodiagnosis and drug sensitivity. *Acta Trop, 184*, 38-52. doi:10.1016/j.actatropica.2017.09.017

Zingales, B., Miles, M. A., Campbell, D. A., Tibayrenc, M., Macedo, A. M., Teixeira, M. M., . . . Sturm, N. R. (2012). The revised Trypanosoma cruzi subspecific nomenclature: rationale, epidemiological relevance and research applications. *Infect Genet Evol, 12*(2), 240-253. doi:10.1016/j.meegid.2011.12.009

Zingales, B., Miles, M. A., Moraes, C. B., Luquetti, A., Guhl, F., Schijman, A. G., & Ribeiro, I. (2014). Drug discovery for Chagas disease should consider Trypanosoma cruzi strain diversity. *Mem Inst Oswaldo Cruz, 109*(6), 828-833. doi:10.1590/0074-0276140156